Design, Modeling and Simulation of P&O Algorithm with Fuzzy Logic Controller for Photovoltaic Water Pumping System

By

Biruk Larago Doboch

A Thesis Submitted to

Electrical Power and Control Engineering (Power Electronics) program

School of Electrical Engineering and Computing

Presented in Partial Fulfillment of the Requirement for the Degree of Master's in Power Electronics

Office of Graduate Studies

Adama Science and Technology University

Adama

September, 2018

Design, Modeling and Simulation of P&O Algorithm with Fuzzy Logic Controller for Photovoltaic Water Pumping System

By: Biruk Larago Doboch

Advisor: Kemal Ibrahim(PhD)

A Thesis Submitted to

Electrical Power and Control Engineering (Power Electronics) program

School of Electrical Engineering and Computing

Presented in Partial Fulfillment of the Requirement for the Degree of Master's in Power Electronics

Office of Graduate Studies

Adama Science and Technology University

Adama

September, 2018

Approval of Board of Examiners

We, the undersigned, members of the Board of Examiners of the final open defense by ____________________________________ have read and evaluated his thesis entitled "____"

and examined the candidate. This is, therefore, to certify that the thesis has been accepted in partial fulfillment of the requirement of the Degree of ………………………………………..

____________________________	______________________	____________________
Supervisor /Advisor	Signature	Date
____________________________	______________________	____________________
Chairperson	Signature	Date
____________________________	______________________	____________________
Internal Examiner	Signature	Date
____________________________	______________________	____________________
External Examiner	Signature	Date

Declaration

I hereby declare that this MSc thesis is my original work and has not been presented for a degree in any other university, and all sources of material used for this thesis have been duly acknowledged.

Name of student: Biruk Larago Doboch

Signature:________________

This MSc Thesis has been submitted for examination with my approval as thesis advisor.

Name of advisor: _______________________________

Signature: ___________________________

Date of submission: ____________________

Advisor's approval sheet

To: Electrical Power and Control Engineering Program (Power Electronics)

Subject: Thesis Submission

This is to certify that the thesis entitled "Design, Modeling and Simulation of Photovoltaic Water Pumping System Controller" submitted in partial fulfillment of the requirements for the degree of Master's in Electrical Power and Control Engineering (Specialization in Power Electronics), the Graduate program of the department of Electrical Power and Control Engineering, and has been carried out by Biruk Larago Doboch Id. No GSR/0030/09 under my supervision. Therefore, I recommend that the student has fulfilled the requirements and hence hereby he can submit the thesis to the department.

____________________________ ____________________ ________________

Name of Advisor Signature Date

ACKNOWLEDGEMENT

First and foremost, praises and thanks to God, the Almighty, for His showers of blessings throughout my thesis work to complete the thesis successfully. Without a relationship with Him, arrival of this day would have been highly doubtful.

There are no proper words to convey my deep gratitude and respect for my thesis advisor, **Kemal Ibrahim (PhD)**, College of Mechanical and Electrical Engineering, Addis Ababa Science &Technology University (AASTU).He has inspired me to become an independent researcher and helped me realize the power of critical reasoning. He also demonstrated what a brilliant and hard-working researcher can accomplish. His dynamism, vision, sincerity and motivation have deeply inspired me. He has taught me the methodology to carry out the thesis and to present the thesis works as clearly as possible. It was a great privilege and honor to work and study under his guidance. I am extremely grateful for what he has offered me. I would also like to thank him for his friendship, empathy, and great sense of humor. Not only is he a competent teacher and advisor, but he is also a genuine human being who really does care for his students.

I am extremely grateful to my families for their love, prayers, caring and sacrifices for educating and preparing me for my future. I am very much thankful to my uncle, Mathewos Selfago, for his love, understanding, prayers and continuing support to complete this thesis work. Besides, I am grateful to thank my friends who spent their time to read and supported me by giving good suggestion for editing the documentation.

I am extending my thanks to Metals & Engineering Corporation(METEC) coordinated with Ethiopian Power Engineering Industry(EPEI), Addis Ababa, for their willingness to give me necessary data like specification and cost of solar panel they provide for the market which is shown in Appendix C.

Table of Contents

LIST OF FIGURES

LIST OF TABLES

LIST OF ACRONYMS

AC	Alternating Current
A/D	Analog into Digital
BDCM	Brushless DC motor
COG	Center of Gravity
CV	Constant Voltage
DC	Direct Current
FIS	Fuzzy Inference System
FLC	fuzzy logic control
GUI	Graphical User Interface
HM	Height Method
INC	Incremental Conductance
LCB	Linear Current Booster
PMDCM	Permanent Magnet DC Motor
MOM	Mean of maximum
MPP	Maximum Power Point
MPPT	Maximum Power Point Tracker
NB	Negative Big
NOCT	Normal Operating Cell Temperature
NS	Negative Small
OV	Open circuit Voltage
PB	Positive Big
P & O	Perturb and Observe
PPV	Photovoltaic Power
PS	Positive Small
PV	Photovoltaic
PWM	Pulse Width Modulation
SC	Short Circuit
SEPIC	Single Ended Primary Inductor Converter
VMPP	Maximum Power Point Voltage
ZO	Zero

LIST OF SYMBOLS

A	Ideal diode quality factor depending on PV technology
A_L	Load friction
B_m	Viscose torque constant for rotational losses
C	Capacitor
D	Duty ratio
d	Diode
D_{mp}	Duty ratio corresponding to the maximum power output
dP	The total power change between two sampling periods
dV	The total voltage change between two sampling periods
e	Induced electromotive force
E_{gap}	Band-gap energy of the semiconductor used in the cell
f_s	dc/dc Converter switching frequency
G	Solar radiation
G_D	The scaling factor the duty ratio variation
G_I	The scaling factor of the PV array output current variation
G_P	The scaling factor of the PV array output power variation
G_S	The scaling factor of the variable step-size
G_ω	The scaling factor of the rotation speed variation
I_a	Armature current of DC motor
I_C	Capacitor current
I_D	Diode internal diffusion current
I_d	Converter Input current
i_L	Inductor current
I_o	Photovoltaic cell reverse saturation current
I_{oc}	Converter output current
I_{Ph}	Photocurrent or light generated current
I_{PV}	Output current of the solar cell
I_{SC}	Short-circuit current of the Photovoltaic model
J	Moment of inertia

k	Boltzmann's constant
K_e	Back electromotive force constant of DC motor
K_L	The proportional constant of the load torque
L	Inductance
La	Armature inductance of DC motor
P_{actual}	The real measured power produced by the PV array
P_e	Electric power of the motor
P_{max}	Maximum power point
P_{out}	Output power of the converter
P_{peak}	Peak power
q	The charge of electron
Ra	Armature resistance of DC motor
R_S	Series resistance of the Photovoltaic cell
R_{Sh}	Shunt resistance of the Photovoltaic cell
S	Switch
T	Photovoltaic cell's operating temperature
T_C	Photovoltaic cell's operating temperature in kelvin
T_e	Electromagnetic torque of DC motor
T_L	Load torque
t_{off}	Off period of converter switch
t_{on}	On period of converter switch
T_p	The torque required to drive the pump
T_S	DC/DC converter switching period
V_a	Armature voltage of DC motor
V_C	Capacitor voltage
V_D	Voltage applied across the diode terminals
V_d	Input voltage of the converter
v_L	Inductor voltage
V_{max}	Voltage at maximum power of the PV array
V_{MPP}	Voltage at maximum power point or optimal voltage

V_{PV}	Output voltage of the solar cell
ΔD	The duty ratio variation
ΔI_{PV}	The PV array output current variation
ΔP_{PV}	The PV array output power variation
$\Delta \omega_m$	The rotation speed variation
Θ	The bias or threshold
Φ	Flux
ω_m	Rotational speed of DC motor

Abstract

*In this thesis work an inquiry into the design of stand-alone Photovoltaic water pumping system controller has been taken into account for supplying a rural area with clean water. It comprises a study of system components and their modeling. Theoretical studies and mathematical modeling techniques of Photovoltaic are undertaken by using equivalent electrical circuits, various tracking algorithms and their control methods are involved in the discussion. The whole system is implemented in the MATLAB/SIMULINK to verify the performance of the planned MPPT technique. The complete system simulation is undertaken by analyzing and modeling each subsystem. It applies SIMULINK to model MPPT, FLC, Photovoltaic module, buck converter, a DC pump motor and the model is moved to MATLAB. Every of these elements have been masked and simulated in an individual subsystem in order that they can be simply controlled and exactly monitored. A model of the complete PV system is presented and discussed along with how all of the subsystem components have been combined to form it. The conventional P&O MPPT technique is changed to P&O with FLC. To verify the practicality of the proposed P&O with FLC MPPT and compare its performance against the conventional P&O algorithm, they are enforced in MATLAB and their simulation is done using existing irradiance data. The simulation result of the proposed P&O with FLC MPPT is compared to conventional P&O algorithm of water pumping system. Based on the simulation results, it is justified that the P&O with FLC has the ability to perturb the operation of the PV module at better approach to MPP compared to conventional P&O algorithm in varying weather and it improves the system performance. It is recommended to apply some other DC-DC converters such as boost, Ćuk and buck-*boost *along with the proposed MPPT technique to improve flexibility in the future research investigation in this area.*

Key words*: Photovoltaic, maximum power point tracker (MPPT), DC-DC converter, P&O algorithm, FLC, MATLAB*

CHAPTER ONE

INTRODUCTION

1.1 Background

Water resources are essential for satisfying human needs, protecting health, ensuring food production and the restoration of ecosystems as well as for social, economic and sustainable development. There is a great need to supply environmentally sound technology for the provision of drinking water. Remote water pumping systems are a key component in meeting this need. It will also be the first stage of the purification and desalination plants to produce potable water. Renewable energy especially solar photovoltaic is important alternative source of energy for the future, and research and development done on this area attained importance in using solar cells to power the electrical systems [5].

According to UN World Water Development Report 2014, it has been estimated that 3.5 billion people do not have satisfied water and 2.5 billion people lack access to improved water supply [3].Water pumping has throughout history been a technical challenge. There has always been a need to supply drinking water and satisfy regular agricultural demands throughout the development of civilization in human societies [4]. There is a great need to supply sustainable energy for the provision of drinking water at very low financial and environmental cost, especially in relatively poor and arid rural regions. Without basic services, such regions are likely to become aid dependent or depopulated and unproductive, especially when expectations are raised by modern information and communications technology. Remote PV water pumping and PV power generation systems, generally, seem to be an excellent solution to assist with this problem into the future.

In the rural areas, pumping systems are needed to pump the water for domestic usage, to irrigate crops, to water cattle and animal stocks, etc. Hence, a source of power is needed to operate the pumping system [5]. An AC powered system would be economic and takes minimum maintenance when the AC power is available from the nearby grid. However, in many rural areas, water sources are spread over many miles of land and the located too far away from the existing grid lines. Installation of a new transmission line and transformers at isolated locations is extremely expensive [5]. There are many internal combustion engines that are used for a stand-alone water pumping systems nowadays. These systems have the same advantages, such as: they are portable and easy to install but they require frequent site visits for refueling and maintenance, and in addition, the diesel is expensive and not readily available in rural areas of many developing countries and even the fuel is available within the country, transporting the fuel to remote, rural villages because there are no roads or supporting infrastructure in most of the remote villages [5].

The consumption of fossil fuels also has an environmental impact; it is considered the major cause of climate change due to their polluting effects. The energy consumption is accompanied by a release of carbon oxide (CO2) into the atmosphere and it contributes for more than of 60% of the global CO2 emitted in the atmosphere each year [6]. The increase in global demand for energy combined with the pollution concern caused by fossil fuels has encouraged scientists to search for environmentally friendly sources of energy. The problem associated with CO2 emissions can be solved through the application of renewable energy technologies, which are already cost competitive with fossil fuels in many situations [24]. Therefore, the use of renewable energy is a very attractive for water pumping systems in the rural areas.

1.2 Photovoltaic system

The photovoltaic system consists of interconnected components designed in a way to achieve the specific target of delivering the desired electricity from a small device to the load. Photovoltaic systems are categorized by the main categories of grid-connected, stand-alone systems and hybrid system which comprises different sources of energy such as PV arrays, diesel generators and wind generators. Hybrid and stand-alone systems are used increasingly in rural areas [25, 26]. Therefore, the PV water pumping system considered in this thesis is a stand-alone system to fulfill the needs of people in the rural locations.

1.2.1 Stand-alone system

The power from the photovoltaic array in the stand-alone system is directly fed to the load without connection to the utility system. The stand-alone system is considered one of the most economic ways of implementing a photovoltaic system especially for application in rural areas that have large periods of intense solar radiation and have no access to the main utility grid. Examples are communication systems, water pumping systems, lighthouses and emergency services or military applications where the auxiliary power units are needed [25, 26].

1.3 Alternatives of PV water pumping system energy storage

Since PV water pumping system constitutes an intermittent source of power, stand-alone systems obviously need some sort of backup energy storage which makes them available through the night or bad weather conditions. Among many possible storage technologies, the lead-acid battery continues to be the workhorse of many PV systems because it is relatively inexpensive and widely available. In addition to energy storage, the battery also has ability to provide surges of current that are much higher than the instantaneous current available from the array, as well as the inherent and automatic property controlling the output voltage of the array so that loads receive voltages within their own range of acceptability [6].

While batteries may seem like a good idea, they have a number of disadvantages. The type of lead-acid battery suitable for PV systems is a deep-cycle battery [6], which is different from one used for automobiles, and it is more expensive and not widely available. Battery lifetime in PV systems is typically three to eight years, but this reduces to typically two to six years in hot climate since high ambient temperature dramatically increases the rate of internal corrosion [28]. Batteries also require regular maintenance and will degrade very rapidly if the electrolyte is not topped up and the charge is not maintained. They reduce the efficiency of the overall system due to power loss during charge and discharge. Typical battery efficiency is around 85% but could go below 75% in hot climate [28]. From all those reasons, experienced PV system designers avoid batteries whenever possible.

For water pumping systems, appropriately sized water reservoirs can meet the requirement of energy storage during the downtime of PV generation. The additional cost of reservoir is considerably lower than that incurred by the battery equipped system [36].

1.4 The proposed PV water pumping system

The water pumping system proposed in this thesis is a stand-alone type with a water storage tank instead of using battery storage, to satisfy an isolated, remote, low maintenance and low cost water-pumping application. The system mainly comprises photovoltaic module as source, converting the sunlight into electrical energy, and a centrifugal pump load driven by permanent magnet DC motor as shown in Fig. 1.1. To achieve high efficiency system performance and to increase the amount of energy extracted from the PV module by the load during the daylight hours, a maximum power point tracker will be included in the system.

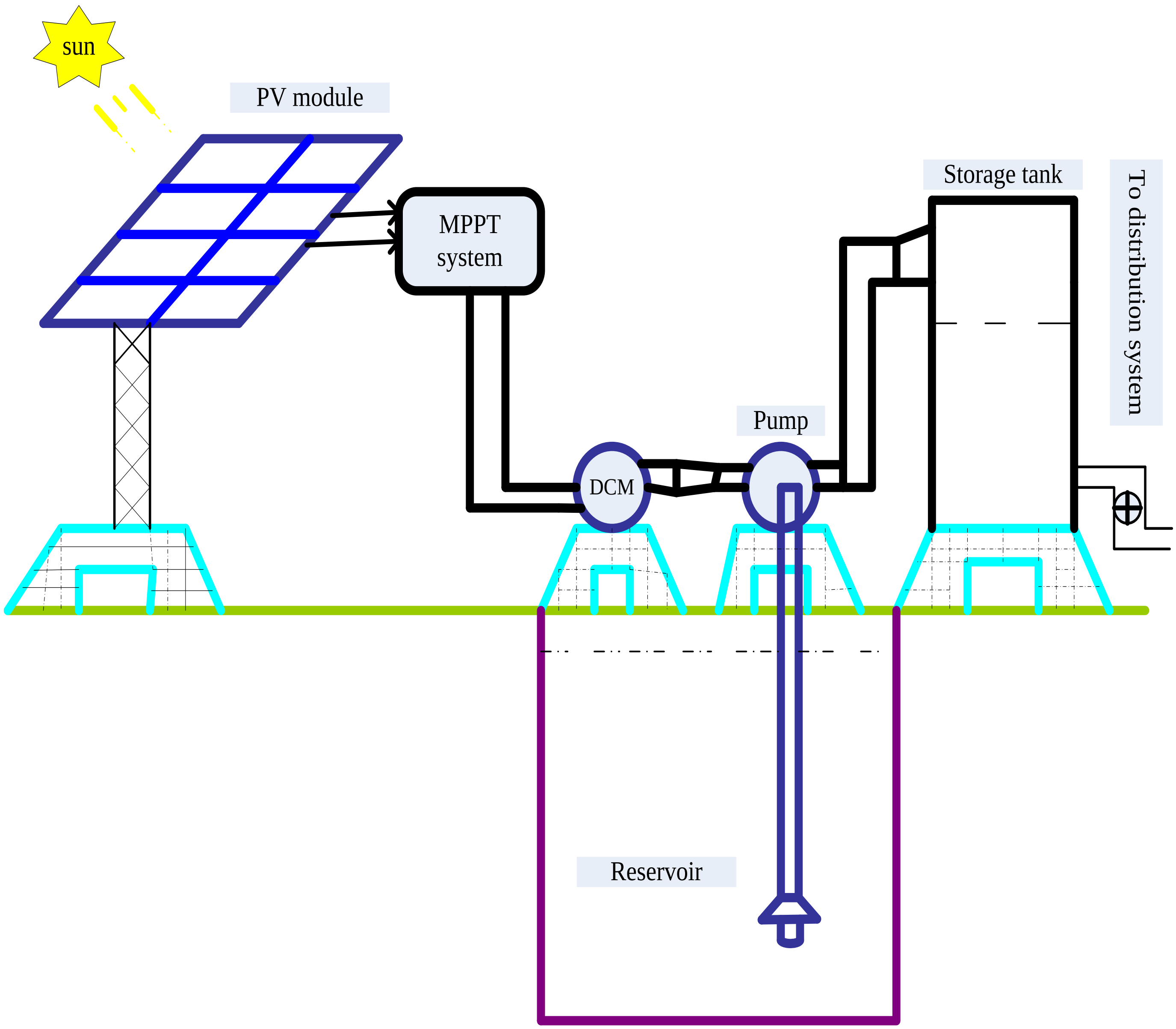

Fig. 1.1 Block diagram of the proposed stand-alone PV water pumping system

The components of such a photovoltaic system will be described in detail in the remaining part of this thesis and mathematical models will be developed to represent the character of each component in a complete system simulation.

1.4.1 PV Module

There are different sizes of PV module commercially available (typically sized from 60W to 170W). Usually, a number of PV modules are combined as an array to meet different energy demands. For example, a typical small-scale desalination plant requires a few thousand watts of power [29]. The size of system selected for the proposed system is 180W, which is commonly used in small water pumping systems for cattle grazing in rural areas [36].

1.4.2 Maximum Power Point Tracker

A maximum power point tracker is a device capable of tracking the MPP, and this device consists of DC-DC power converter its duty cycle adjusted by MPPT controller. While the photovoltaic panels may seem like a good source of electricity, their conversion efficiency is not very high. Their ability to convert sunlight energy to electrical power is relatively imperfect, with conversion efficiency typically in the range 12 ~ 20%. The range of efficiency can drop further during variable solar irradiation, panel temperature and load conditions [29]. Therefore, if the load is directly coupled to the PV array, the PV array must usually be oversized to supply the required power to the load. This leads to an over-sized expensive system. It is important to operate the PV-cells of the array at the maximum power point, MPP, or as near to it as possible, by using an electronic load-matching circuit, since this gives a worthwhile improvement in the available power in comparison with direct load connection [1]. The output current and power of a PV array depends on the terminal voltage. The maximum power point tracker (MPPT) is now prevalent in grid-tied PV power systems and is becoming more popular in stand-alone systems. It should not be confused with sun trackers, mechanical devices that rotate and/or tilt PV modules in the direction of sun. MPPT is a power electronic device interconnecting a PV power source and a load, maximizes the power output from a PV module or array with varying operating conditions, and therefore maximizes the system efficiency. MPPT is made up with a switch-mode DC-DC converter and a controller.

1.4.3 MPPT Controller

Analog controllers have traditionally performed control of MPPT. However, the use of digital controllers is rapidly increasing because they offer several advantages over analog controllers. First, digital controllers are programmable thus capable of implementing advanced algorithm with relative ease. It is far easier to code the equation, $x = y \times z$, than to design an analog circuit to do the same [37]. For the same reason, modification of the design is much easier with digital controllers. They are immune to time and temperature drifts because they work in discrete, outside the linear operation. As a result, they offer long-term stability. They are also insensitive to component tolerances since they implement algorithm in software, where gains and parameters are consistent and reproducible [37].They allow reduction of parts count since they can handle various tasks in a single chip. Many of them are also equipped with multiple A/D converters and PWM generators, thus they can control multiple devices with a single controller.

1.4.4 Water Pump

Two types of pumps are commonly used for PV water pumping applications: positive displacement and centrifugal [20]. Positive displacement types are used in low-volume pumps [36]. Centrifugal pumps have relatively high efficiency [7] and are capable of pumping a high volume of water [36]. Water pumps are driven by various types of motors. AC induction motors are cheaper and widely available worldwide. The system, however, needs an inverter to convert DC output power from PV to AC power, which is usually expensive, and it is also less efficient than DC motor-pump systems [7]. In general, DC motors are preferred because they are highly efficient and can be directly coupled with a PV module or array. Brushed types are less expensive and more common although brushes need to be replaced periodically (typically every two years) [7]. There is also an aforementioned brushless type. The water pump chosen here for its size and cost is centrifugal pump as it is inexpensive, simple, requires low maintenance and is available in a wide range of flow rates and heads. Therefore a centrifugal pump is considered in this work. It has flow rates up to 20.0L/min (5.4GPM) [13]. The typical daily output is between 3000L and 6,500L [13].

1.5 Statement of the problem

According to UNESCO, Water.org in 2018, 61 million Ethiopians lack access to safe water and 65 million lack access to improved sanitation [3]. Of those who lack access to improved sanitation, staggering 27 million practice open defecation. In rural Ethiopia, a Water.org survey found that many women and children walk more than three hours to collect water, often from shallow wells or unprotected ponds they share with animals. Even from addressed areas, it is hand pumping system without waste water treatment. Recurring droughts result in famine, food shortages, and water-related diseases, as people are forced to rely heavily on contaminated or stagnant water sources. Water sources are spread over many depth of land and power lines are scarce. Installation of a new transmission line and transformer to the location is often prohibitively expensive. There is a great need to supply environmentally sound technology for the provision of drinking water. Remote water pumping systems are a key component in meeting this need.

1.6 Motivation

Solar energy is the most abundant energy source we know. The sun is the biggest energy generator on Earth. We receive 173,000 terawatts continuously. The sunlight reaching the Earth every hour could potentially satisfy the global energy needs. However; we are able to use only 0.001 per cent of the solar energy that is available to us. Using solar energy does not lead to air or water pollution, and does not release greenhouse gases. It is Applicable Everywhere. Solar Panels and solar water heaters are most effective in areas with constant exposure to the sun. However, they also generate electricity or heat when it is cloudy or cold. So solar energy is still a viable source in that kind of regions. This is due to the fact that solar panels need sunlight, not sun heat, to generate electricity of heat. Albert Einstein experimented with solar energy and photovoltaic. He wrote a paper in 1905 explaining the photoelectric effect. The paper won him a Nobel Prize in 1921 and also built the foundations for further development of the solar technologies. Even though effective generation from solar panels will not happen until 50 years later, Einstein's work was the cornerstone. The space industry was one of the first to acknowledge the usefulness of solar energy and to implement it. As early as the 1960s the industry began to use solar energy to provide power aboard the space crafts. Vanguard 1 is the first artificial earth satellite powered by solar energy. The Russian Lunokhod Rover was also powered by solar energy when it landed on the Moon in 1973. But, direct application of this source of clean energy cannot generate the required amount of energy. Hence, these are some of the interesting facts about photovoltaics, which are capable of motivating electrical engineers to design a controller to maximize the power being generated from the sun which is the clean source of energy.

1.7 Objectives

1.7.1. General Objective

The general objective of this proposed thesis is to Design, Mathematical Modeling and Simulation of the Photovoltaic Water Pumping System Controller.

1.7.2. Specific Objectives

- Model the selected PV module
- Design appropriate DC-DC buck converter and P&O with FLC
- Simulate the system by P&O with FLC using MATLAB/SIMULINK
- Analyze the influence of the controller on the performance PV module

- Justify and record the improvements done by using proposed controller
- Draw conclusions and recommendations

1.8. Significance of the Thesis

The use of Photovoltaic system for water pumping not only provides potable pure water but also it is important for the reduction of global warming. The advantages of the proposed system are:

- Once the system is implemented, unattended operation proceeds.
- It provides smoke and fume free energy.
- System is modular and closely matched to need.
- It provides better life for rural areas with low cost.
- It makes recommendation on the control strategies needed on the current energy source to get better advantage.

1.9 Scope of the Thesis

This proposed thesis is limited to providing theoretical design, modeling and simulations of PV water pumping system controller with MPPT. The system will not include hardware implementation. That is left for future work.

1.10 Thesis Organization

The thesis is organized into five chapters. The first chapter discusses the introduction part in which the background, problem statement, motivation, objective and significance of the study are discussed. It presents a brief introduction to PV energy, its history and how increasing fuel cost and emissions make PV water pumping systems attractive and economically viable in remote locations. Literature review on the Converter, MPPT algorithms and control strategies are described in the second chapter of the thesis. The third chapter deals with methodology through which methods of analyzing MPPT, Converter and Fuzzy Logic Controller has been discussed how to apply it in this thesis for controlling. In fourth chapter; design and simulation of the system are illustrated by using MATLAB. Based on the results and analysis, conclusions and recommendations are drawn in fifth chapter.

CHAPTER TWO

LITERATURE REVIEW

This chapter reviews and discuses several popular MPPT techniques for solar PV systems like CV, P&O, INC, SC and OV that are reviewed in the literature along with their advantages and disadvantages to get better understanding of each MPPT technique and its influence on the system performance. Besides that, this chapter presents a comparison between these techniques in terms of steady-state oscillation, tracking speed and efficiency.

2.1 Maximum power point tracking (MPPT)

The first attempt to study MPPT was made by Dang [4] of California Polytechnic State University, Pomona. The thesis built a small PV module simulator and a buck converter without a controller. Then, it provided a rudimentary computer simulation of MPPT with a resistive load. The study was, however, far from comprehensive. Another was done here by Day [5], and it centered round a power system for a miniature satellite. It included MPPT in the system, but the functionality of MPPT was not tested. The theoretical study was insufficient, and it lacked simulations and experiments to ensure the functionality of MPPT. The efficiency of a PV plant is affected mainly by three factors: the efficiency of the PV module, efficiency of inverter (93-95%) and the efficiency of the Maximum Power Point Tracking (MPPT) algorithm.

2.2 MPPT algorithms classification`

Several MPPT algorithms have been proposed for PV power systems in recent years, to locate the MPP and increase the system efficiency. The MPPT algorithms may be divided into two types, which are indirect control or “quasi tracking techniques” and direct control or “true tracking techniques” [23, 35]. In the indirect control techniques, the MPP is calculated either by measuring the voltage and current of the PV array, the solar insolation, or by the use of mathematical functions obtained from empirical data. Therefore, these techniques are incapable of tracking the MPP with varying irradiation and temperature. The indirect control techniques are look-up table technique, constant voltage technique, fractional open-circuit voltage and fractional short-circuit current. However, the true tracking techniques have the ability to find the optimum operating point even under changing atmospheric conditions, because they do not rely on previous knowledge of or calculated data from the PV array *V-I* characteristics. The true tracking techniques are the perturbation and observation (P&O)

technique, incremental conductance (INC) technique; but artificial intelligence techniques can also be included in this category, such as, fuzzy logic control (FLC) techniques and the neural network techniques. In the tracking process one or two variables are used for calculating the MPP. The fractional open-circuit voltage and fractional short-circuit current use only one variable, either the PV array output voltage or current respectively, though the P&O and INC methods need both variables to determine the MPP [10, 23].

2.2.1 Simple panel load matching

The simple panel load matching technique is one of the simplest techniques to operate a PV array close to its maximum power point. In this technique the optimum operating point of the PV array is determined either by a series of measurements under average operating conditions or theoretical calculation. The load is designed to produce the values of PV voltage and current corresponding to the MPP. There is another commonly used simple method that is widely used all over the world in PV battery charger systems, which involves choosing the average battery voltage close to the average solar panel V_{MPP} [21]. This method has the advantages of simplicity and no additional circuitry is used, therefore, the power loss between the panel and the battery is reduced and the risk of component failure is kept low for the whole system. However, the system does not take into consideration the changes of solar irradiation or temperature [31].

2.2.2 Load switching technique

The load switching technique was proposed in 1993 by Huang Yongji and Lin Deheng to optimize the output power produced by the PV array. The MPPT technique is based on the use of an array reconfiguration controller [33]. In this configuration different panels are connected in series and parallel in an appropriate manner to form a PV array. Then, the PV array is connected to a number of controllable battery cells connected in series to fulfill the load matching process. However, this technique has the drawbacks that it requires extra switching circuits and wiring. Hence, the stepwise switched operating voltage cannot guarantee accurate tracking of MPP. Moreover, it is difficult to keep an equal charge level on all the battery cells, hence degrading battery life in the long term [31].

2.2.3 Constant voltage method (CV)

If the PV system is implemented without a battery to tie the bus voltage to an approximately constant level, a simple control scheme of the constant voltage method can be applied as presented in [12]. In this method the feedback of the PV voltage is compared with a fixed reference voltage and the resultant signal adjusts the duty ratio of the DC-DC converter to keep the operating point of the PV array at the MPP or close to it. The reference voltage is set to be equal to the V_{MPP} of the characteristic PV array or to another calculated best fixed voltage.

This method is simple, economical and only one feedback-loop control is required. However this technique has the drawback that it does not correct for environmental variation such as change in irradiation and temperature [31].

2.2.4 Perturb and observe (P&O) algorithm

The perturb and observe algorithm is considered to be the most commonly used MPPT algorithm among the other techniques because of its simple structure and ease of implementation. It is based on the concept that on the power-voltage curve, the change in the PV array output power is equal to zero (ΔP_{PV} = 0) on the top of the curve as illustrated in [13, 14, 20]. The P&O operates by periodically perturbing (incrementing or decrementing) the PV array terminal voltage or current and comparing the corresponding output power of PV array *P(n+1)* with that at the previous perturbation *P(n)*. If the perturbation in terminal voltage leads to increase in the PV power (ΔP_{PV} > 0), the perturbation should be kept in the same direction; otherwise the perturbation is moved to the opposite direction. The perturbation cycle is repeated until reaching the maximum power at (ΔP_{PV} = 0). There are two different ways to implement the P&O algorithm. In the conventional way a reference voltage is used as a perturbation parameter; therefore a PI controller is needed to adjust the duty ratio [14, 19]. The second way is that, the duty ratio is directly perturbed and the power is measured every PWM cycle [13]. The advantages of this technique are simplicity, ease of implementation and it does not require a previous knowledge of the PV array.

2.2.5 Incremental conductance (INC) method

The basic idea of the incremental conductance is that the slope of P-V curve (the derivative of PV array output power with respect to its output voltage) becomes zero ($dP/dV=0$) at the MPP. It is also possible to find a relative location of the operating point to the MPP by looking at the slopes. The slope is the derivative of the PV module's power with respect to its voltage. It is negative on the right of MPP and positive on the left of the MPP [18].

The INC method performs erratically during transient conditions. Also the computational time is increased due to the slowing down of the sampling frequency as a consequence of the algorithm's high complexity in contrast to the P&O technique.

2.2.6 Fractional short-circuit current (SC)

The basis for short-circuit current method is that, the maximum operating current I_{MPP} is approximately linearly related to the short-circuit current I_{SC} under varying atmospheric conditions; in other words:

$$I_{MPP} \approx K_{SC} \, . \, I_{SC} \tag{2.1}$$

Where K_{SC} is a proportional constant and it depends mainly on the metrological conditions and fill factor. The proportional constant K_{SC} is usually found to be between (75% - 92%). To measure I_{SC} an additional switch has to be introduced in parallel with the PV array to satisfy the short circuit condition. However the author in [30] provided another option by using a boost converter and the switch of the converter is used for short circuiting the PV array. Once K_{SC} is known and I_{SC} is measured the I_{MPP} can be calculated from Equation (2.1). The advantages of this method are its simplicity and low cost of implementation. On the other hand, the momentary interruption required for measuring I_{SC} leads to some loss of generated power, and the value of K_{SC} changes slightly [15].

2.2.7 Fractional open-circuit voltage (OV)

The open-circuit technique is based on the fact that the ratio of PV array output voltage V_{MPP}at the maximum power point to its open circuit voltage V_{OC} is approximately constant under varying irradiation and temperature levels as shown in the Equation (2.2) [22].

$$V_{MPP} \approx K_{V} \, . \, V_{OC} \tag{2.2}$$

K_V is the proportional constant which depends on the characteristic of the photovoltaic array being used. Therefore it has to be estimated by empirically determining V_{OC} and V_{MPP} for the particular PV array at different levels of temperature and irradiation. However the value of K_V has been reported to range between 71% and 80%. The open circuit voltage V_{OC} is measured by momentarily interrupting the normal operation of the system. This is done by introducing a static switch in series with the PV array. Once K_V is known and V_{OC} is measured, the V_{MPP} value can be calculated from (2.2) as a reference and a feed forward voltage control scheme is implemented to bring the PV array voltage to the point of peak power.

This method has an advantage that it is very simple, cheap to implement and it uses only one feedback loop. However, its drawback is that the interrupted system operation at the time of measuring V_{OC}results in some generated power loss. To prevent this, the authors in [38] used pilot cells to obtainV_{OC}. The pilot cells are solar cells that represent the PV array's cells, which are not used to produce electricity but to obtain the characteristic parameters such as V_{OC} without interrupting the main PV system. The pilot cells must be carefully chosen to represent the characteristics of photovoltaic array. Hence, each pair of pilot cell/solar array must be calibrated, consequently increasing the energy cost of the system.

2.3 Discussion of different techniques addressed

Different MPPT techniques have been reviewed and discussed in this chapter along with their advantages and disadvantages. Many comparisons have been carried out amongst different MPPT techniques. The authors in [12, 47, 48] provided comparison in different aspects between the main MPPT techniques (CV, P&O, INC, SC and OV). The CV technique was the worst amongst the other MPPT techniques, because it fixes the reference voltage to a best fixed voltage value and holds it constant under any operating condition instead of following the MPP [12].

The OV and SC techniques have better performance with their moderate complexity compared to the CV technique. However the P&O and INC techniques OV and SC techniques provide higher energy supply than this because the OV and SC require an additional static switch to perform the open-circuit and short circuit condition, which increases the losses and hence reduces their performance.

In the literature [12, 47] it has been highlighted that, the P&O and INC techniques are the most efficient compared to the other MPPT techniques. Moreover, the relative cost of P&O and INC techniques are not high, because they do not require additional static switches as in the OV and SC techniques. Though the INC technique has the similar performance as P&O technique, but its implementation cost is higher [47].

2.4 Summary

Based on the review of the performance comparison made on different MPPT techniques, it is recommended that the P&O and INC techniques have the potential to perform better than other MPPT techniques. However, because of the higher implementation cost of the INC technique, its use would not be justified by the relatively small improvement in the performance. This makes the P&O technique more attractive than the INC technique in this thesis work.

CHAPTER THREE

METHODOLOGY

In this chapter, an explanation of component characteristics, circuit design and the mathematical modeling of the PV water pumping system are provided. It starts with the explanation of Proposed Variable Step-size Perturb and Observe algorithm with FLC and its flow chart followed by solar cells, reviewing the physical structure of the semiconductor of the PV cell and the basic concept of how does it convert the sunlight into electrical energy. The mathematical model of the solar cell, and module are presented to show and analyze the effect of the atmospheric conditions on their *I-V* and *P-V* output characteristics. This chapter introduces and investigates various DC-DC converters, which are commonly used in MPPT power converter of PV systems, to select the most suitable converter for a DC motor pump load. This chapter discusses the type of DC motor and pump which will be used in the system and selecting the appropriate and efficient DC motor pump combination. The load characteristics will be analyzed and discussed with the PV module characteristics when directly connected without the MPPT.

3.1 Proposed Variable Step-Size Perturb and Observe algorithm with FLC

The proposed MPPT algorithm is based on the conventional P&O algorithm, but a fuzzy logic controller block is used to provide a variable step-size to overcome the limitation that exists in the implementations of the conventional P&O algorithm. The flow chart of the proposed modified P&O algorithm with variable step-size is illustrated in Fig. 3.1. The inputs to the fuzzy logic controller are the change in the PV module power ΔP_{PV} and the change in the PV module currentΔI_{PV} so that controller adjusts the step-size ΔS for the P&O algorithm according to the existing solar irradiation and temperature. As the FLC uses the measurement of the PV array voltage and current as input signals, it can share the same sensors with the P&O to reduce the controller implementation cost and complexity. The conventional P&O operates by periodically perturbing the PV output voltage V_{PV} and calculates the change in the PV output power $P_{PV}$by comparing the instantaneous power with that of the previous perturbation cycle. If the change in the power is positive, the perturbation will continue in the same direction in the next perturbation cycle, otherwise the perturbation will move to the opposite direction. By repeating this process, the operating point will gradually move towards the maximum power point. The perturbation variable chosen in the proposed algorithm is the duty-cycle, however; the step-size is not fixed and it is calculated by the adapted FLC block. The principle of the adopted FLC block is to adjust the value of the step-size according to the position of the operating point. The FLC sets the step-size to a large value when the operating point is far away from the MPP conversely, if the operating point is close to the MPP, the step-size value is adjusted to small value. This process continues until the MPP is reached, hence the FLC sets the step-size to zero value. Therefore, this ensures that a fast dynamic response and eliminates the oscillations around the MPP when a steady-state is reached.

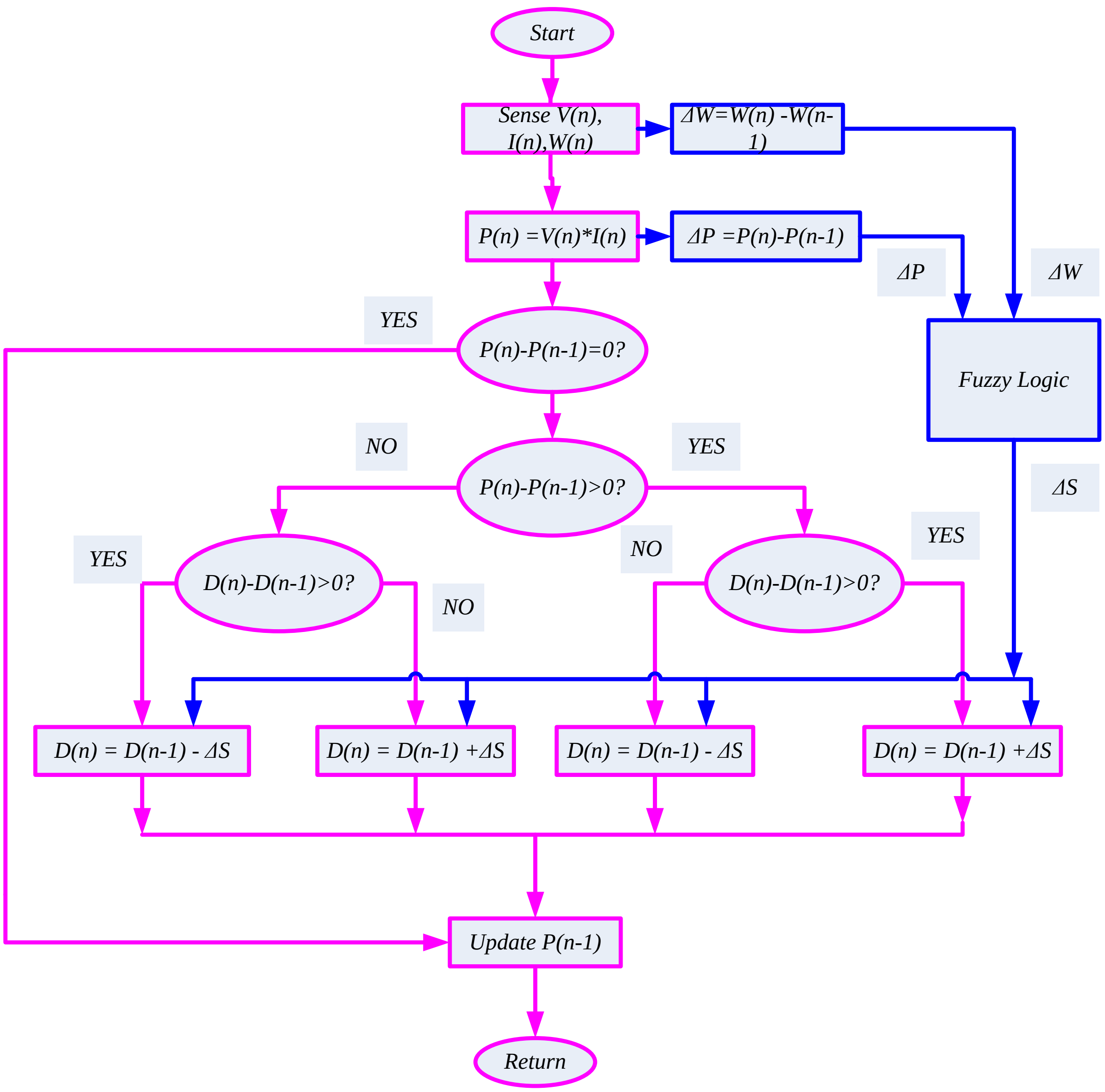

Fig. 3.1 Flow chart of the proposed Perturb & Observe algorithm with Fuzzy Logic Controller.

3.2 Fuzzy logic

Fuzzy logic is based on a mathematical model which deals with uncertainty and imprecise, ambiguous, noisy, or missing input information. It compares an analog input signal to a predetermined logic variable membership function or fuzzy sets that correspond to values in the range 0 and 1. Fuzzy logic is implemented in a control system to emulate human-like decisions in control. FL techniques have been widely used in a wide range of engineering applications due to their heuristic nature associated with simplicity and effectiveness for both linear and nonlinear systems [53]. It can be implemented in software, hardware or a combination of both. Fuzzy sets are considered as the brain of the fuzzy control system which in turn is responsible for converting analog input values into a scale of 0 to 1.

The concept of fuzzy logic was first known 40 years ago, since the fundamental theory was introduced by Zadeh in 1965 [50, 51]. However, the theory of FL was not applied to control system until ten years later, because of insufficient small computer capability before that time. In the early 70's, the theory began to produce results when it was applied in a practical application to control an automatic steam engine by Mamdani in 1974 [52]. In 1976, an industrial application to control cement kilns was developed in Denmark by Blue Circle Cement and SIRA and the system started working in 1982 [53]. Over the past few decades fuzzy logic controllers have been successfully applied to many industrial applications. Starting from 1980s it was implemented in applications such as industrial manufacturing, banks, automatic control, automobile protection, banks, and to control consumer products: washing machines, dish washers, televisions, air conditioners, rice cookers and video cameras [53].Some of the essential characteristics of FL are listed below [52]:

In fuzzy logic, exact reasoning is viewed as a limiting case of approximate reasoning.

- In fuzzy logic, everything is a matter of degree.
- In fuzzy logic, knowledge is interpreted a collection of elastic or, equivalently, fuzzy constraint on a collection of variables.
- Interface is viewed as a process of propagation of elastic constraints.
- Any logic system can be fuzzified.

There are two main characteristics of fuzzy systems that give them better performance for specific applications.

- Fuzzy systems are suitable for uncertain or approximate reasoning, especially for a system with a mathematical model that is difficult to derive.
- Fuzzy logic allows decision making with estimated values under incomplete or uncertain information.

3.3 Fuzzy Logic Controller Structure

The general structure of a fuzzy controller and its main parts is shown in Fig. 3.2. The fuzzy logic controller consists of four components: fuzzification interface, knowledge base, interface engine, and defuzzification interface [53].

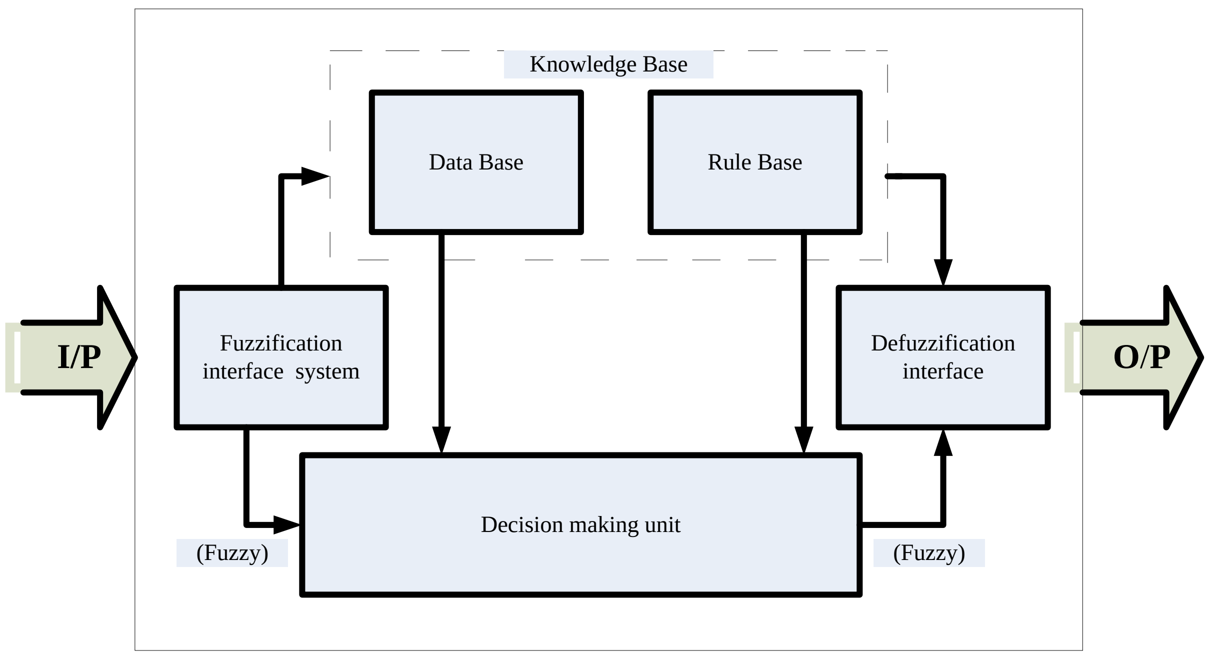

Fig. 3.2 General structure of fuzzy interface system.

The fuzzifier transforms crisp inputs into the fuzzy subsets to obtain degrees of memberships and represent them with linguistic variables, which in turn are used to activate rules. The fuzzy inference engine process those data to obtain the desired output. The defuzzifier converts those fuzzy outputs to crisp variables to complete the desired fuzzy logic control objectives.

Every fuzzy set can be represented by its membership function. In practice the membership functions can have a number of different shapes depending on the application. They can be triangular, trapezoidal, Gaussian, bell-shaped, sigmoidal or S-curve. Some popular waveforms of the membership functions are shown in Fig. 3.3 [52, 53].

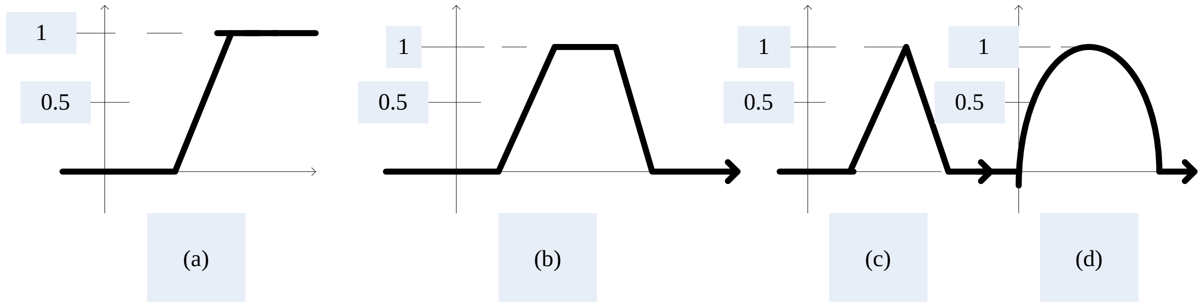

Fig. 3.3 Different graphs of membership functions (a) monotonic (b) trapezoidal (c) triangular (d) Gaussian.

Trapezoidal or triangular membership functions are usually used in systems that require significant dynamic variation in a short period of time. A Gaussian or S-curve membership function is always selected if the system requires very high control accuracy [53].

3.3.1 Knowledge base

The knowledge base is the heart of the fuzzy control system. It is the inference basis for fuzzy control. The knowledge base, defines all relevant language control rules and parameters. The derivation of fuzzy control rules can be performed in four modes. These four modes are not mutually exclusive, and it is necessary to combine them to obtain an effective system [51, 52].

- Expert experience and control engineering knowledge: the fuzzy control rule is based on information obtained from the controlled system.
- Operators' control actions: observation of human controller's actions in terms of input-output operating data.
- Based on the fuzzy model of process: linguistic description of the dynamic characteristics of a process.
- Based on learning: ability to modify control rules such as self-organizing controller such as neural network and genetic algorithm.

The number of base rules can be defined based on the number of membership in the fuzzy set and the inputs. For example if the system contains two inputs and each of them contains five memberships then the total base rules will be $5^2 = 25$ base rule. The higher the number of memberships, the better the system efficiency will be, but the system implementation will become more complex [53].

3.3.2 Fuzzy interface procedure

There are several techniques for performing the fuzzy interface process, such as, the Mamdani method, Takagi-Sugeno_Kang (TSK) method, Tsukamot method and Larsen method. The Mamdani and TSK methods are the most commonly used methods in fuzzy controllers [52, 53]. However, the Mamdani method is usually more popular for most control engineering applications because this method is computationally more efficient and has better interpolative properties than the other interface methods [52].

A. Mamdani method

The Mamdani method is the most widely used fuzzy interface strategy. Since it was proposed in 1975, by Professor Ebrahim Mamdani of London University who built one of the fuzzy systems to control a combination of steam engine and boiler. In Mamdani‘s method a set of fuzzy if-then rules was applied, and these were supplied by experienced human operators [51].

Mamdani fuzzy logic uses the linguistic variables to describe the process states and uses these variables as inputs to control rules. The terms of the linguistic variables are fuzzy sets with certain shape. Mamdani fuzzy logic usually uses the trapezoidal or triangular fuzzy set but other shapes are possible. The fuzzy interface process of the Mamdani method can be formed in four steps [51]:

- Fuzzification
- Rule evaluation
- Aggregation of the rule outputs
- Defuzzification

Step 1: Fuzzification

Fuzzification is the first step in fuzzy logic processing, in which the crisp quantities are converted to fuzzy inputs. The transformation process of fuzzy values is represented by the membership function [51,52].

There might be some error, when measuring the voltage, current, temperature, solar insolation, etc., in most real applications. This will result in vague data. Therefore, the vagueness can be represented by the membership functions.

Step 2: Rule evaluation

In this step the fuzzified inputs are applied to the antecedents of the fuzzy rule, then applying the fuzzy operator to fuzzy rule that has multiple antecedents to resolve the antecedents to a single number between 0 and 1. The fuzzy operator (AND or OR) is used to obtain this signal number. If the OR fuzzy operation is used, thus the classical fuzzy operation union is used [51]:

$$\mu A \cup B(x) = max[\mu A(x), \mu B(x)] \tag{3.1}$$

Similarly, in order to evaluate the conjunction of the rule antecedents, the AND fuzzy operation intersection is applied as in equation (3.2).

$$\mu A \cap B(x) = min[\mu A(x), \mu B(x)] \tag{3.2}$$

The most common method of correlating the rule consequent with the truth value of the rule antecedent is the clipping method. In this method, the consequent membership function is being cut at the level of the antecedent truth. Since the top of the membership function is sliced, the clipped fuzzy set loses some information. However, clipping method is widely used because it involves less complex and faster mathematics, generates an aggregated output surface that is easier to defuzzify [51, 52].

There is another method which generally loses less information by providing a better approach for preserving the original shape of the fuzzy set, which is called scaling. In this method, the original membership function of the rule consequent is adjusted by multiplying all its membership degrees by the truth value of the rule antecedent [53].

Step 3: Aggregation of the rule outputs

After finding the output of each rule, the aggregation process is applied to unify all the rules outputs to become one output. The input to the aggregation process is the combination of truncated or scaled consequent membership function, and the output is the combined output fuzzy set [53].

Step 4: Defuzzification

The defuzzification is the last step in the process of the fuzzy inference, and its reverse of the fuzzification process. The output of the fuzzy inference process result from the combination of the control inputs and it is still linguistic variable. However, the final output of the fuzzy control has to be a crisp number. Hence the defuzzification process is needed to convert the fuzzy output back to the crisp output to be available for real application controllers [53].

There are several defuzzification techniques which are used, but there is one systemic procedure for selecting a good defuzzification strategy. Selection of the defuzzification technique relies on the system or the application characteristics [52].

The following three defuzzification techniques are the most commonly used techniques:

- **Mean of maximum method (MOM)**

The MOM defuzzification strategy computes the average value of all the control actions whose membership functions reach the maximum. In the case of a discrete universe, the control action can be expressed by the following Equation (3.3) [53].

$$MOM = \sum_{i=1}^{l} \frac{w_j}{l} \tag{3.3}$$

In Equation (3.3), w_j is the support value when the membership function reaches the maximum value $\mu z(wj)$, and l is the number of support values.

- **Height method (HM)**

The HM defuzzification method can only be applied when the output membership function is an aggregated union result of symmetrical functions [53]. In the HM method, the first step involves evaluating the centroid of each output membership function for each rule and then the final output is calculated as the average of individual centroids weighted by their heights (degree of membership) as in the Equation (3.4) [51].

$$Z = \frac{\sum_{j=1}^{n} w_j \cdot \mu(w_j)}{\sum_{j=1}^{n} \mu(w_j)} \tag{3.4}$$

- **Centre of gravity method (COG)**

The Centre of gravity method is the most widely used defuzzification technique in real applications. The advantage of COG method is the defuzzified values tend to move smoothly around the output fuzzy region [51]. The COG technique is a basic general defuzzification technique that computes the value of the abscissa of the Centre of gravity of the area below the membership. The output of COG can be represented by Equation (3.5) [51, 53].

$$COG = \frac{\sum_{j=1}^{n} w_j \cdot \mu(w_j)}{\sum_{j=1}^{n} \mu(w_j)} \tag{3.5}$$

Where n is the number of quantization levels of the output. According to Fig. 3.4, the COG is calculated as a follows:

$$COG = \frac{(0+10+20)*0.1+(30+40+50+60)*0.2+(70+80+90+100)*0.5}{0.1+0.1+0.1+0.2+0.2+0.2+0.2+0.5+0.5+0.5+0.5} = 67.4$$

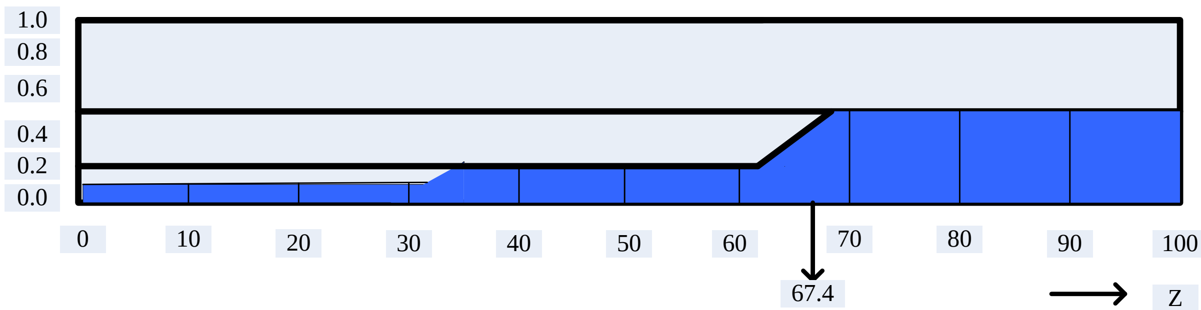

Fig. 3.4 Defuzzification example.

3.4 P&O algorithm with FLC based MPPT of PV water pumping system

This section presents the proposed controller for MPPT of the PV supplied DC water pump. The variation of solar radiation is the most important factor in the MPPT of PV system. It is changing periodically and nonlinearly, hence an FLC based MPPT is proposed to solve the problem and to deliver the maximum available power of the PV module to the load. A schematic of the photovoltaic module and water pumping system used to investigate the fuzzy logic controller performance is shown in Fig.3.5. The system comprises a PV module, buck converter, fuzzy based MPPT control unit and DC permanent magnet motor coupled to a centrifugal pump. The power produced by the PV module is supplied to the DC motor through a buck converter. The changes in output power of the PV module, ΔP_{PV}, and the change in rotation speed of the pump, $\Delta\omega_m$, are used as input variables of the fuzzy control unit to determine the duty-ratio, *D*, control signal for the buck converter.

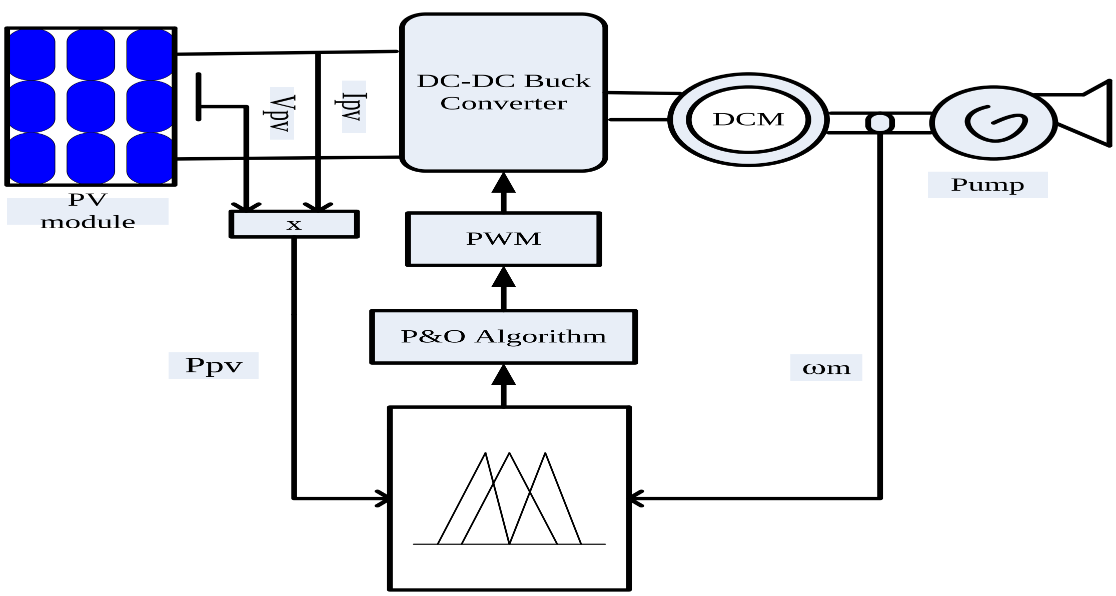

Fig. 3.5 Schematic diagram of the proposed MPPT water pumping system.

3.4.1 Fuzzy logic controller

The control objective is to track the maximum power point and maintain the system operating on this point at all levels of temperature and solar irradiation, which will lead consequently to maximizing the dc motor speed and the water discharge rate of the coupled centrifugal pump. At the time when output power of the PV module is maximum, the hydraulic power, $P_P = K_T$ $\omega_m 3$, is maximum. Consequently, the rotational speed ω_m, is a maximum at the maximum power point. By making use of the relation between the PV module output power and the rotational speed, a fuzzy logic controller has been proposed to adjust the buck converter duty ratio which adapts online the PV module output power to maximize the rotational speed, which in turn increases the water discharge of the centrifugal water pump.

In the fuzzification stage, numerical input variables are calculated or converted into linguistic variables based on subsets called membership function [49, 53]. The proposed FLC MPPT method has two input variables and one output variable as shown in Fig.3.6. The input variables are the PV module output power variation ΔP_{PV} (k) and rotation speed variation $\Delta\omega_m$ (k) at sampling instant k. The output variable is the duty ratio D of the buck converter. The input variables ΔP_{PV} (k) and $\Delta\omega_m$ (k) are expressed by Equation (3.6) and Equation (3.7) respectively.

$$\Delta P_{PV} (k) = G_P (P_{PV} (k) - P_{PV} (k-1)) \quad (3.6)$$

$$\Delta\omega_m (k) = G\omega (\omega_m (k) - \omega_m (k-1)) \quad (3.7)$$

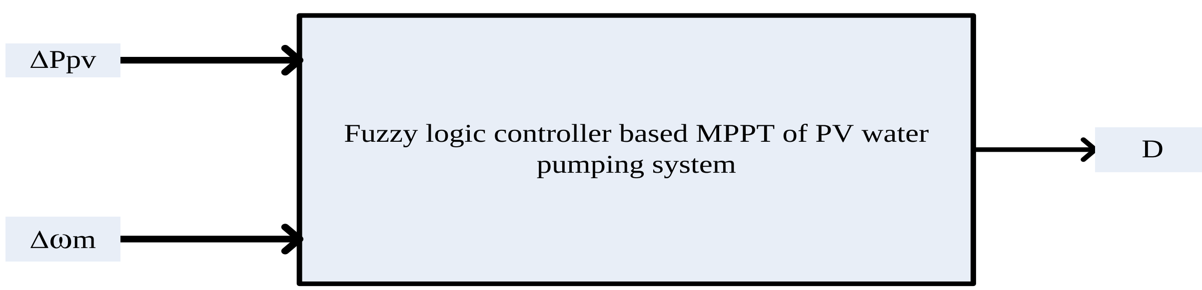

Fig. 3.6 General diagram of the proposed FLC of water pumping MPPT.

In (3.6) and (3.7), G_P and $G_\omega$are scaling factors used to normalize the ΔP_{PV} (k) and $\Delta\omega_m$ (k), respectively. The scaling factors play an important role in optimizing performance and can be chosen using trial and error. The membership functions of the both inputs and output variables are represented by symmetric triangular functions and defined in common normalized range of (-1, 1). The membership functions of the input variables ΔP_{PV} and $\Delta\omega_m$ which are assigned for fuzzy sets have the same shape and range, and they are shown in Fig. 3.7. The membership function of the output variable also has the same number of sets as the input variables, and is shown in Fig. 3.7. The membership function of both inputs and output variables are assigned five sets, including positive big (PB), positive small (PS), zero (ZO), negative big (NB), and negative small (NS).

Fuzzy rules comprise a set of rules in linguistic form which associate the fuzzy inputs with the fuzzy output. These are based on an expert knowledge and understanding of the system behavior that is required to achieve the control objectives. The fuzzy control rules have been set up using a set of IF-THEN statements that contain all information for the controlled parameters. The fuzzy control rule includes 25 rules as described in Table 3.1. These rules are used for the control of the buck converter such that the maximum power is achieved at the output of the PV module. The fuzzy rules are designed to incorporate the following considerations keeping in view the overall tracking performance.

1. If a positive variation in the rotation speed is accompanied with a positive variation of PV module output power, then the chopper duty ratio should be increased. Otherwise if the variation of PV module output power is negative, then chopper ratio should be decreased.
2. If the rotation speed variation is zero or sufficiently close to zero which means that its maximum is reached, then there should be no change in the chopper ratio.
3. If a negative variation in the rotation speed is accompanied with a positive variation in PV module output power, then the chopper duty ratio should be decreased. Otherwise if the variation of PV module output power is positive, then chopper ratio should be increased.

In the defuzzification stage and inference mechanism the output of fuzzy logic control is converted from linguistic variables to numerical variables. The inference mechanism determines the matching degree of the current fuzzy input with respect to each rule and the controller has to resolve the conflict between different rules being obeyed at the same time and decides which rules are to be obeyed according to the input field. Then the obeyed rules are combined to form the control actions. There are different methods of defuzzifying an outcome fuzzy set. The method used for this is called Centre of Gravity (COG) or centroid. The idea of

(COG) is to find the variable value of the center of gravity of the composite membership function for the fuzzy value [49].

The crisp value of the output variable ΔD (k) is computed by Equation (3.8).

$$D(k)=D(k-1)+G_D\Delta D(k) \quad (3.8)$$

Where G_D is the output scaling factor of the fuzzy logic controller and $D(k)$ is the final output signal sent to the system.

Table 3.1: Rule table

If $\Delta\omega_m > 0$ If $\Delta P > 0$ $D(K) = D(K-1) + \Delta D$ else $D(K) = D(K-1) - \Delta D$ end	If $\Delta\omega_m$ is PB and ΔP is PB then ΔD is PB
	If $\Delta\omega_m$is PB and ΔP is PS then ΔD is PB
	If $\Delta\omega_m$ is PB and ΔP is NB then ΔD is NB
	If $\Delta\omega_m$ is PB and ΔP is NS then ΔD is NB
	If $\Delta\omega_m$ is PB and ΔP is ZO then ΔD is NS
	If $\Delta\omega_m$ is PS and ΔP is PB then ΔD is PS
	If $\Delta\omega_m$ is PS and ΔP is PS then ΔD is PS
	If $\Delta\omega_m$ is PS and ΔP is NB then ΔD is NS
	If $\Delta\omega_m$ is PS and ΔP is NS then ΔD is NS
	If $\Delta\omega_m$ is PS and ΔP is ZO then ΔD is NS
If $\Delta\omega_m = 0$ $D(K) = D(K-1)$	If $\Delta\omega_m$ is ZO and ΔP is PB then ΔD isPB
	If $\Delta\omega_m$ is ZO and ΔP is PS then ΔD is PB
	If $\Delta\omega_m$ is ZO and ΔP is ZO then ΔD is ZO
	If $\Delta\omega_m$ is ZO and ΔP is NB then ΔD is NB
	If $\Delta\omega_m$ is ZO and ΔP is NS then ΔD is NB
If $\Delta\omega_m < 0$ If $\Delta P > 0$ $D(K) = D(K-1)$- ΔD else $D(K)$= $D(K-1)$+ ΔD end	If $\Delta\omega_m$ is NB and ΔP is PB then ΔD isNB
	If $\Delta\omega_m$ is NB and ΔP is PS then ΔD is NB
	If $\Delta\omega_m$ is NB and ΔP is NB then ΔD is PB
	If $\Delta\omega_m$ is NB and ΔP is NS then ΔD is PB
	If $\Delta\omega_m$ is NB and ΔP is ZO then ΔD is PS
	If $\Delta\omega_m$s NS and ΔP is PB then ΔD is NS
	If $\Delta\omega_m$ is NS and ΔP is PS then ΔD is NS
	If $\Delta\omega_m$ is NS and ΔP is NB then ΔD is PS
	If $\Delta\omega_m$ is NS and ΔP is NS then ΔD is PS
	If $\Delta\omega_m$is NS and ΔP is ZO then ΔD is PS

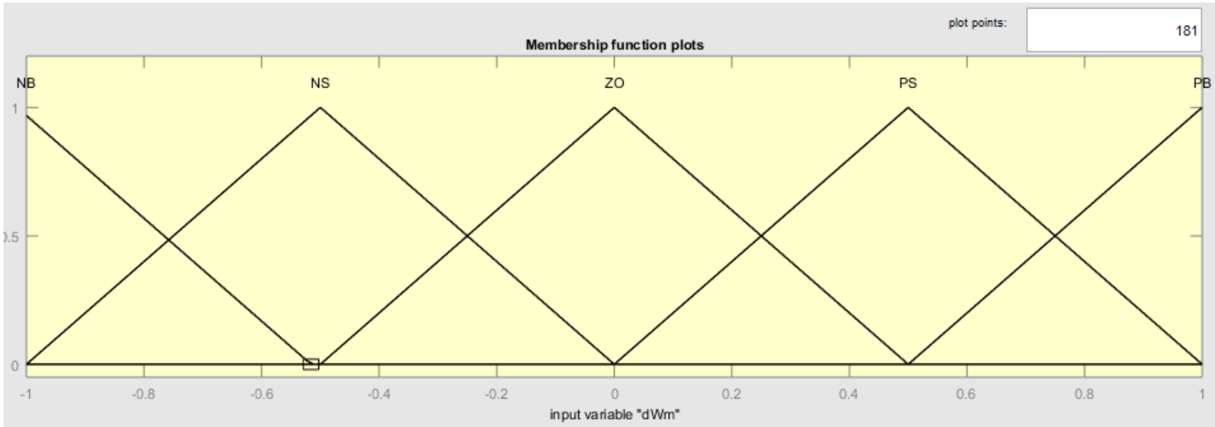

Fig. 3.7 Membership functions of the 1st input variable (δP_{PV}), 2nd input variable ($\delta\omega_m$) and the output variable (δd).

3.5 Photovoltaic cell simplified model

The basic solar cell is usually represented by a p-n junction diode connected in parallel with current source. This conventional equivalent circuit as illustrated in Fig.3.8 [17]. The basic model does not provide a high range of accuracy but it shows the basic behavior of the solar cell.

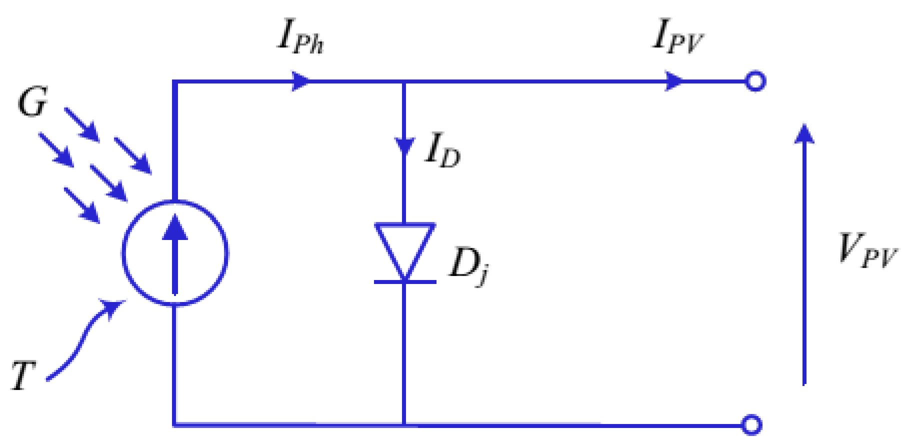

Fig. 3.8. Simple model of photovoltaic cell.

The current source represents the photocurrent produced by sunlight and the diode determines the current-voltage characteristic of the cell. The current-voltage characteristic function can be gained by applying Kirchhoff's current law in the Fig 3.8 gives the following equation.

$$I_{PV} = I_{Ph} - I_D \tag{3.9}$$

Where: I_{Ph} is the photon generated current, and I_D is the current shunted through the intrinsic diode.

In the circuit shown in Fig.3.8 above, D_j is the ideal p-n diode, I_D the diode internal diffusion current and I_{Ph} the photocurrent, or light generated current, which is proportional to the radiation and surface temperature. The output current and voltage of the solar cell is represented by I and V, respectively. The diode internal diffusion current is modeled by the Shockley's diode Equation (3.10) given below.

$$I_D = I_0(e^{qV_D/KT} - 1) \tag{3.10}$$

Where: I_o is the reverse saturation current of diode (A),

q is the electron charge (1.602×10^{-19} C),

V_D is the voltage across the diode (V),

K is the Boltzmann's constant (1.381×10^{-23} J/K),

T is the junction temperature in Kelvin (K).

Replacing I_D of the equation (3.9) by the equation (3.10) gives the current-voltage relationship of the PV cell.

$$I = I_{Ph} - I_0(e^{qV/KT} - 1) \tag{3.11}$$

Where: V is the voltage across the PV cell, and I is the output current from the cell. The reverse saturation current of diode (I_o) is constant under the constant temperature and found by setting the open-circuit condition as shown in Fig.3.8. Using the equation (3.11), let $I = 0$ (no output current) and solve for I_o.

$$0 = I_{Ph} - I_o(e^{qV_{oc}/KT} - 1) \tag{3.12}$$

$$I_{Ph} = I_o\left(e^{qV_{oc}/KT} - 1\right) \tag{3.13}$$

$$I_o = \frac{I_{Ph}}{(e^{qV_{oc}/KT} - 1)} \tag{3.14}$$

To a very good approximation, the photon generated current I_{Ph}, which is equal to I_{sc} is directly proportional to the irradiance, the intensity of illumination, to PV cell [2]. Thus, if the value $I_{Ph} = I_{sc}$ is known from the datasheet, under the standard test condition, Go=1000W/m^2 at the air mass (AM) = 1.5, then the photon generated current at any other irradiance, G (W/m^2), is given by:

$$I_{Ph}I_G = \left(\frac{G}{Go}\right) I_{Ph}I_{Go} \tag{3.15}$$

3.6 Photovoltaic cell the More Accurate Model

There are a few things that have not been considered in the simple model and that will affect the performance of a PV cell in practice.

i) Series Resistance: In a practical PV cell, there is a series of resistance in a current path through the semiconductor material, the metal grid, contacts, and current collecting bus [2]. These resistive losses are lumped together as a series resister (R_s). Its effect becomes very conspicuous in a PV module that consists of many series-connected cells, and the value of resistance is multiplied by the number of cells.

ii) Parallel Resistance: This is also called shunt resistance. It is a loss associated with a small leakage of current through a resistive path in parallel with the intrinsic device [1]. This can be represented by a parallel resister (R_p). Its effect is much less conspicuous in a PV module compared to the series resistance, and it will only become noticeable when a number of PV modules are connected in parallel for a larger system.

iii) Recombination: Recombination in the depletion region of PV cells provides non-ohmic current paths in parallel with the intrinsic PV cell [2, 34]. As shown in Figure 3.9, this can be represented by the second diode (d_2) in the equivalent circuit.

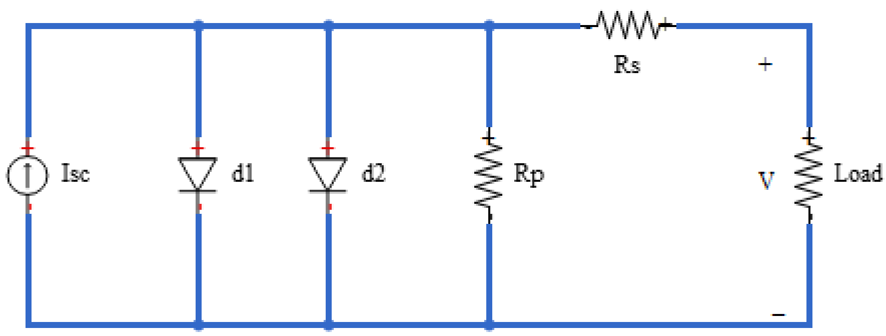

Fig. 3.9: More accurate equivalent circuit of PV cell

Summarizing these effects, the current-voltage relationship of PV cell is written as:

$$I= I_{Ph} - I_{o1}[e^{\frac{q(V+IR)}{KT}} - 1] - I_{o2}\left[e^{\frac{q(V+IR)}{2KT}} - 1\right] - \left(\frac{V+IRs}{Rp}\right) \quad (3.16)$$

It is possible to combine the first diode (d_1) and the second diode (d_2) and rewrite the equation (3.16) in the following form.

$$I=I_{Ph} - I_o\left[e^{\frac{q(V+IRs)}{nKT}} - 1\right] - \left(\frac{V+IRs}{Rp}\right) \quad (3.17)$$

Where: n is known as the “ideality factor” (“n” is sometimes denoted as “A”) and takes the value between one and two [28].

3.7 Photovoltaic Module

A single cell produces an output voltage less than 1V, about 0.6V for crystalline silicon (Si) cells, thus a number of PV cells are connected in series to achieve a desired output voltage. When series-connected cells are placed in a frame, it is called as a module. Most of commercially available PV modules with crystalline-Si cells have either 36 or 72series-connected cells. Furthermore, the advent of high efficiency DC-DC converters has alleviated the need for modules with specific voltages. When the PV cells are wired together in series, the current output is the same as the single cell, but the voltage output is the sum of each cell voltage. Also, multiple modules can be wired together in series or parallel to deliver the voltage and current level needed. The group of modules is called an array.

3.7.1 Modeling of a PV module by using appropriate model

The strategy of modeling a PV module is no different from modeling a PV cell. It uses the same PV cell model. The parameters are all same, but only a voltage parameter (such as the open-circuit voltage) is different and must be divided by the number of cells. The electric model with moderate complexity, shown in Figure 3.8, provides fairly accurate results. The model consists of a current source (I_{SC}), an ideal diode (D_j), and a series resistance (R_S). The small variation in R_s has a significant effect on the output power of the PV panel. On the other hand, the PV efficiency is insensitive to the variation in R_{sh}, which can be assumed to approach infinity without leakage current. Therefore, the R_{sh} can be neglected to give the appropriate model with suitable complexity. Neglecting the shunt resistance, the model of PV module consists of a current source (I_{sc}), an ideal diode (D_j), and a series resistance (R_s) and it becomes an appropriate model with suitable accuracy as shown in Fig 3.10. To make a better model, it also includes temperature effects on the short-circuit current (I_{SC}) and the reverse saturation current of diode (I_O). It uses a single diode with the diode ideality factor (n).

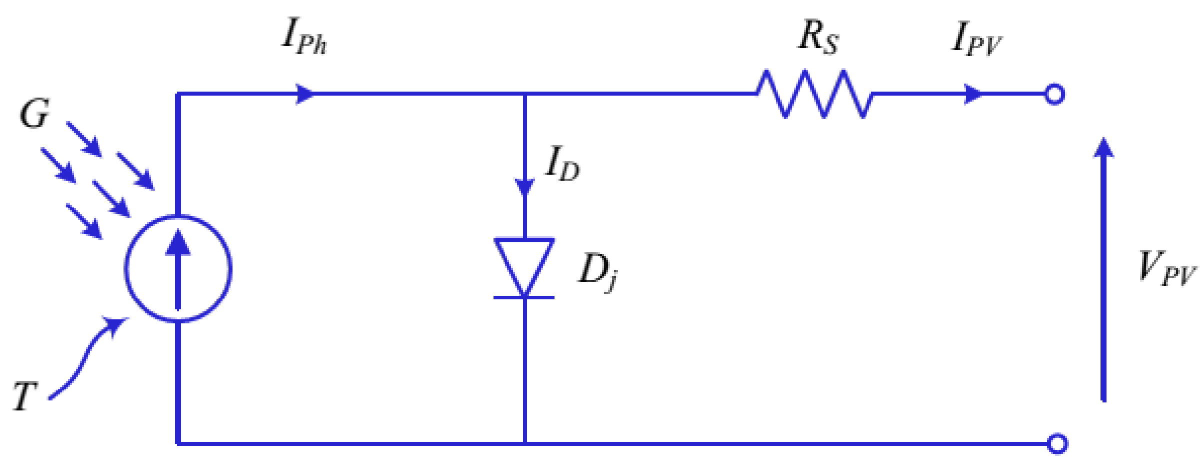

Fig. 3.10 Appropriate equivalent circuit model.

To make a better model, it also includes temperature effects on the short-circuit current (I_{sc}) and the reverse saturation current of diode (I_o). It uses a single diode with the diode ideality factor (n) set to achieve the best I-V curve match. Since it does not include the effect of parallel resistance (R_p), letting $R_p = \infty$ in the equation (3.17) gives the equation (3.18) [39] that describes the current-voltage relationship of the PV cell, and it is shown below.

$$I = I_{Ph} - I_o \left[e^{\frac{q(V+IR_S)}{nKT}} - 1 \right] \tag{3.18}$$

Where: I is the cell current (the same as the module current),

V is the cell voltage = {module voltage} ÷ {Number of cells in series},

T is the cell temperature in Kelvin (K).

First, the photon current ($I_{Ph} = I_{sc}$) at a given cell temperature (T) is calculated as:

$$I_{Ph} = I_{Ph}\left[1 + a(T - T_{ref})\right] \tag{3.19}$$

where: I_{Ph} at T_{ref} is given in the datasheet (measured under irradiance of (1000 W/m^2), T_{ref} is the reference temperature of PV cell in Kelvin (K), usually 298K (25 °C), a is the temperature coefficient of I_{Ph} in percent change per degree temperature also given in the datasheet. The photon current ($I_{Ph} = I_{sc}$) is proportional to the intensity of irradiance, thus I_{Ph} at a given irradiance (G) is:

$$I_{Ph} = \left[\frac{G}{G_o}\right] \tag{3.20}$$

Where: G_o is the nominal value of irradiance, which is normally 1KW/m^2.

The reverse saturation current of diode (I_o) at the reference temperature (T_{ref}) is given by the equation (3.14) with the diode ideality factor added:

$$I_o = \frac{I_{Ph}}{(e^{qV_{oc}/KT} - 1)} \tag{3.21}$$

The reverse saturation current (I_o) is temperature dependent and the I_o at a given temperature (T) is calculated by the following equation (3.22) [50].

$$I_o I_T = I_o I_{T_{ref}} \left(\frac{T}{T_{ref}}\right)^{3/n} e^{\frac{-qE_g}{nk}\left(\frac{1}{T} - \frac{1}{T_{ref}}\right)} \tag{3.22}$$

The diode ideality factor (n) is unknown and must be estimated. It takes a value between one and two; the value of n=1 (for the ideal diode) is, however, used until the more accurate value is estimated later by curve fitting [35].

The series resistance (R_s) of the PV module has a large impact on the slope of the I-V curve near the open-circuit voltage (V_{oc}), hence the value of R_s is calculated by evaluating the slope dV/dI of the I-V curve at the V_{oc} [19]. The equation for R_s is derived by differentiating the equation (3.10) and then rearranging it in terms of R_s.

$$I = I_{Ph} - I_o \left[e^{\frac{q(V+IRs)}{nKT}} - 1\right] \tag{3.23}$$

$$dI = 0 - I_o \text{q} \left(\frac{dV + R_s dI}{nKT}\right) e^{q\left(\frac{V+IR_s}{nKT}\right)} \tag{3.24}$$

$$R_s = -\frac{dI}{dV} - \frac{nKT/q}{I_o\, e^{q\left(\frac{V+IR_s}{nKT}\right)}} \tag{3.25}$$

Then, evaluating the equation (3.25) at the open circuit voltage that is V=V_{oc} (also let I=0)

$$R_s = -\left.\frac{dV}{dI}\right|_{v_{oc}} - \frac{nKT/q}{I_o \cdot e^{\frac{qV_{oc}}{nKT}}} \tag{3.26}$$

where: $\left.\frac{dV}{dI}\right|_{v_{oc}}$ is the slope of the I-V curve at the V_{oc}use the I-V curve in the datasheet then divide it by the number of cells in series), V_{oc} is the open-circuit voltage of cell (found by dividing V_{oc} in the datasheet by the number of cells in series).

The calculation using the slope measurement of the I-V curve published on the SANYO HIT180 datasheet gives a value of the series resistance per cell, R_s= 5.1mΩ.

It is possible to solve the equation of I-V characteristics. It is however, complex because the solution of current is recursive by inclusion of a series resistance in the model. Although it may be possible to find the answer by simple iterations, the Newton's method is chosen for rapid convergence of the answer [12]. The Newton's method is described as:

$$f(x) = X_n - \frac{f(x)}{f'(X_n)} \tag{3.27}$$

Where: $f'(x)$ is the derivative of the function, $f(x)$= 0, X_n is a present value, $X_{n+1}$is a next value. Rewriting the equation (3.18) gives the following function:

$$f(I) = I_{Ph} - I - I_o\left[e^{\frac{q(V+IRs)}{nKT}} - 1\right] = 0 \tag{3.28}$$

Inserting equation (3.28) into the equation (3.27) gives a following recursive equation, and the output current (I) is computed iteratively.

$$I_{n+1} = I_n - \frac{I_{Ph} - I_n - I_o\left[e^{q\left(\frac{V+I_nR_S}{nKT}\right)} - 1\right]}{-1 - I_o\left(\frac{qR_S}{nKT}\right)e^{q\left(\frac{V+I_nR_S}{nKT}\right)}} \tag{3.29}$$

Figure3.11 shows the plots of I-V characteristics at various module temperatures simulated with the MATLAB model for SANYO HIT180 module. Data points superimposed on the plots are taken from the I-V curves published on the manufacturer's datasheet [1]. After some trials with various diode ideality factors, the MATLAB model chooses the value of *n* = 1.62 that attains the best match with the *I-V* curve on the datasheet. The figure shows good correspondence between the data points and the simulated I-V curves. As the temperature increases with a fixed irradiation level it results in a slight increase in the short circuit current, I_{SC}, because the band gap energy decreases and more photons have enough energy to create electron-hole pairs. On the other hand, the increase of temperature has an obvious reduction in the PV panel output power due to the drop in the open circuit voltage V_{OC} [42].

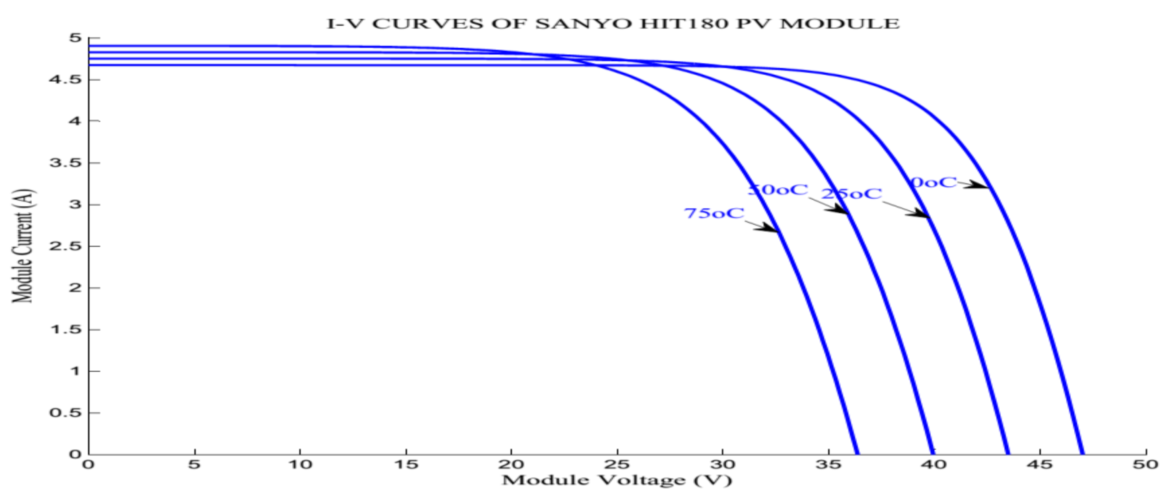

Figure 3.11: I-V curves of SANYO HIT180 PV module at various temperatures simulated with the MATLAB model (1kw/m^2, 25 ℃).

3.8 DC-DC converters

The main part of MPPT hardware is a switch-mode DC-DC converter. It is widely used in DC power supplies and DC motor drives for the purpose of converting unregulated DC input into a controlled DC output at a desired voltage level [17]. The same converter is used for a MPPT to provide load matching for the maximum power transfer by regulating the input voltage at the PV module MPP by controlling the duty ratio (*D*).

3.9 Topologies of DC-DC converters

There are a number of different topologies for DC-DC converters. They are categorized into isolated or non-isolated topologies. The isolated topologies use a small-sized high-frequency electrical isolation transformer which provides the benefits of DC isolation between input and output, and step up or down of output voltage by changing the transformer turns ratio. They are very often used in switch-mode DC power supplies [18]. Popular topologies for a majority of the applications are fly back, half-bridge, and full-bridge [22]. In PV applications, the grid-tied systems often use these types of topologies when electrical isolation is preferred for safety reasons. Non-isolated topologies do not have isolation transformers. They are almost always used in DC motor drives [17]. These topologies are further categorized into three types: step down (buck), step up (boost), and step up & down (buck-boost). The buck topology is used for voltage step-down. In PV applications, the buck type converter is usually used for charging batteries and in LCB for water pumping systems. The boost topology is used for stepping up the voltage. The grid-tied systems use a boost type converter to step up the output voltage to the utility level before the inverter stage. Then, there are topologies able to step up and down the voltage such as: buck-boost, Ćuk, and SEPIC (stands for Single Ended Primary Inductor Converter). For PV system with batteries, the MPP of commercial PV module is set above the charging voltage of batteries for most combinations of irradiance and temperature. A buck converter can operate at the MPP under most conditions, but it cannot do so when the MPP goes below the battery charging voltage under a low-irradiance and high-temperature condition. Thus, the additional boost capability can slightly increase the overall efficiency [27].

3.9.1 Buck converter

In this type of DC-DC converter, the average output voltage V_o produced is always lower than the DC input voltage. The buck converter is used for voltage step-down in PV applications, such as for charging batteries and in water pumping systems. The basic circuit of the step-down converter as illustrated in Fig. 3.12 [45]. The diode (*d*) is used to enhance the output filtering effect and prevent the switch from absorbing or dissipating the inductive energy because this would lead to overheating the switch. In addition to that, there is an inductor and capacitor at the output of the converter which forms a low-pass filter to attenuate the output voltage fluctuation.

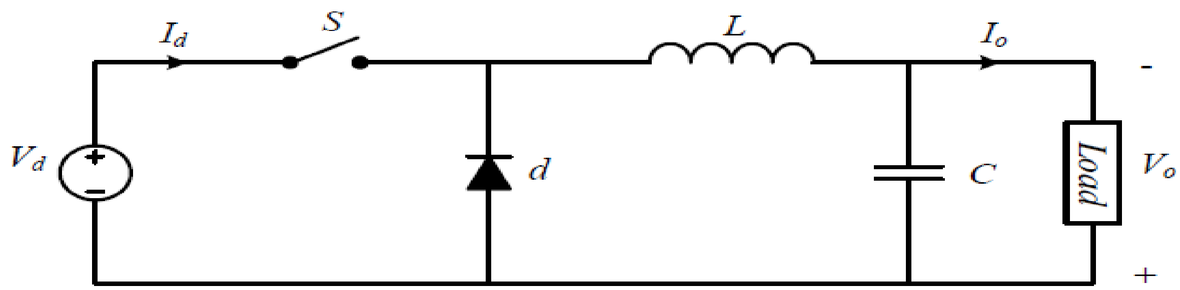

Fig. 3.12 Step-down buck converter.

Fig. 3.15 illustrates the wave forms of the inductor current (i_L) and voltage (v_L) of the step-down converter operating in a continuous conduction mode.

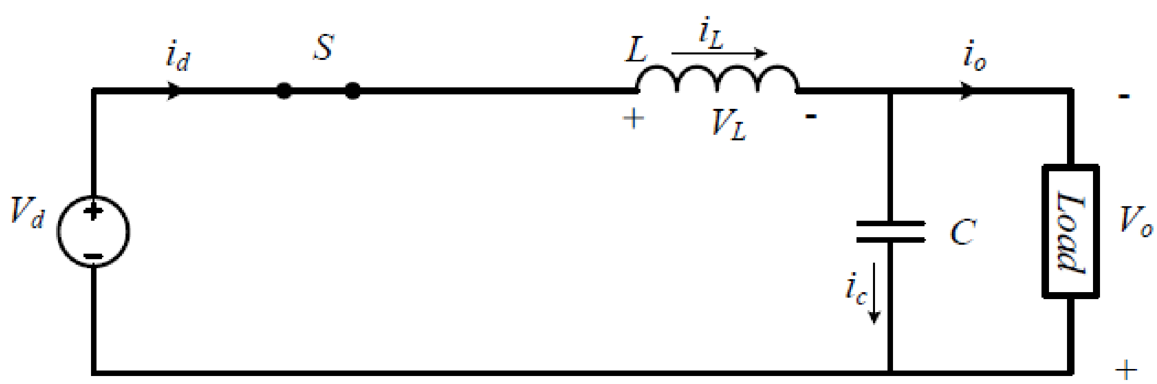

Fig. 3.13 Step-down buck converter switch closed.

At the time duration when the switch *S* is on as shown in Fig. 3.13, the diode *d* becomes reverse biased and the input voltage V_d appears across the inductor leading to linear increase in the inductor currenti_L. In addition, the capacitor *C* is charged in the same cycle [44].

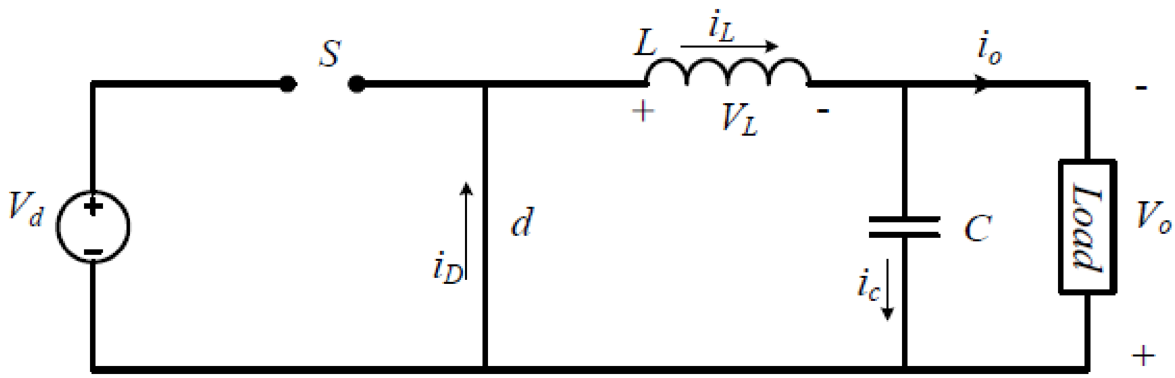

Fig. 3.14 Step-down buck converter switch open.

When the switch *S* is turned off as shown in Fig. 3.14, the diode *d* becomes forward biased and the voltage across the inductor is reversed $V_L = -V_o$. Therefore, current in the inductor freewheel through the diode and starts decreasing linearly. In this cycle the capacitor is charged by the inductor energy.

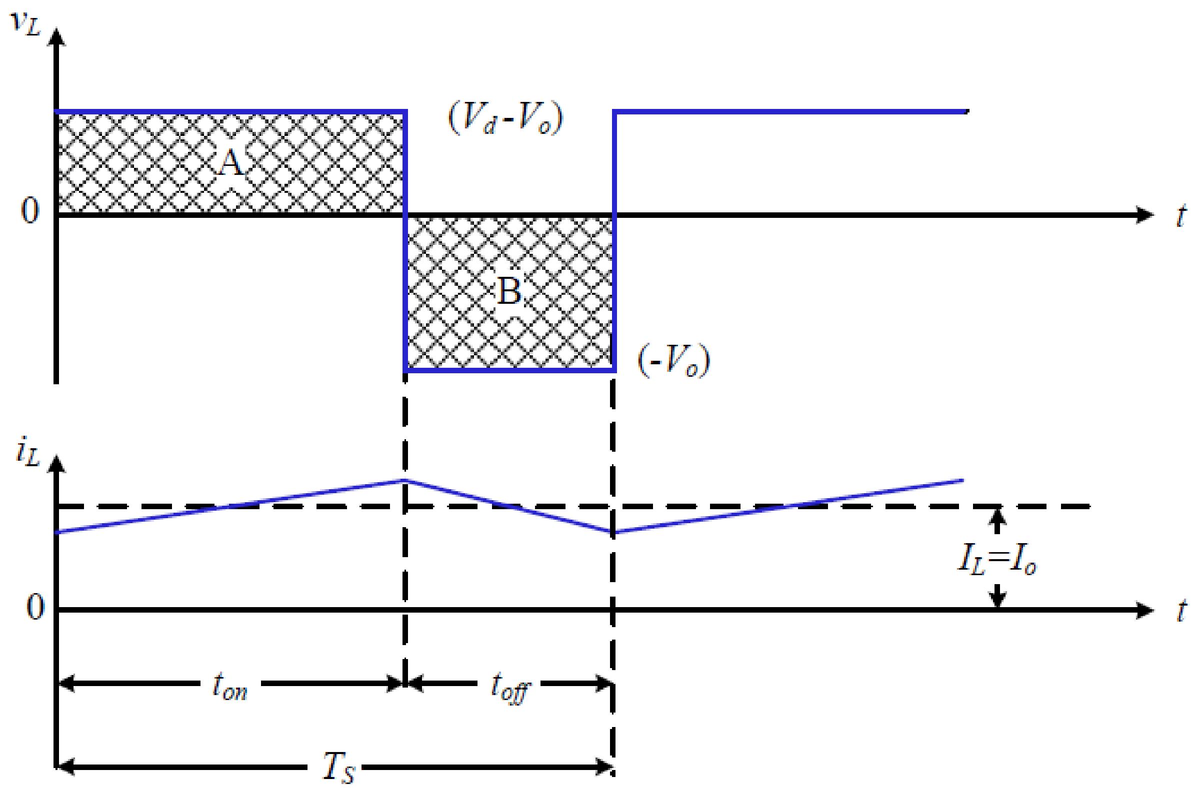

Fig. 3.15 Step-down converter wave form of the inductor current and voltage in continuous current mode.

The waveform must repeat from one time period to the next during steady-state operation. The relation between the input and output voltage, input and output current and the duty ratio D can be defined by Equation (3.30) and (3.31) [44].

$$\frac{V_o}{V_d} = \frac{t_{on}}{T_s} = D \tag{3.30}$$

$$\frac{I_{oc}}{I_d} = \frac{1}{D} \tag{3.31}$$

$$L = \frac{V_S(1-D)}{2\Delta I_S f_S} \tag{3.32}$$

$$C = \frac{\Delta I_o}{8\Delta V_o f_s} \tag{3.33}$$

In Equations (3.30) and (3.31) T_S is the switching period, or time period of square pulse that controls the electronics switch *S*, t_{on} is the on time of controlling square-wave, I_{oc} is the converter output current, I_d is the converter input current.

3.9.2 Boost converter

Example applications of boost converter operation are the regenerative braking circuit of DC motors and in regulated DC power supplies. In this type of converter the output voltage is always greater than the input voltage. Therefore the step up converter can be applied to MPPT systems where the output voltage needs to be greater than the input voltage. Such as in a grid-connected system where the boost converter maintains a high output voltage even if the PV module voltage falls to low values. The circuit topology of the step-up converter as illustrated in Fig. 3.16 [44].

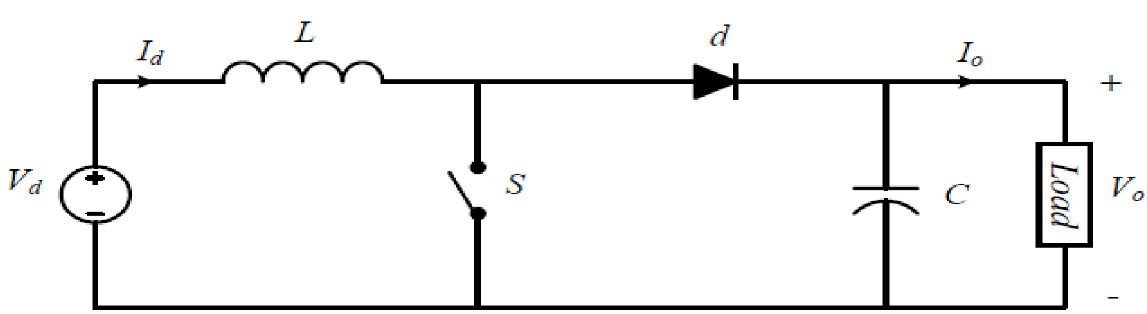

Fig. 3.16 Step-up boost converter.

When the switch *S* is on the diode *d* is reverse based. Consequently, the current in the inductor *L* rises linearly due to the input voltage source, and in this case the output stage is isolated and the capacitor *C* is partially discharged supplying the current load. When the switch is off during the second interval the diode is conducting, and during this time the output stage receives energy from both the inductor and the input source. When the converter is operating at steady-state condition, the duty ratio, *D*, can be expressed by Equation (3.34) [44].

$$D = 1 - \frac{V_d}{V_o} \tag{3.34}$$

Where *D* denotes the duty ratio, V_d and V_o denotes the input and the output voltages of the converter, respectively. From the above equation it can be seen that, the increase in the duty ratio *D* will increase the value of the output voltage, V_o. In addition the change in the duty ratio results in change in the input and the output current of the converter.

The filter inductor and capacitor to operate the converter in the continuous conduction mode can be calculated by the following equations;

$$L = \frac{V_d D}{2\Delta I_L f_s} \tag{3.35}$$

$$C = \frac{I_{oc} D}{\Delta V_o f_s} \tag{3.36}$$

3.9.3 Buck-Boost converter

A Buck-Boost converter is cascade connection of two basic converters, the buck converter and boost converter. The Buck-Boost converter provides an output voltage can be higher or lower than the input voltage. Also this type of converter produces a negative polarity output with respect to the common terminal of the input voltage [44]. The main application of Buck-boost converter is in regulated DC power supplies. Fig. 3.17 shows the circuit topology of Buck-Boost converter [45].

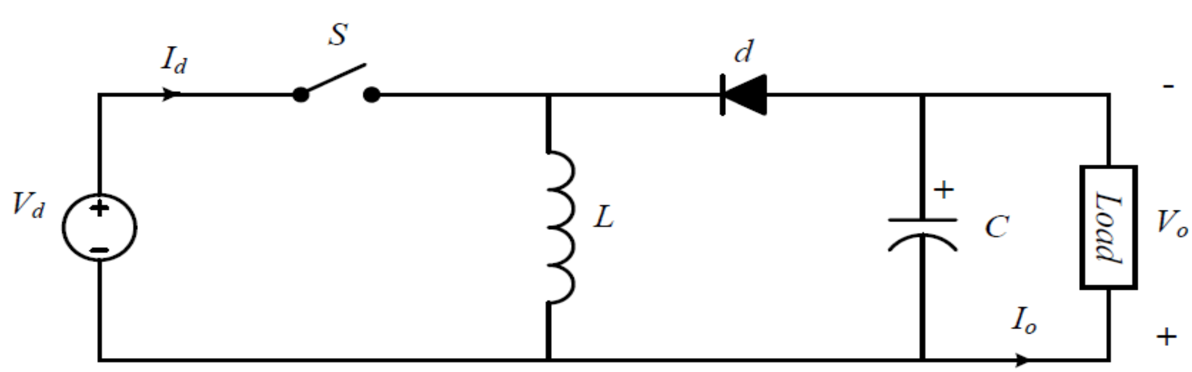

Fig. 3.17 Buck-boost converter [45].

In the equivalent circuit shown in Fig. 3.17 when the switch *S* is turned on during the first time interval t_{on} of the switching period T_s, the diode *d* is reverse based and input provides energy to the inductor causing the inductor current i_L, to increase. When the switch is off during the second time interval t_{off}, the diode is forward biased so the energy stored in the inductor is transferred to the load. In this case the inductor current i_L, is forced to flow backwards through the load and results in a negative polarity in the converter output voltage.

During the steady-state condition the relation between the output voltage V_o and the duty ratio of the converter can be defined by the following equation.

$$\frac{V_o}{V_d} = \frac{D}{1-D} \tag{3.37}$$

From the above equation the output voltage could be higher or lower than the input voltage according to the value of the duty ratio. For the duty ratio condition $D > 0.5$, the output is higher than the input as in a boost converter. If $D < 0.5$ the output is lower than the input as in a buck converter.

$$L = \frac{(1-D)^2 R}{2 f_s} \tag{3.38}$$

$$C = \frac{D}{R f_s (\Delta V_o / V_o)} \tag{3.39}$$

3.9.4 Cuk Converter

The Cuk converter can be obtained by using the duality principle on the circuit of a Buck-Boost topology. The circuit diagram of Cuk converter is shown in Fig. 3.18. It is clear that the input circuit of Cuk converter is a boost converter and the output circuit is seen to be a buck converter. Hence the Cuk converter is similar to the Buck-Boost converter; it provides a negative polarity regulated output voltage with respect to its terminal of the input voltage [44].

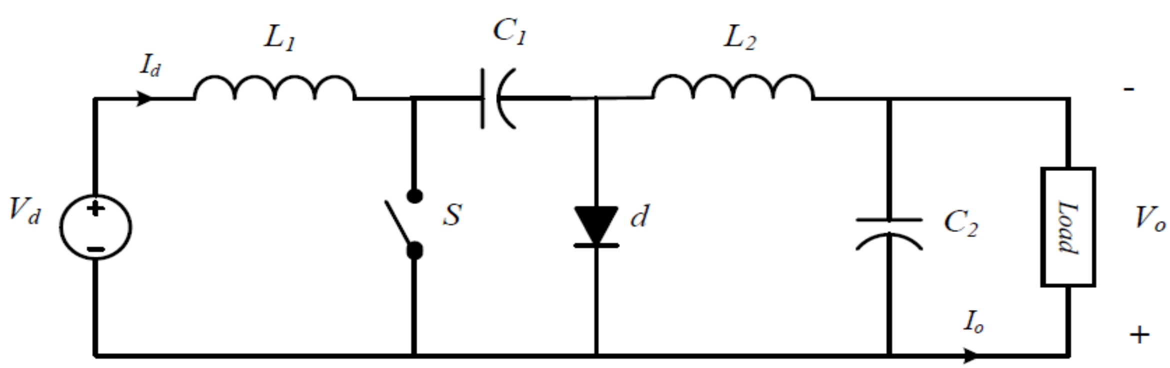

Fig. 3.18 Cuk converter.

In steady-state operation, the average voltage of the inductor is zero, therefore by applying Kirchhoff's voltage law to the circuit shown in Fig. 3.18.

$$V_{c1} = V_d + V_o \tag{3.40}$$

Cuk converter shows two different operating modes. The first mode obtained when the switch S is off. In this case the diode d is conducting as shown in Fig. 3.19. Therefore, the capacitor C_1 is charged by the input V_d through the inductor L_1. The energy stored in the inductor L_2 feeds the load. Hence, the following relationship is obtained [44].

$$I_{C1} = I_{L1} \tag{3.41}$$

The second mode of operation exists when the switch S is on. The diode d is not conducting because it is reverse-based due to C_1. The capacitor C_1 discharges through the switch S, transferring its energy to the load and L_2. Assume the inductor currents are ripple free, because the inductors are large enough. Therefore, the following relationship is obtained [45].

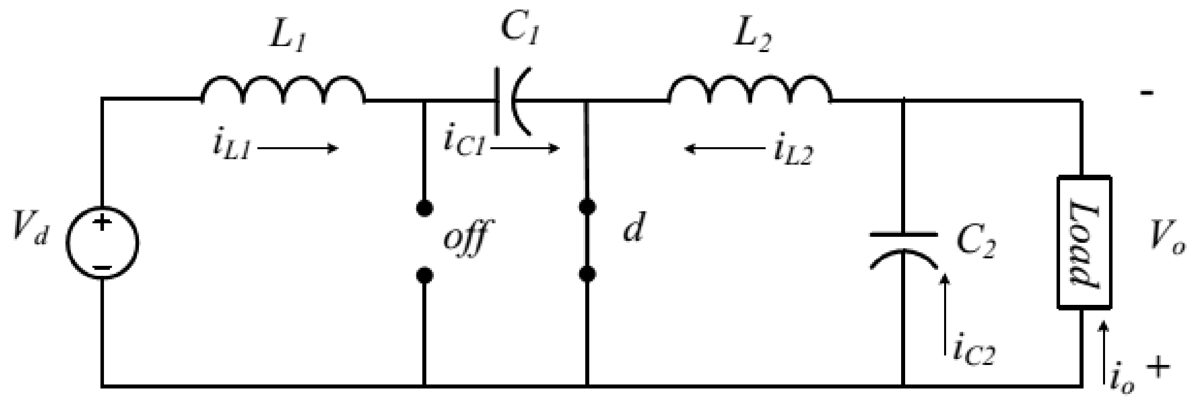

Fig. 3.19 Cuk converter when the switch is off.

$$-I_{C1} = I_{L2} \tag{3.42}$$

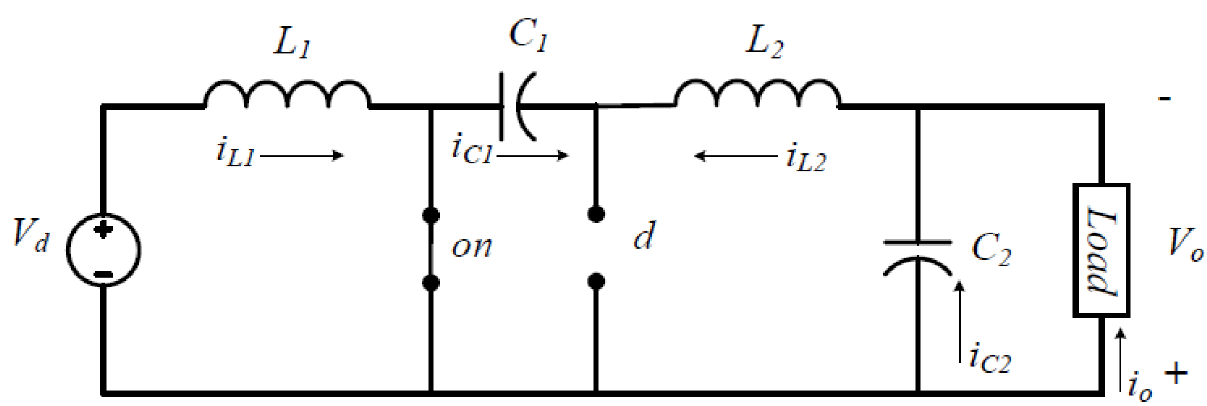

Fig. 3.20 Cuk converter when the switch is on.

For one time period of operation, the average capacitor current is zero. Therefore, by rearranging the Equations (3.41) and (3.42) yields [44],

$$[I_{C1}|_{S_{on}}].DT_s + \left[I_{C1}|_{S_{off}}\right].(1-D)T_s = 0 \tag{3.43}$$

$$-I_{L2}DT_S + I_{L1}.(1-D)T_S = 0 \tag{3.44}$$

$$\frac{I_{L1}}{I_{L2}} = \frac{D}{(1-D)} \tag{3.45}$$

Where D is the duty ratio of the converter and it is the ratio of the conduction time t_{on} to the switching period T_S. The value of D changes between 0 and 1 [44].

Assuming the converter is ideal in other words there are no losses. Therefore, the input power of the converter P_{in} is equal to the output power P_{out} [44].

$$P_{in} = P_{out} \tag{3.46}$$

$$V_d.I_{L1} = V_o.I_{L2} \tag{3.47}$$

$$\frac{I_{L1}}{I_{L2}} = \frac{V_o}{V_d} \tag{3.48}$$

Combining the Equations (3.45) and (3.48), the following relation is obtained [44].

$$\frac{V_O}{V_d} = \frac{D}{(1-D)} \tag{3.49}$$

- If 0 < D < 0.5 the output is smaller than the input.
- If D = 0.5 the output is the same as the input.
- If 0.5 < D < 1 the output is larger than the input.

In the literature, many types of DC-DC converters have been studied to see which converter is suitable for the MPPT stage of the PV system. For water pumping systems, the output voltage needs to be stepped down, unlike in the grid connected systems, in order to provide a higher starting current for a pump motor. Therefore, the Cuk, SEPIC, Buck-Boost and Buck converters are a good choice since step-down or step up voltage conversion may be performed by converter transistor duty-cycle adjustment. The Cuk and SEPIC converters have the advantage that their input current is continuous, and they can draw ripple free current from a PV module [5]. However, Cuk, SEPIC and Buck-Boost converters have a higher number of passive components and high current, voltage and switched power stresses in the switch or transistor compared to the Buck converter. This also affects the whole system efficiency [46], since the switched current and voltage are higher for the same output power as an individual buck or boost. Also, the higher voltage devices required generally switch less rapidly and have higher on-state voltage, which further increases conduction and switching losses. Therefore, in this work it was decided to use a Buck converter because of its higher efficiency, less complex control requirements, more robust and predictable operating characteristics than other topologies.

3.10 Modeling of DC motor and pump

Using DC motors to PV pumping systems instead of AC motors have been the objective of many studies and it was concluded that DC motors can be directly coupled to the PV module. Therefore, the overall system cost and complexity will be significantly reduced. A permanent magnet DC motor is employed in this work. The permanent magnet DC motors are reliable, efficient and require low maintenance [44]. In addition, the PMDCM coupled with centrifugal pump has suitable matching characteristics with the PV module characteristics and has low starting torque compared to the other PV electro-mechanical systems.

3.10.1 PMDC motor modeling

The equivalent circuit of the permanent magnet DC motor is shown in Fig. 3.21 [15], where R_a is the armature winding resistance (Ω), L_a is the armature self-inductance (H), I_a is the motor armature current (A) and V_a is the applied voltage (V).

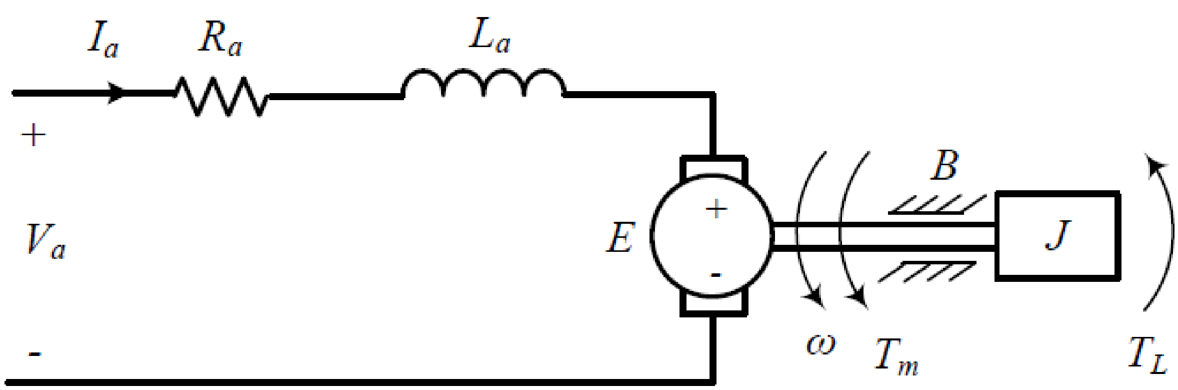

Fig. 3.21 Circuit model for dc permanent magnet motor with pump load.

From the equivalent circuit shown in Fig. 3.21, the armature DC voltage can be calculated by using Equation (3.50).

$$V_a = R_a I_a + L_a \frac{dI_a}{dt} + e \tag{3.50}$$

e is the induced voltage when the motor is turning, and it is known as a back emf, or a counter electromotive force. The induced voltage e is proportional to the angular speed of the rotor ω_m, the constant proportionality, K_e, and the field flux Φ as given by Equation (3.51).

$$e = K_e \Phi \omega_m \tag{3.51}$$

In the case of separately exited motors with constant field voltage or permanent magnet motors the field flux remains constant. Accordingly, Equation (3.51) becomes;

$$e = K_e \omega_m \tag{3.52}$$

Hence Equation (3.52) becomes;

$$V_a = R_a I_a + L_a \frac{dI_a}{dt} + K_e \omega_m \tag{3.53}$$

The torque balance equation is given by:

$$T_e = J \frac{d\omega_m}{dt} + B_m \omega_m + T_L \tag{3.54}$$

Where J is the moment of inertia, B_m is the viscous torque constant for rotational losses, T_e and T_L are the electromagnetic torque and the load torque respectively. The electromagnetic torque T_e is equal to the product of the torque constant $K_t$and the current through the armature winding as given by:

$$T_e = K_t I_a \tag{3.55}$$

Therefore Equation (3.54) can be rewritten as:

$$K_t I_a = J \frac{d\omega_m}{dt} + B_m \omega_m + T_L \tag{3.56}$$

For a constant flux machine the torque constant is equal to the back emf constant (K_e) [18]. Also the torque developed by the armature can be written as in (3.57).

$$T_e = \frac{P_e}{\omega_m} = \frac{eI_a}{\omega_m} = \frac{K_e \omega_m I_a}{\omega_m} = K_t I_a \tag{3.57}$$

Where P_e is the electric power of the motor and $B_m\ \omega_m$ represents the rotational losses torque. In a steady-state condition, Equations (3.50) and (3.54) become:

$$V_a = R_a I_a + E \tag{3.58}$$

$$K_t I_a = B_m \omega_m + T_L \tag{3.59}$$

3.10.2 Interfacing the PV module to the DC water pumping load

In this section, how to maximize the power delivered from the PV module to the load at all insolation levels is presented. A buck converter without the output filter, which is essentially a step-down converter, also known as a chopper, inserted between the PV module and the load as shown in Fig. 3.22.

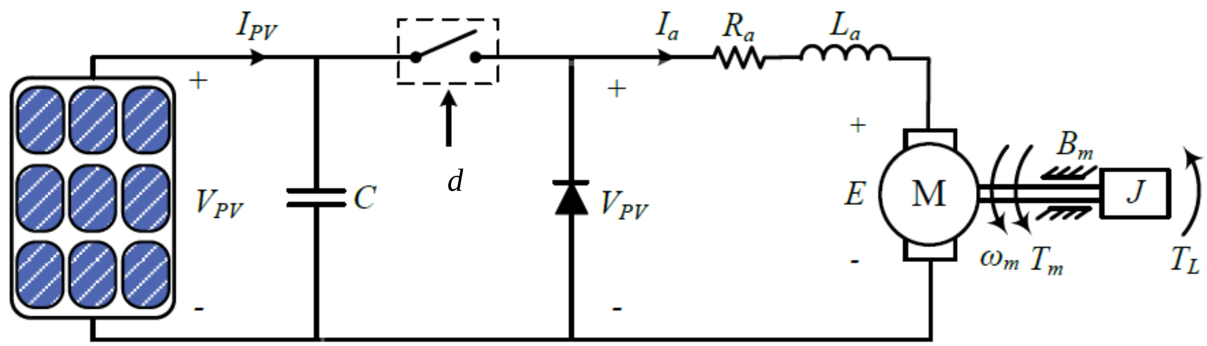

Fig. 3.22 PV module supplying dc pump through step-down converter.

In block diagram shown above, the maximum power can be transferred to the load by the chopper when it is driven with optimal duty ratio *D*. The peak power P_{peak} delivered to the load under steady-state conditions at any solar insolation levels can be derived using (3.60).

$$P_{peak} = R_a {I_a}^2 + EI_a \tag{3.60}$$

The duty ratio is expressed in terms of the motor speed to define how the motor speed is affected by changing the buck chopper duty ratio. Therefore, Equation (3.50) can be expressed in terms of the speed. From Equations (3.57) and (3.59), the torque developed by the motor under steady-state condition is given by either Equation (3.61) or (3.62).

$$\frac{EI_a}{\omega_m} = B_m \omega_m + T_L \tag{3.61}$$

$$EI_a = B_m {\omega_m}^2 + T_L \omega_m \tag{3.62}$$

Similarly from Equation (3.59), the armature current is given by

$$I_a = \frac{B_m \omega_m + T_L}{K_t} \tag{3.63}$$

Substituting Equations (3.61) and (3.63) into (3.60) yields

$$P_{peak} = \left(\frac{B_m \omega_m + T_L}{K_t}\right)^2 R_a + B_m {\omega_m}^2 + T_L \omega_m \tag{3.64}$$

$$P_{peak} = \frac{R_a}{{K_t}^2}\left({B_m}^2 {\omega_m}^2 + 2B_m \omega_m T_L + {T_L}^2\right) + B_m {\omega_m}^2 + T_L \omega_m \tag{3.65}$$

Equation (3.65) results in a polynomial whose order depends on the type of load torque T_L. Equation (3.65) is solved for ω_m for various insolation levels taking the real and the positive values. To determine the variation of the duty ratio *D* with the speed ω_m corresponding to peak powers associated with different levels of solar insolation, the output voltage V_o of the buck chopper is calculated from

$$V_o = R_a I_a + E = K_e \omega_m \tag{3.66}$$

Where ω_m is the speed corresponding to maximum power point of Equation (3.65) and then I_a can be obtained by substituting this value of ω_m into Equation (3.63).

Since the buck converter is operating in the continuous conduction mode, its duty ratio is defined by the Equation (3.67).

$$D = \frac{V_o}{V_d} \tag{3.67}$$

Then at different insolation levels the duty ratio D is calculated by:

$$D = \frac{V_o}{V_{max}} \tag{3.68}$$

Where V_o is given by Equation (3.66) and V_{max} is the voltage at maximum power of the solar panel for different insolation.

For a constant type of load torque, Equation (3.65) is a second order polynomial given by

$$\left(\frac{{B_m}^2 R_a}{{K_t}^2} + B_m\right) {\omega_m}^2 + \left(\frac{2 B_m T_L R_a}{{K_t}^2} + T_L\right) \omega_m + \frac{{T_L}^2 R_a}{{K_t}^2} - P_{peak} = 0 \tag{3.69}$$

3.10.3 Centrifugal pump load

Although the volumetric pump and the centrifugal pump are widely used in PV pumping systems, it was reported in [39] that a load composed of a DC motor driving a constant volume pump represents a non-matched load for a PV module because the motor driving a constant volume pump requires a nearly constant current. However, it was found in [40] the PV module energy utilized by the centrifugal pump is much higher than by the volumetric pump, because the centrifugal pump works for longer periods even for low insolation levels and its load characteristic is well matched to the maximum power locus of the PV module. Also centrifugal pumps are inexpensive, simple, require low maintenance and are available in a wide range of flow rates and heads. Therefore a centrifugal pump is considered in this work. It has flow rates up to 20.0L/min (5.4GPM) [13]. The typical daily output is between 3000L and 6,500L [13]. The rated maximum power consumption is 180W. It operates with a low voltage (14~35V DC), and its power requirement is as little as 42W [13].

The centrifugal pump load develops speed dependent torques. The speed-torque characteristics of centrifugal pump including friction torque are approximately given by (3.70)[21].

$$T_p = T_L = A_L K_L {\omega_m}^{1.8} \tag{3.70}$$

T_p is the torque required to drive the pump, A_L is the load friction (Nm) and K_L the proportional constant of the load torque $\mathrm{N.m}/(rad/sec)^2$.

Since the load torque $T_L = T_p$, hence Equation (3.65) becomes:

$$\left(\frac{{B_m}^2 R_a}{{K_t}^2} + B_m\right){\omega_m}^2 + \left(\frac{2B_m T_p R_a}{{K_t}^2} + (T_p)\right)\omega_m + \frac{(T_p)^2 R_a}{{K_t}^2} - P_{peak} = 0 \qquad (3.71)$$

$$\left(\frac{{K_L}^2 R_a}{{K_t}^2}\right){\omega_m}^4 + \left(\frac{2B_m K_L R_a}{{K_t}^2} + K_L\right){\omega_m}^3 + \left(\frac{{B_m}^2 R_a}{{K_t}^2} + B_m\right){\omega_m}^2 - P_{peak} = 0 \qquad (3.72)$$

Equation (3.72) is implemented in MATLAB to calculate the rotation speed of the motor ω_m for a given value of peak powerP_{peak}. For the MATLAB script of this equation please refer to Appendix A.1.2.

3.11 Summary

In this chapter presents a discussion of the selection of the strategy and modeling of the proposed fuzzy logic based MPPT control for the PV water pumping system. The chapter begins with a brief introduction about the fuzzy logic development history and applications. Next it provides an overview of fuzzy controller basic structure with brief illustration of its main components which are: the fuzzification interference, knowledge base, interface engine, and defuzzification interference. The fuzzy interface process has also been discussed and explained however, there are several methods for performing the fuzzy interface process, the Mamdani method was thoroughly explained and used in this work. This is because the Mamdani method is computationally more efficient and has better interpolative properties than the other interface methods.

The design of the proposed fuzzy logic based MPPT controller for the PV water pumping system is also discussed in this chapter and illustrated with a the complete schematic diagram of the system. The proposed FLC is designed to track the maximum power of the PV array and deliver it to pump load under variable temperature and insolation conditions. The controller uses the variation of the PV module output power ΔP_{PV} and variation of the motor-pump rotational speed $\Delta\omega_m$ as the input variables to continuously adjust the buck converter's duty ratio, which constitutes the output variable of the control, to maintain system operating at the MPP.

This chapter also deals with the model development for the component parts of the proposed PV water pumping system are discussed. The component parts are: PV module, power electronic interfacing device (DC-DC converter), permanent DC motor and centrifugal pump load.

This part begins with the physical structure of PV cells along with the fundamental concept and principles of converting the solar energy to electrical energy. The modeling of equivalent electrical circuit of PV cell presented and discussed. The model is implemented using MATLAB to study the PV characteristics. Furthermore, the low output power of the single cell is discussed and how to connect number of cells in series and parallel to form a PV module to meet the desired load power. The effect of temperature and solar radiation on the I-V and P-V characteristics of PV cell also discusses this chapter to show the importance of MPPT in the PV system.

This chapter introduces and investigates various DC-DC converters used in the MPPT of PV systems. As the PV system is proposed in this work is a stand-alone system therefore, the focus was on the non-isolated converter: Buck converter, Boost converter, Buck-Boost converter and Cük Converter. The electrical circuits of these converters were presented and operating concept of each convert was thoroughly discussed. And then followed by a discussion mentioning advantages and disadvantages of each converter and which the most reliable converter to be implemented in the PV water pumping system. It was concluded that, the DC-DC buck converter is the suitable converter if the load comprises a DC motor and it will be simulated in the MATLAB using the SimPowerSystems block-set.

The discussion and mathematical modeling part extends to the DC motor and load pump used in proposed PV water pumping system. The DC motor type chosen is a permanent magnet brushed motor hence it can be directly coupled to the PV module without inverter and it is efficient, require low maintenance. The mathematical model of the PMDC motor is presented and the problem of the motor directly connected to the PV module discussed. The load pump driven by the PMDC motor is a centrifugal pump this is because it is inexpensive, requires low maintenance, and available in a wide range of flow rates and heads. Additionally, the centrifugal pump works for longer periods even for low insolation levels and its load characteristic is well matched to the maximum power locus of the PV module. Mathematical equations also are derived in this chapter to be implemented in MATLAB/SIMULINK using various functional blocks develop the PMDC motor and the pump models.

CHAPTER FOUR

DESIGN SIMULATION AND ANALYSIS

In this part, the implementation of the proposed PV control system is done in MATLAB/SIMULINK to give how the control system is applied to test and confirm its usefulness in MPP tracking and each block of the photovoltaic water pumping system is described as well. In this thesis work, two cases are considered in simulation. The first case is simulation using conventional P&O algorithm to assess its viability and the benefits. In the second case, the PV system is similarly simulated in MATLAB by replacing the conventional P&O algorithm by modified P&O with FLC to show the practicality and execution of the proposed fuzzy logic controller concerned on MPPT of water pumping system. Besides, a comparison has been done between the proposed P&O with FLC and the conventional P&O algorithm in PV water pumping system controlling based on simulation results. The simulation is kept running with variable-step solver for exactness and to keep the solver from endlessly circling on the m-file during execution. The solver integration technique applied is the (ode 23) [39].

4.1 System Design and Simulation

System modeling and simulation has been undergone in MATLAB/SIMULINK. The total SIMULINK model of the proposed system is shown in Fig. 4.1. The modeled system comprises basically of PV module, PMDC, DC/DC buck converter model used to interface PV output to the pump load to track MPP of the PV module. To carry out the tracking of MPP, a perturbation and observation algorithm has been applied.

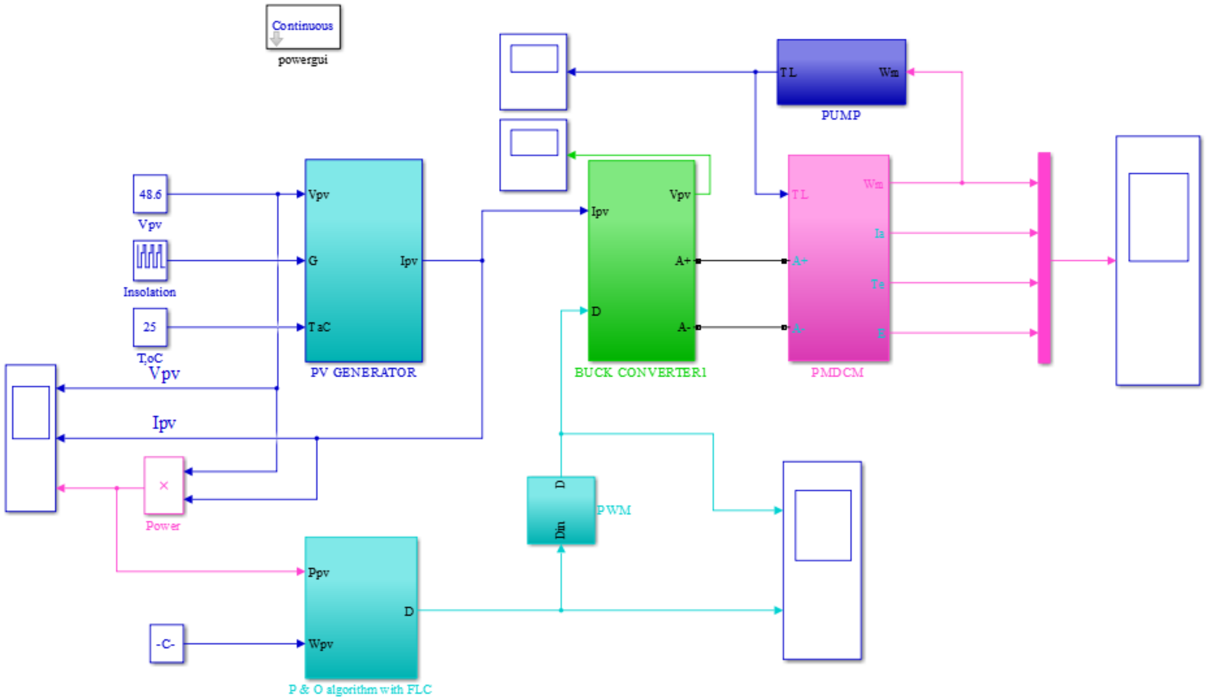

Fig. 4.1 SIMULINK model of PV water pumping system with MPPT algorithm.

4.1.1 PV module

The electrical specification of the PV module is given in the table 4.1 demonstrated as follows. The PV demonstrate test system was implemented in MATLAB as m-file code by using Equation (3.29) as shown in Appendix A1.1 and the code electrically works as a voltage controlled current source.

The PV panel used as a part of the simulation is 96 SANYO HIT180 panels associated in 12×8 matrix. The temperature T, isolation G and PV voltage VPV are fed to the Embedded MATLAB Function and the output is the current produced by the panel. The basic performance of the PV panel differs from one to other; hence typical parameters are generally given in a datasheet. The performance and salient parameters regarding the characteristic of PV panel under standard test conditions are provided in the datasheet. The parameters of PV panel applied as a part of this thesis work are shown in the Table 4.1.

Table 4.1 Electrical characteristics data of PV module taken from the datasheet [12]

Electrical Characteristics	Rated value
Current at P_{max} (I_{mp})	3.33 A
Rated Maximum Power(P_{max})	180W
Normal Operating Cell Temperature(NOCT)	47 ± 2 ℃
Open-circuit voltage (V_{oc})	66.4V
Short-circuit current (I_{sc})	3.65A
Temperature coefficient of I_{sc}	1.10 mA / °C
Temperature coefficient of power	-0.33% / °C
Temperature coefficient of V_{oc}	-0.173 V / °C
Voltage at P_{max} (V_{mp})	54V
Series Resistance (R_s)	0.3345Ω

4.1.2 Buck Converter Design

The simulation model of the switching mode buck converter is masked by the SIMULINK and made into just a single block as appeared in Fig. 4.2. There are two inputs and two outputs in the Buck converter subsystem block appeared in Fig. 4.2. The input terminal g stands for the gate signal from the PWM block, $I_{PV}$and $V_{PV}$are the current and voltage inputs respectively and A+ and A- are secondary positive and negative outputs of buck converter respectively.

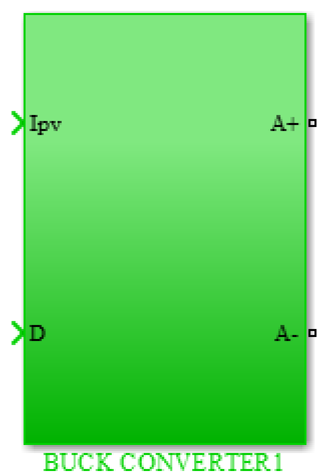

Fig. 4.2 One block representation of buck converter.

The detail of the masked buck converter is directed in MATLAB and simulated using SimPowerSystems components and the circuit diagram is shown in Fig.4.3. The converter comprises of IGBT switch and freewheeling diode. Also, input and output filters are incorporated. The inductor is in charge of diminishing the output current ripple; the bigger the inductor, the smaller the ripple.

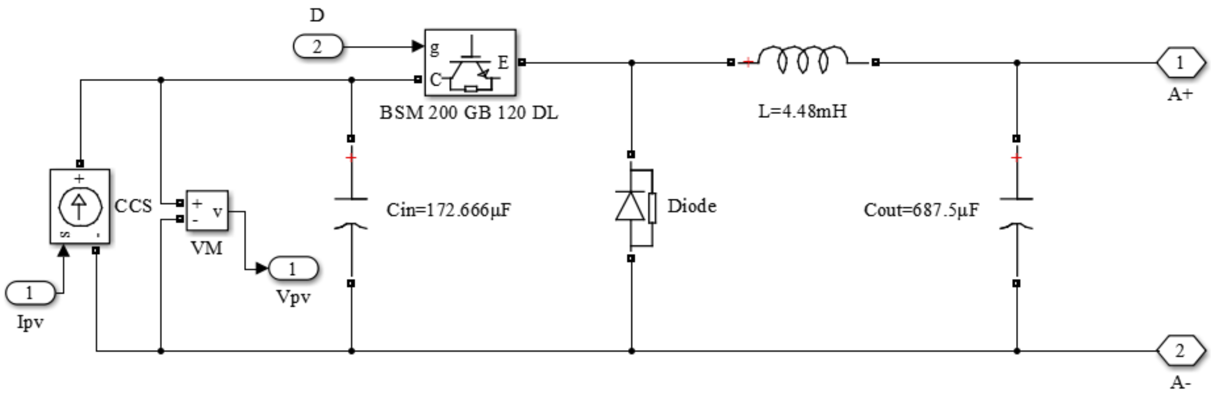

Fig. 4.3 Simulation model of DC-DC buck converter.

4.1.3 Buck converter parameters scaling

As the output power conveyed by the PV module will shift with temperature and irradiation, it is important to first expect a fixed working voltage while deciding the parameters of the buck converter to be utilized.

The proposed buck converter, which keeps up the output voltage of the PV module at the greatest power point, has a target output voltage of around 24V. In this work, 54V is the best output voltage of the PV module used. This working voltage is used for selecting the underlying duty cycle and for choosing the best possible estimations of the buck converter components.

The circuit of step down converter is displayed in Fig. 4.3. The greatest input voltage V_{inm} of the converter is 54.0V as shown below in Table 4.2 and it is equivalent to the maximum output voltage of the PV module. The greatest output voltage of the converter is V_{om} has been 24V. Therefore, the converter duty ratio D_{mp} relating to the maximum power output is manipulated by the Equation (4.1). The parameters estimations of the buck converter are shown in the Table 4.2, whereas I_{inm}, I_{om} are the maximum input and output currents of the buck converter respectively, and f_s is the converter switching frequency.

$$D_{mp} = \frac{V_{om}}{V_{inm}} \tag{4.1}$$

Table 4.2 Buck converter parameters

Maximum input Voltage	(V_{inm})	54.0V
Maximum output Voltage	(V_{om})	24.0V
Maximum input Current	(I_{inm})	3.33A
Maximum output Current	(I_{om})	7.5A
Duty ratio corresponding to the maximum power output	(D_{mp})	44.4%
Switching frequency	(f_s)	20KHz

❖ **Input filter**

The input capacitor is used to reduce the converter input voltage ripple and determines the amount of peak current drawn from the source. The input capacitor can be calculated by Equation (4.2) with maximum voltage ripple of 2% [16].

$$C_{in} = \frac{I_{inm}(1 - D_{mp})}{\Delta V_{inm} f_s} \tag{4.2}$$

$$C_{in} = \frac{3.33(1-0.44)}{0.02\times 54\times 10\times 10^3} = 172.666\mu F$$

❖ **Output filter**

The output filter comprises inductor L and capacitor C_{out} .

1) Inductor

The buck converter inductor value required to operate the converter in the continuous conduction mode can be calculated by Equation (4.3).

$$L = \frac{V_{om}(1 - D_{mp})}{2\Delta I_{om} f_s} \tag{4.3}$$

$$L = \frac{24(1-0.44)}{2\times 0.02\times 7.5\times 10\times 10^3} = 4.48mH$$

2) *Capacitor*

The output capacitor value is calculated by the Equation (4.4) assuming the voltage ripple (2%) to give the desired peak to peak output voltage ripple [16].

$$C_{out} = \frac{D_{mp} I_{om}}{\Delta V_{om} f_s} \tag{4.4}$$

$$C_{out} = \frac{0.44\times 7.5}{0.02\times 24\times 10\times 10^3} = 687.5\mu F$$

4.1.4 The P&O Controller

The perturb and observe (P&O) algorithm with Fuzzy Logic Controller is implemented in MATLAB/SIMULINK as shown in Fig. 4.4. The P&O comprises two blocks, the conventional P&O algorithm and FLC. The conventional P&O was implemented in a similar manner as the PV module. Its MATLAB script is written as M-file code in an embedded MATLAB function, the MATLAB script is illustrated in Appendix A.1.1.

MATLAB/SIMULINK is applied to implement Fuzzy Logic Controller by using the accessible Fuzzy Logic Toolbox. The FLC was designed by applying a viable Graphical User Interface (GUI) tool given by the fuzzy logic toolbox in MATLAB/SIMULINK to sustain the design of the Fuzzy logic controller. This is known as the Fuzzy Interface System (FIS) editor as outlined in Appendix B.1 in Fig. B.1.To design the fuzzy logic controller, FIS is applied. The detailed design of the Fuzzy Interface System (FIS) editor, Membership Function Editor and Rule Editor are as shown in the Appendix B1. Determination of input and output signals is done by selecting not only the desired shape but also number of membership functions in the Membership Function Editor as appeared in Appendix B in Fig. B.2 to Fig B.4. The FLC uses the PV module Power P_{PV} and the pump motor speed ω_m as input signals and produces duty ratio D as a control signal for the buck converter.

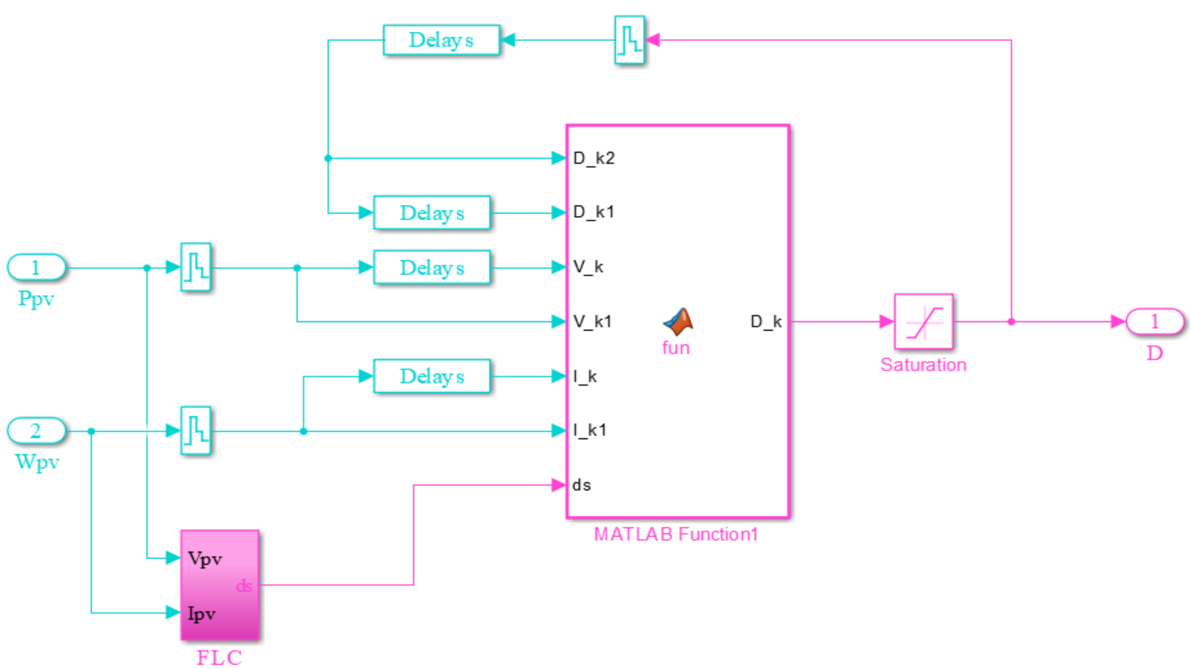

Fig. 4.4 SIMULINK model of the P&O controller FLC.

Fuzzy rules are a set of rules that the fuzzy controller applies. These rules can be determined in the Rule Editor as shown in Appendix B.1 in Fig. B.5.

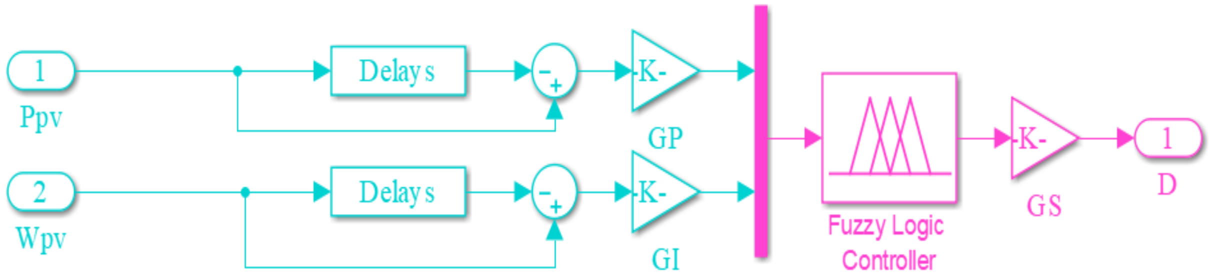

Fig. 4.5 FLC SIMULINK block for step-size tuning.

Table 4.3: FLC SIMULINK block parameters

Fuzzy logic control parameters	
The scaling factor of the PV module output power variation (GP)	0.58
The scaling factor of the PV module output current variation (GI)	0.18
The scaling factor of the variable step-size (*GS*)	0.0186

Once the FLC has been designed, the FIS editor is saved as an (fis) file. The fis file is exported to the MATLAB workspace and the name of the file is entered in the Fuzzy logic control block in SIMULINK shown in Fig. 4.5. The SIMULINK model of the proposed P&O can also be further integrated into one model block as in Fig. 4.6.

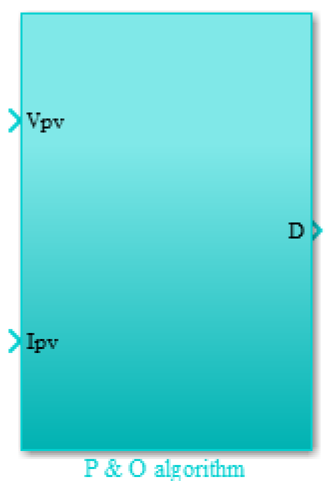

Fig. 4.6 One block representation of P&O with FLC.

4.1.5 Permanent magnet DC motor model

The PMDCM simulation model is built in MATLAB environment using the SimPowerSystems and SIMULINK library as shown in Fig. 4.7. The PMDCM model implements Equations (3.53) and (3.54).

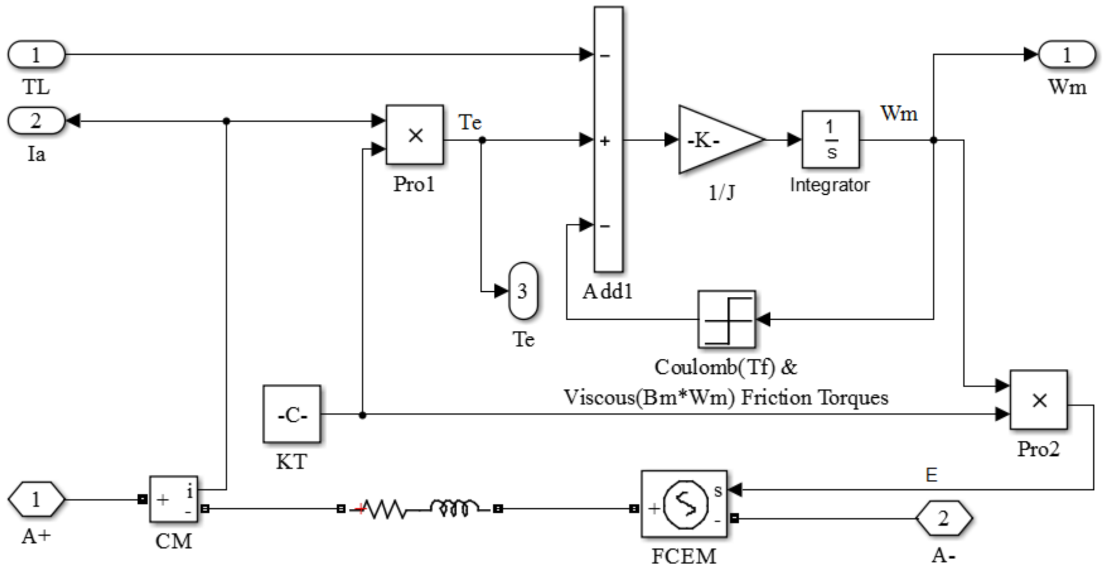

Fig. 4.7 Simulink model of PMDC motor.

4.1.6 Centrifugal pump load

The centrifugal pump was simulated in MATLAB/SIMULINK by implementing Equations (3.70) using various functional blocks. The model shown in Fig.4.8 is centrifugal water pump.

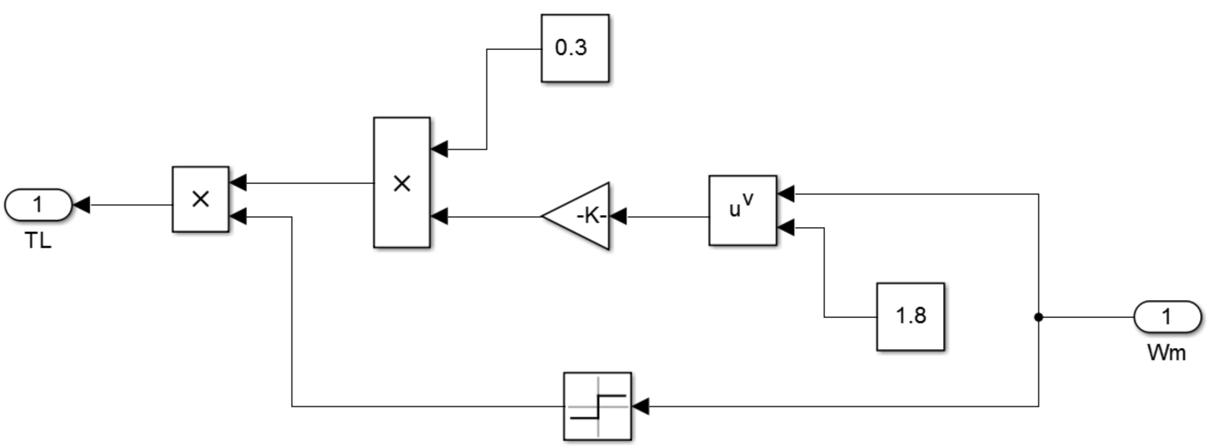

Fig. 4.8 Simulink model of centrifugal pump load.

The pump block has one input and one output terminals; the motor speed ω_m is fed into the pump as an input which in turn outputs load torque, T_L.

Table 4.4: Parameters of DC permanent magnet motor and pump load

DC PM Motor data	
Rated motor voltage (V_a)	12V
Rated motor current (I_a)	15A
Rated motor speed (ω)	3000rpm
Rated torque	0.39Nm
No load motor current (I_a)	4A
No load motor speed (ω)	3400rpm
Starting torque	3.1Nm
Starting current	96A
Ambient temperature	-10℃$\sim +$ 40℃
Load pump data	
Moment of inertia (J)	0.02365 Kg.m^2
Viscous friction coefficient (B)	0.002387 Nm/(rad/sec)
Load torque constant (K_e)	0.00039 Nm/(rad/sec)
Load friction (A_L)	0.3 Nm

To better assess the overall performance of the PV water pumping system, the combined SIMULINK model shown in Fig. 4.1 is subjected to slow and rapid changes in solar irradiation using the proposed MPPT controller to display the behavior of the MPPT controller during the passing of clouds.

4.2 Simulation results of the P&O and P&O with FLC MPPT technique

The simulations offer a valuable opportunity to verify the feasibility and the performance of the variable step-size P&O with FLC algorithm.

In actuality, the great influence on output power of a photovoltaic cell is done by ambient temperature and solar irradiation, in spite of the fact that the change in ambient temperature affects the PV cell and it isn't specifically identified with the speed of dynamic response. Hence, the cell working temperature is settled at 25℃ in all simulations. But, in practice the clouds sometimes move rapidly prompting a sudden change in the PV panel output power. As a result, the algorithm must be tried under various irradiation levels to check the speed of tracking.

4.2.1 Conventional perturb & observe algorithm (P&O)

To analyze the conventional perturb and observe (P&O) algorithm and the perturb and observe (P&O) with FLC, the conduct of P&O will be introduced by the simulation results in this part. Fig. 4.9 to Fig. 4.13 demonstrates the dynamic performance of the PV current, PV voltage, PV power and duty ratio of the conventional P&O. The P&O MPPT controls by adjusting the duty ratio, D, until the maximum power output is reached. The operating power points deviate from the peak power when the irradiation changes. The P&O readjusts the control variables to bring the maximum power operating point back. The MPPT responds to the irradiation change through controlling the PWM input of the DC-DC buck converter by adjusting its duty ratio D. The most commonly chosen parameters that define the behavior of the response are Rise Time (t_r), Overshoot, Undershoot, Settling Time (t_s) and Steady State Error (e_{ss}).

- ✓ **Rise Time (t_r):** the time taken for the output to go from 10% to 90% of the final value.
- ✓ **Overshoot**:$(\text{max value } - \text{final value})/(\text{final value }) \times 100\%$.
- ✓ **Undershoot**: Occurs when the transition is from higher to lower and its value is lower than the final value.
- ✓ **Settling Time (t_s):** The time taken for the signal to be bounded to within a tolerance of x% of the steady state value.
- ✓ **Steady State Error (e_{ss}):** The difference between the input value and the final value.

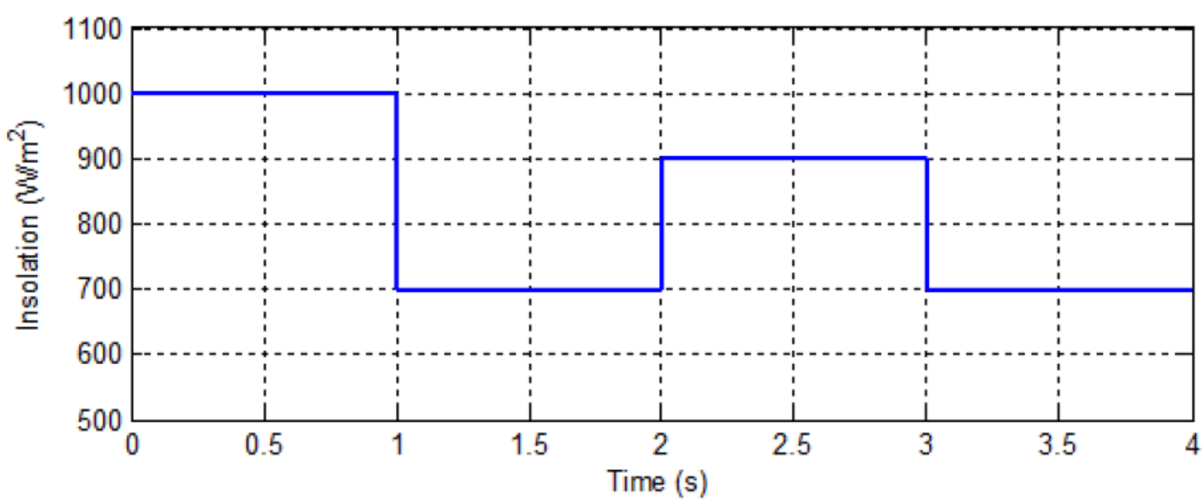

Fig. 4.9 Solar Irradiation.

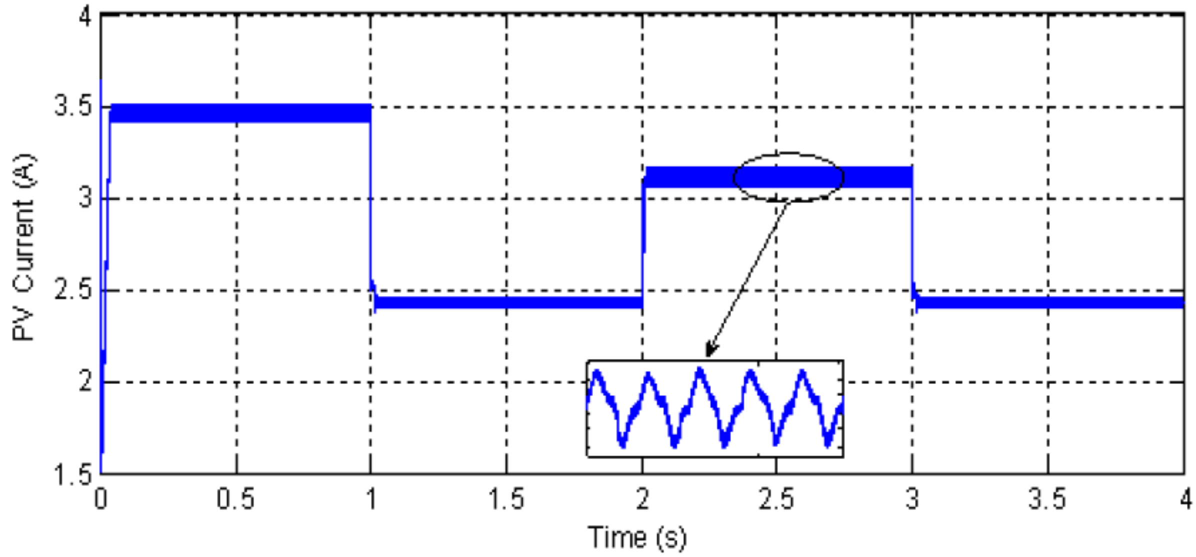

Fig. 4.10 PV module output current using conventional P&O algorithm

t_r=0.1S, Overshoot=1.4%, Undershoot=0%,t_s=0.15S

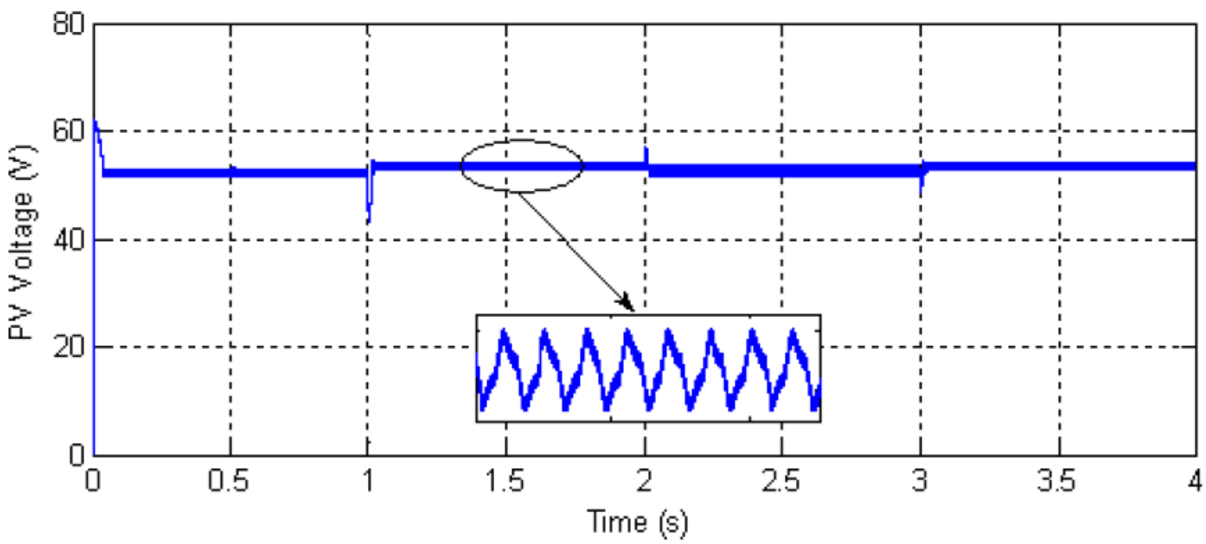

Fig. 4.11 PV module output voltage using conventional P&O algorithm

t_r=0.01μS, Overshoot=5.3%,Undershoot=0%,t_s=0.15S

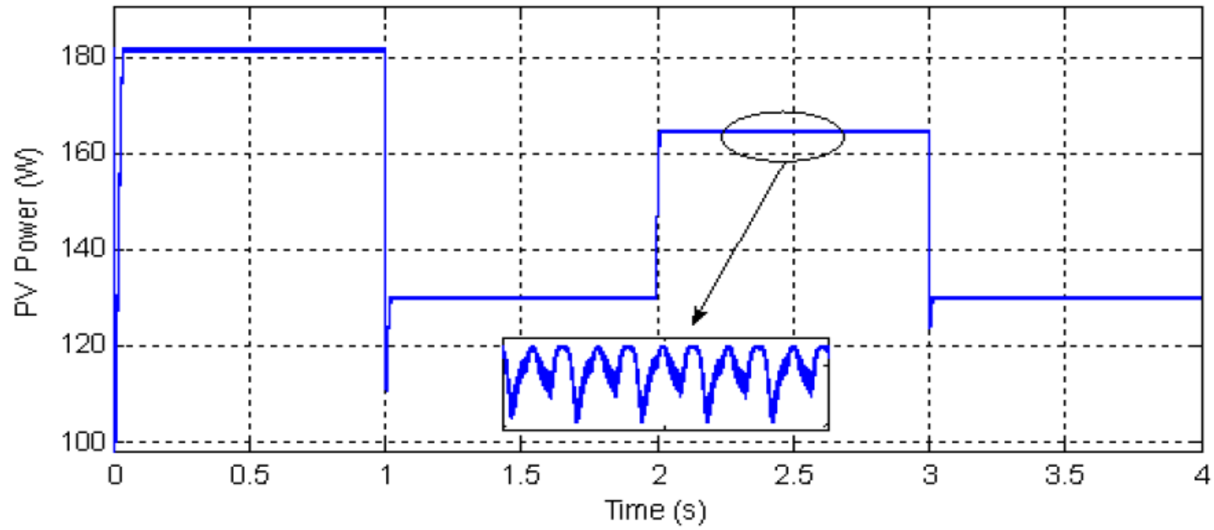

Fig. 4.12 PV module output power using conventional P&O algorithm

t_r=0.1S, Overshoot=0.27%,Undershoot=0%,t_s=0.15S

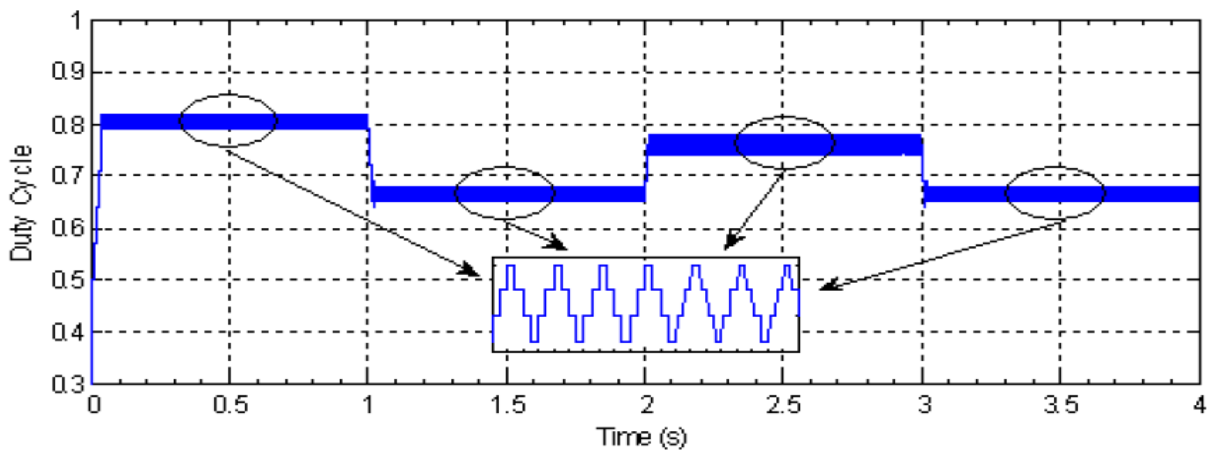

Fig.4.13 Duty ratio waveform of conventional P&O algorithm

t_r=0.1S, Overshoot=1.25%, Undershoot=0%,t_s=1.25S

4.2.2 Perturb & observe algorithm with fuzzy logic controller

The proposed perturb and observe method with FLC was introduced and clarified previously in chapter three. The P&O with FLC depends on a conventional perturb and observe algorithm, P&O. It was upgraded using a fuzzy logic control. Simulation outputs by P&O with FLC are presented and analyzed in this part. To test the execution of the proposed technique and to make a better comparison, the simulations are done under similar conditions from the previous simulations with the regular P&O algorithm. The output waveforms of the P&O with FLC MPPT are shown from Fig. 4.14 to Fig. 4.14. The proposed P&O with FLC MPPT prevails with regards to working a fast change of the duty ratio D to reach maximum output power. After achieving the maximum power point, the proposed MPPT stops changing the duty ratio D and keeps up operation now, except if it recognizes any adjustment in the PV power. Fig. 4.16 demonstrates that at the beginning, the operating power points move away from MPP because of the change in the irradiation. Consequently, the P&O with FLC MPPT starts adjusting again the duty ratio D to track the new maximum power tracking point and continue working at this point.

As the following simulation results show, the proposed P&O with FLC MPPT algorithm shows better performance compared to conventional P&O algorithm. The simulation results show that, the P&O with FLC accurately tracked the maximum power point under varying irradiation levels and it stops changing the duty ratio D once the maximum power point is reached.

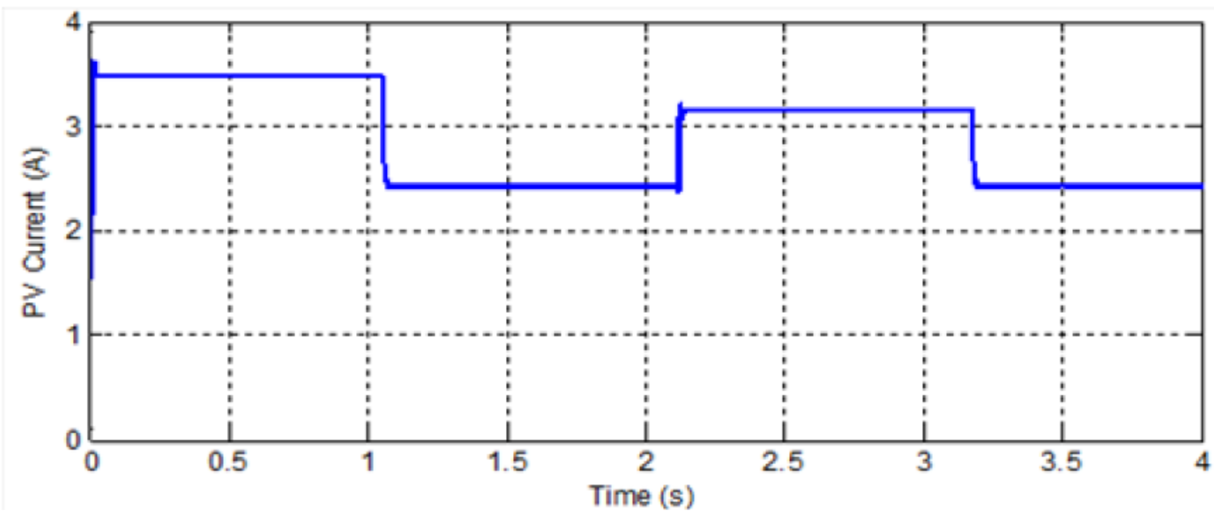

Fig. 4.14 PV module output current using P&O with FLC algorithm.

t_r=0.01S, Overshoot=1.14%, Undershoot=0%,t_s=1.1S

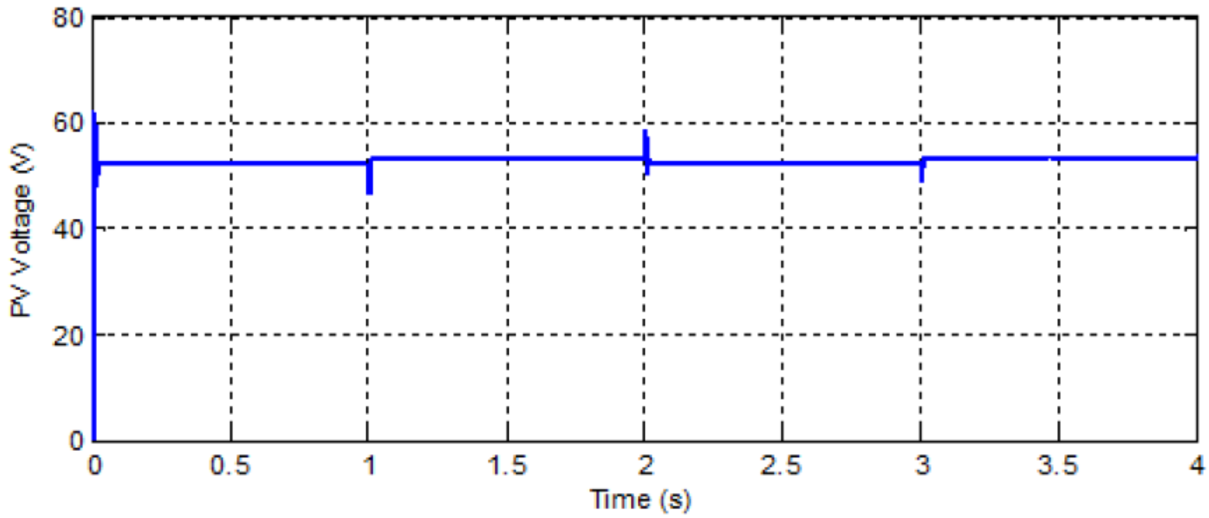

Fig. 4.15 PV module output voltage using P&O with FLC algorithm.

t_r=0.01µS, Overshoot=0%, Undershoot=0%,t_s=1.1S

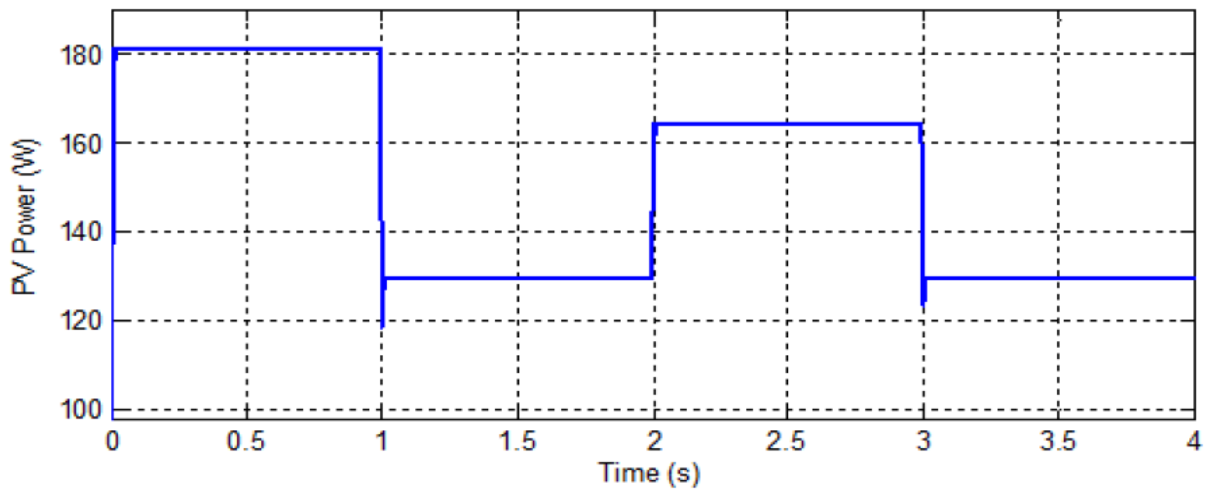

Fig. 4.16 PV module output power using P&O with FLC algorithm

t_r=0.01µS, Overshoot=0%, Undershoot=0%,t_s=1.1S

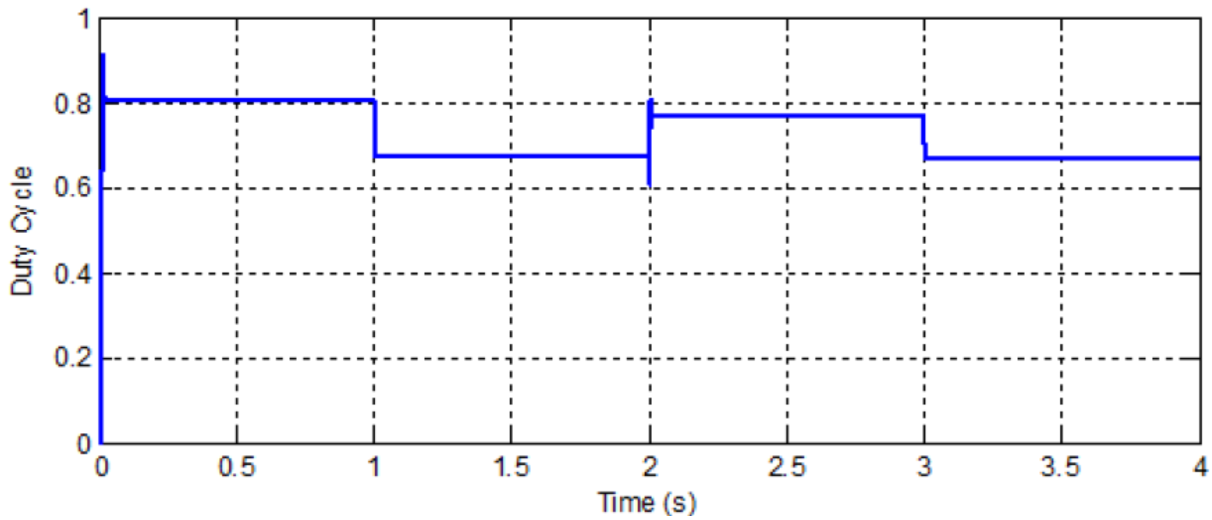

Fig.4.17 Duty ratio waveform of P&O algorithm with FLC

t_r=0.01μS, Overshoot=0%, Undershoot=0%,t_s=1.1S

4.2.3 Comparative performance between P&O with FLC and conventional P&O

In this part, the same condition is considered to compare P&O with FLC and conventional P&O to show the performance of the both techniques. To show the performance of the proposed P&O with FLC MPPT algorithm with the P&O MPPT algorithm, the P&O was tested under three step changes of in irradiation levels.

Table 4.5 provides a summary of tracking performance for the P&O with FLC MPPT and conventional P&O MPPT methods with different levels of irradiation. It ought to be noticed that the performance is manipulated in view of a simulation. In practice, the PV module will operate all day. Keeping in mind the goal to compare the manipulation of the P&O with FLC against the conventional P&O in tracking the maximum power, the simulation power of the PV module is looked against the calculated power at the theoretical MPP for the same level of solar irradiation. The proposed P&O with FLC presented better performance compared to the conventional P&O algorithm. It succeeded in tracking the MPP and maintains operation at this point by adjusting the duty ratio. The PV module output power is obtained from multiplication of PV module current from Equation (3.29) and its corresponding voltage. The MPPT efficiency is evaluated using Equation (4.5).

$$\eta_{MPPT} = \frac{P_{pv}}{P_{max}} \times 100\% \qquad (4.5)$$

Where P_{pv} is *the simulated maximum* power and P_{max} is the calculated maximum power.

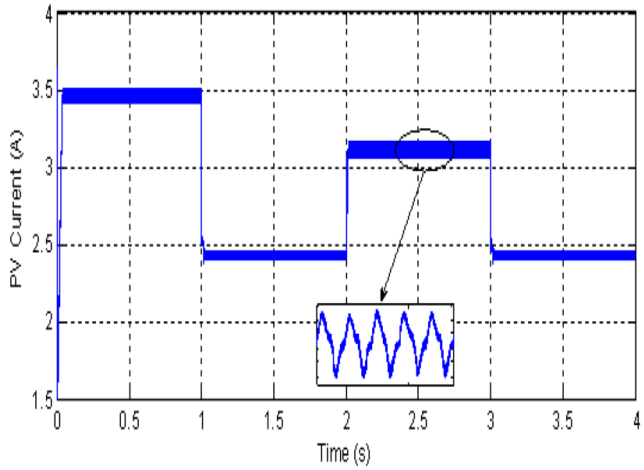

Fig. 4.18 PV module output current using conventional P&O algorithm

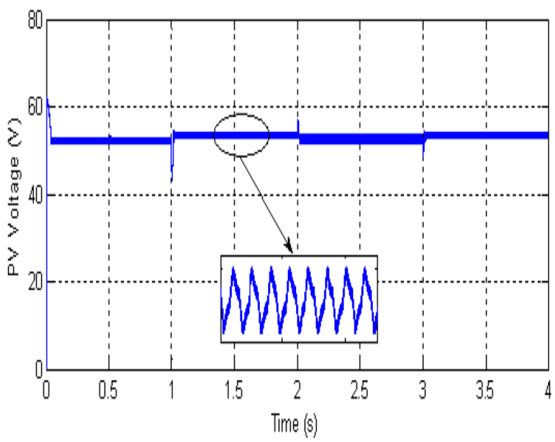

Fig. 4.19 PV module output voltage using conventional P&O algorithm

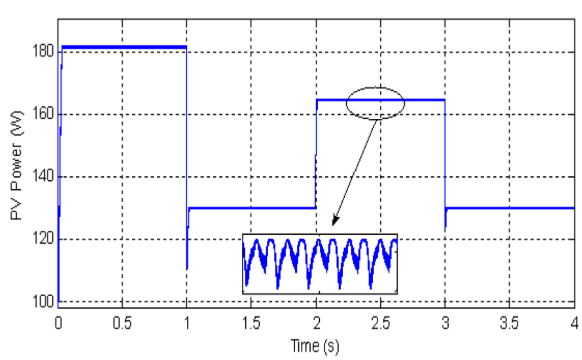

Fig. 4.20 PV module output power using conventional P&O algorithm

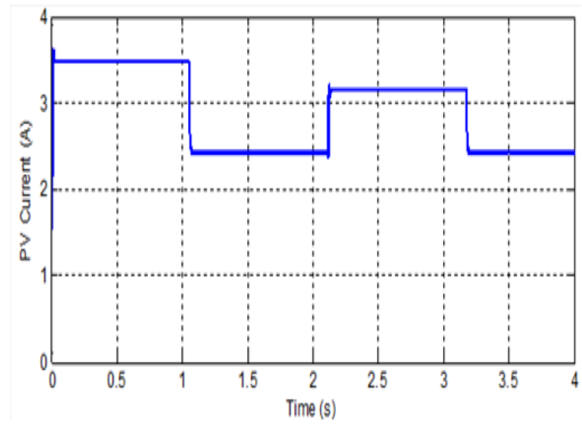

Fig. 4.22 PV module output current using P&O with FLC algorithm

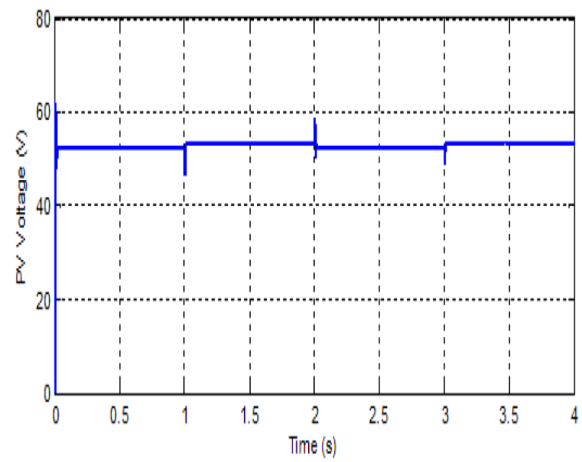

Fig. 4.23 PV module output voltage using P&O with FLC algorithm.

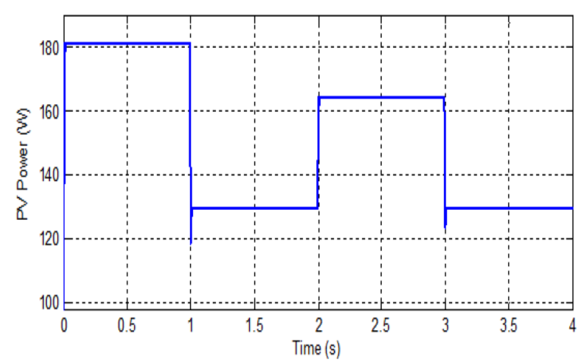

Fig. 4.24 PV module output power using P&O with FLC algorithm

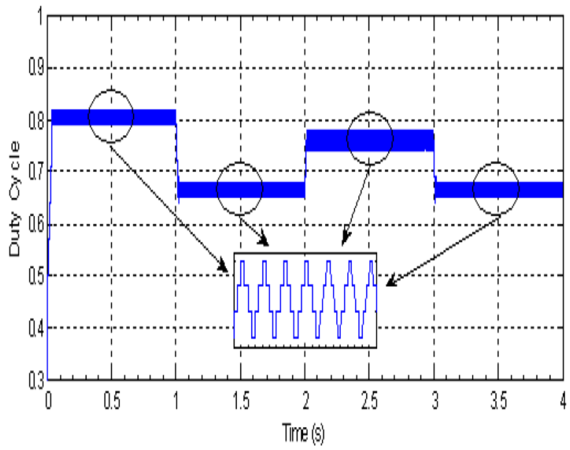

Fig.4.21 Duty ratio waveform of conventional P&O algorithm

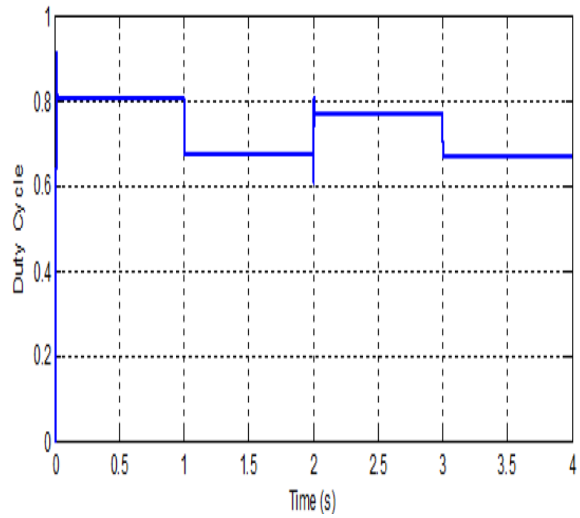

Fig.4.25 Duty ratio waveform of P&O algorithm with FLC

Table 4.5: Tracking performance comparison between P&O with FLC MPPT and conventional P&O MPPT methods.

Irradiation	G(W/m2)	1000	700	900	700
With conventional P&O algorithm	P_{pv}(W)	178.9	127.8	163.4	127.8
	Power oscillation at steady state	High	High	High	High
P&O with FLC	P_{pv}(W)	179.9	129	164.35	129
	Power oscillation at steady state	None	None	None	None

4.3 Summary

This chapter provides the design and MATLAB simulation of the proposed PV water pumping system controller to test the performance of the proposed MPPT technique and to verify its functionality. The system comprises of PV module, DC-DC buck converter, MPPT controller and DC motor load pump. Each of these components has been simulated and masked in an individual subsystem so that they can be easily controlled and precisely monitored. Then, these subsystems are combined to form the complete system. To verify the functionality of the proposed P&O with FLC MPPT algorithm and compare its performance against the conventional P&O algorithm, they were implemented in MATLAB. The simulation was performed under changing irradiation levels. The outputs demonstrate that the P&O with FLC has improved results compared with the conventional P&O algorithm. The outputs demonstrated that the P&O with FLC has enhanced the tracking speed and has removed the oscillation around the MPP. To check the advantages of the proposed MPPT algorithm, the output of P&O with FLC MPPT algorithm was compared to the conventional P&O algorithm. The simulation was completed under various levels of solar irradiation, and it was begun at 1000 W/m^2,700 W/m^2, 900 W/m^2 and back to700 W/m^2.

CHAPTER FIVE

CONCLUSION AND RECOMMENDATION

5.1 CONCLUSION

In this thesis work, a PV water pumping system is brought to presentation to provide the pure water in remote rural areas with a clean and sustainable supply of energy, solar irradiation. Hence, the thesis mainly focuses on the way how to improve the full system performance by implementing better controller so that the transfer of available maximum power is possible irrespective of the changing atmospheric conditions.

While managing this work, some existing MPPT controller strategies were reviewed in Chapter 2, like constant voltage technique, P&O, INC, fractional short-circuit current, fractional open-circuit voltage, and showed their ability to trace the MPP along with changing weather condition. The benefits and drawbacks of each MPPT technique tracking performance were illustrated.

The planned technique is a perturb and observe algorithm with FLC. The conventional P&O MPPT technique is simple compared with P&O with FLC that makes it the best to design and implement. However, a P&O algorithm technique with fastened perturbation step makes it troublesome to attain each a quick response and best steady-state in operation conditions once atmospheric conditions are changeable. P&O MPPT was developed using Fuzzy Logic Controller (FLC) to repeatedly modify the step-size in step with the modification of atmospheric conditions. The P&O with FLC with variable step-size was shown to possess a quicker dynamic response and eliminates the oscillation around the MPP thereby; it improves the MPPT performance of the PV system. Explanation of the design and simulation results of the developed P&O with FLC MPPT technique was presented and discussed. Comparatively straightforward operation of the FLC was achieved by applying as inputs the modification within the PV power and speed therefore the variable step-size of the P&O as the output.

The simulation results were presented in order to show the benefits of MPPT and evaluate the performance and functionality of the proposed MPPT technique. The simulations were performed using MATLAB/SIMULINK. A model of the complete PV systems was presented and discussed along with how all of the subsystem components have been combined to form this system. A more detailed SIMULINK model of each component was also presented, starting with the PV module, buck converter, DC load and MPPT controllers, and then each component in the subsystem.

The simulation results were considered in two cases: in the first case the PV system feeds a pump load to evaluate and test the performance of the conventional P&O algorithm under changing solar irradiation conditions. The PV output power harvested in this case is 178.9W, 127.8W, 163.4W and 127.8W at irradiation of 1000W/m^2, 700W/m^2, 900 W/m^2 and back to 700 W/m^2 respectively.

In the second case, the conventional P&O algorithm was replaced by the proposed P&O with FLC to validate its performance and functionality under changing irradiation. The PV output power harvested in this case is 179.9W, 129W, 164.35W and 129W at irradiation of 1000W/m^2, 700W/m^2, 900 W/m^2 and back to 700 W/m^2 respectively.

The output results of the P&O with FLC were compared to the output results of the conventional P&O algorithm. The simulation results clearly showed that, the P&O with FLC method at the same irradiation changes has the ability to improve the performance of tracking the MPP and thereby increasing the total efficiency of the PV system.

The major contributions of this thesis work are:

- The proposed perturb and observe with FLC MPPT method with a variable step-size. The conventional P&O was modified to overcome the drawbacks in the conventional P&O MPPT algorithm. This is done by combining the conventional P&O with the fuzzy logic control, FLC. When a step change in the solar irradiation or temperature occurs, the FLC automatically tunes the step-size according to the change in the operating power. If the operating point is far from the MPP, the FLC increases the step-size to enable fast tracking of the MPP. A comparison with conventional P&O MPPT algorithm showed that the proposed P&O with FLC algorithm has improved performance of the photovoltaic power generation system.
- The proposed two-input Fuzzy logic controller for the MPPT of PV water pumping system. The PV module output power change, ΔP_{pv}, and the change in rotation speed of the pump, $\Delta\omega_m$, are used as inputs for this controller, which in turn adjusts the duty-ratio, ΔD, of the buck converter to track the MPP of the system. The FLC was proposed by making use of the relation between the PV module output power and the rotational speed to adjust the duty ratio of the buck converter which adapts the PV module output power to maximize the

rotational speed. At the time when output power of the PV module is at a maximum, the hydraulic power, $PP = KT\omega_m{}^3$, is at a maximum. Consequently, the rotational speed, ω_m, is at a maximum at the MPP. By maximizing the rotational speed, the daily volume of water discharge by the centrifugal water pump will be increased.

5.2 RECOMMENDATION

To enable the MPPT process, the buck converter is used as an interconnection in this thesis work. Future research investigations could be applied to some other converters such as boost, Ćuk and buck-boost along with the proposed MPPT technique to improve flexibility in the choice and configuration of the PV module connection.

In this work, simulation models were developed and used to compare the performance of the proposed MPPT technique. However, practical hardware tests at a representative power level and under the typical climatic conditions of an application need to be conducted to verify the simulation results. The simulation results achieved in this work will hopefully be applied to future investigations involving building prototype models to test experimentally the developed MPPT algorithm for the Photovoltaic water pumping system.

REFERENCES

[1] Mahesh Kumar,"*Modeling and Simulation of Solar Photovoltaic dc water pumping system Using MPPT*," International Research Journal of Engineering and Technology (IRJET), Volume: 04 Issue: 05, May, 2017.

[2] Sumedha Sengar,"*Maximum Power Point Tracking Algorithms for Photovoltaic System*", International Review of Applied Engineering Research. ISSN 2248-9967 Volume 4, Number 2, pp. 147-154, 2014.

[3] UNESCO, "*The UN World Water Development Report*," viewed on www.unesco.org/water/wwap/wwdr/), 2018.

[4] A. Z. Sahin and S. Rehman, "*Economical Feasibility of Utilizing Photovoltaic for Water Pumping in Saudi Arabia*," International Journal of Photo energy, vol. 2012, pp. 9, 2012.

[5] CEO Alicia Barton, "*Green strategic Outlook: Towards a clean energy Future*," New york State of Opportunity, 2018.

[6] S. S. Chandel, etal., "*Review of solar photovoltaic water pumping system technology for irrigation and community drinking water supplies*," Renewable and Sustainable Energy Reviews, vol. 49, pp. 1084-1099, 2015.

[7] M. Dursun and S. Ozden, "*Application of Solar Powered Automatic Water Pumping in Turkey*, "International Journal of Computer and Electrical Engineering Vol.4, April 2012.

[8] J. M. Enrique, etal., "*A reliable, fast and low cost maximum power point tracker for photovoltaic applications*," Solar energy, vol. 84, pp. 79-89, 2010.

[9] Sanae Dahibi, etal. "*A new method to improving hydrogen production by an Adaptive Photovoltaic System and P&O Algorithm*", Journal of Theoretical and Applied Information Technology, Vol. 84, Feb 10, 2016.

[10] N. Onat, "*Recent developments in maximum power point tracking technologies for photovoltaic systems*," International Journal of Photo energy, Vol. 2010, pp. 11, 2010.

[11] Haider Islam, etal. "*Performance Evaluation of Maximum Power Point Tracking Approaches and Photovoltaic Systems*," Power Electronics and Renewable Energy Research Laboratory, Department of Electrical Engineering, University of Malaya, Malaysia, Feb 4, 2018.

[12] R. Faranda and S. Leva,"*Energy comparison of MPPT techniques for PV Systems*," WSEAS transactions on power systems, Milano, Italy, Vol.3, Issue 6, 2008.

[13] Nasir Hussein Selman, etal., "*Comparison between Perturb and Observe, Incremental Conductance and Fuzzy Logic MPPT Techniques at Different Weather Conditions*," International Journal of Innovative Research in Science, Engineering and Technology, Department of Communication Engineering, Iraq, Vol. 5, Issue 7, July 2016.

[14] Luigi Piegari, etal. "*Optimized Adaptive Perturb and Observe Algorithm for Photovoltaic Maximum Power Point Tracking*, "Department of Electronics, Information and Bioengineering, Milano, Energies, 2015.

[15] M. H. Rashid, "*Incremental Conductance MPPT Technique for PV System*", International Journal of Advanced Research in Electrical, Electronics and Instrumentation Engineering, Vol. 2, Issue 6, June 2013.

[16] S. T. Buddha, "*Topology Reconfiguration to Improve The Photovoltaic (PV) Array Performance*," Master Thesis, Arizona State University, Dec. 2011.

[17] T. Huan-Liang, "*Insolation-oriented model of photovoltaic module using Matlab/Simulink*," Solar Energy, vol. 84, pp. 1318-1326, 2010.

[18] Anukool Korde, "*Assessment of a Solar PV Re-Powering Project in Sweden Using Measured and Simulated Data"*, Master Thesis, European Solar Engineering School, Sept. 2017.

[19] R.Prakash, etal. "*Modeling and Design of MPPT Controller Using Stepped P&O Algorithm in Solar Photovoltaic System*," World Academy of Science, Engineering and Technology, Vol.8, 2014.

[20] Saleh Elkelani Babaa, etal. "*Overview of maximum power point tracking control techniques used in photovoltaic systems*," School of Electrical Engineering & Electronic Engineering, Newcastle University, UK, pp. 59-72, August, 2014.

[21] Luigi Piegari, etal. "*Optimized Adaptive Perturb and Observe Maximum Power Point Tracking Controller for Photovoltaic Generation*," Journal of Energies, 2015.

[22] Long-Yi Chang Chung, etal., "*Smart Global Maximum Power Point Tracking Controller of Photovoltaic Module Arrays*," Department of Electrical Engineering, National Changhua University of Education, Taiwan, March 6,2018.

[23] V. Salas, etal., "*Review of the maximum power point tracking algorithms for stand-alone photovoltaic systems*," Solar Energy Materials and Solar Cells, vol. 90, pp. 1555-1578, 2006.

[24] M. Thomson, "*Reverse-osmosis desalination of seawater powered by photo voltaic without batteries*," Doctoral Thesis, Loughborough University, June 30, 2003.

[25] E.T.E1 Shenawy, etal. "*Design and Optimization of Stand-alone PV System for Egyptian Rural Communities*," International Journal of Applied Engineering Research, India Publications, Vol.12, 2017.

[26] M. A. Eltawil and Z. Zhao, "*Grid-connected photovoltaic power systems: Technical and potential problems-A review*," Renewable and Sustainable Energy Reviews, vol. 14, pp. 112-129, 2010.

[27] J. Gonzalez-Llorente, etal., "*Analyzing the optimal matching of dc motors to photovoltaic modules via dc-dc converters*," in Applied Power Electronics Conference and Exposition (APEC), 2010 Twenty-Fifth Annual IEEE, pp. 1062-1068, 2010.

[28] Protap Kumar Mahanta, etal "*Modeling and Simulation of a PV Module Based Power System using MATLAB/SIMULINK*," Department of Applied Physics, Electronics and Communication Engineering, Dhaka University, Bangladesh, March, 2014.

[29] S. Yuvarajan, etal "*A novel power converter for photovoltaic applications*," Electrical and Computer Engineering Department, North Dakota State University, Frago, USA, Journal of Power Sources pp. 327-331,15 June 2004.

[30] M.S. Aït Cheikh, etal, "*Maximum power point tracking using a fuzzy logic control scheme*," Review of Renewable Energies, Vol. 10, 387 – 395, 2007.

[31] Mohammed Redha Rezoug, etal., "*Fuzzy Logic-Based Perturb and Observe Algorithm with Variable Step of a Reference Voltage for Solar Permanent Magnet Synchronous Motor Drive System Fed by Direct-Connected Photovoltaic Array*," Department of Electrical Engineering, Kasdi Merbah University Ouragla, Algeria, February, 2018.

[32] Fatima Zohra Zerhouni, etal "*Proposed Methods to increase the Output Efficiency of a Photovoltaic (PV) System*," University of Science and Technology Mohamed Boudiaf,Ageria Vol 7,2010.

[33] V. V. Tyagi, etal. "*Progress in solar PV technology: Research and achievement*," Renewable and Sustainable Energy Reviews, vol. 20, pp. 443-461, 2013.

[34] P. Bhatnagar and R. Nema, "*Maximum power point tracking control techniques: State-of-the-art in photovoltaic applications*," Renewable and Sustainable Energy Reviews, vol. 23, pp. 224-241, 2013.

[35] A. Al-Badi and H. Yousef, "*Design of Photovoltaic Water Pumping System as an Alternative to Grid Network in Oman*", International Conference on Renewable Energies and Power Quality, Spain, Madrid, May 2016.

[36] Texas Instruments, "*Converting Analog Controllers to Smart Controllers with TMS320C24X DSPs for Optimal Digital Control*" Application Report, (downloaded from dspvillage.ti.com/), June 2004.

[37] Srushti R.Chafle, etal "*Design of Cuk Converter With MPPT Technique*," International journal of innovative research in Electrical, Electronics, Instrumentation and Control engineering Vol. 1, Issue 4, July 2013.

[38] The MathWorks, Inc "*MATLAB User Guide*," Technical Manual, 2015.

[39] Pie Basalike, "*Design, Optimization and Economic Analysis of photovoltaic Water Pumping Technologies*," School of Business Society and Engineering, 2015.

[40] Michael Gratzed and Jacques-E, "*Solar Energy Conversion"*, Laboratory for Photonic and Interfaces, Institute of Physical Chemistry, Switzerland Vol.3, pp. 589-644, 2001.

[41] N. Mohan and T. M. Undeland, "*Power electronics: converters, applications, and design"*: Wiley-India, 2007.

[42] Amevi Acakpovi and Essel Ben Hagan, "Novel *Photovoltaic Module Modeling using Simulink/Matlab*," Accra Institute of Technology, vol. 83, 2013.

[43] Mnimekalai.P, etal. "*An Overview of Converters for Photovoltaic Power Generating Systems",* International Conference in Communication and Computing Technologies, 2012.

[44] J.Surya Kumari, etal, "*Comparison of Maximum Power Point Tracking Algorithms for Photovoltaic System,*" Progress in Photovoltaic: Research and Applications, ISSN: 2231-1963, Nov 2011.

[45] Mounir Derri, Mostafa Bouzi, etal., "*Maximum Power Point Tracking using Fuzzy Logic Controller for Stand-Alone photovoltaic System,*" International Journal of Engineering Research & Technology (IJERT), Vol. 3, Issue 11, November, 2014.

[46] Anass Ait Laachir.etal.," *Maximum Power Point Tracking Using Adaptive Fuzzy Logic control for Photovoltaic System*," Int. Journal of Engineering Research and Applications, Vol. 5, Issue 1(Part 2), pp.65-70, January 2015.

[47] Shubhechchha Rane, etal, "*Performance of Mamdani Fuzzy Inference System for Tracking Multiple Targets Using Autopilot System*," International Journal of Electrical and Electronics Research Vol. 5, Issue 1, pp. 34-42, March 2017.

[48] Akash Garg[1], R.Saida Nayak[2], Sushma Gupta[3] ," *Comparison of P&O and Fuzzy Logic Controller in MPPT for Photovoltaic PV Applications by Using MATLAB/SIMULINK*,'' Journal of Electrical and Electronics Engineering, India, Vol. 10, Issue 4, pp. 53-62, August, 2015.

[49] Saravana selvan.D, etal. "*Simulation of Fuzzy Logic Control Based MPPT Technique for Photovoltaic System*," 2nd International Conference on Innovations in Engineering and Technology, Penang (Malaysia), Sept. 19-20, 2014.

[50] R.Arulmurugan[1] and N.Southanthira Vanitha[2], "*Fuzzy Logic Controller with Maximum Power Point Tracking Using Creative Design of DC to DC Buck Converter for Photovoltaic Power System*," Department of EEE, Knowledge Institute of Technology, Affiliated to Anna University, India, 2013.

[51] Deepa S. Bhandare, etal. "*Advanced Fuzzy Logic Tools for Industrial Applications-A Survey*", Department of Electrical Engineering, Modern College of Engineering, Pune University, India, Vol-4, Issue 7, 2016.

[52] Basil M. Hamed and Moayed N.Al-Mobaied, "*Fuzzy Logic Speed Controllers Using FPGA Technique for Three-Phase Induction Motor Drives*," Dirasat, Engineering Sciences, Vol 37, 2010.

[53] Basil M.Hamed and Mohammed S.El-Moghany, "*Fuzzy controller design using Field Programmable Gate Array (FPGA) for sun tracking in solar array system*," Electrical Engineering Department, Islamic University of Gaza, Gaza, Palestine,pp.46-52, 2012.

Appendix A

A.1 MATLAB Functions and Scripts

A.1.1 MATLAB Function for Modeling PV Module

function $I_a = PV(V_a, G, T_a C)$

% calculates module current under given voltage, irradiance and temperature

% Out: I_a *= Module operating current (A), vector or scalar*

% In: V_a *= Module operating voltage (V), vector or scalar*

% G = Irradiance (1G = 1000 W/m^2*), scalar*

% $T_a C$ *= Module temperature in deg C, scalar*

% Define constants

k = 1.381e-23; % Boltzmann's constant

q = 1.602e-19; % Electron charge

% constants taken from the datasheet of PV module and

% curve fitting of I-V character (Use data for 1000W/m^2)

A = 1; % Diode ideality factor (A),

% 1 (ideal diode) < A < 2

E_g*= 1.12; % Band gap energy; 1.12eV (Si), 1.42 (*G_a*As),*

% 1.5 (C_d*Te), 1.75 (amorphous Si)*

*Ns = 36*4; % # of series connected cells (BP SX150s, 72 cells)*

%for $T_a C$ *=0:25:75*

Go=1000;

T_{ref} *= 298; % Reference temperature (25C) in Kelvin*

$V_{oc\_}T_{ref}$ *= 21.6*4/Ns; % Voc (open circuit voltage per cell) @ temp* T_r*K*

$I_{sc\_}T_{ref}$ *=2.4*5; % Isc (short circuit current per cell) @ temp TrK*

% Define variables

$T_a K$ *= 273 +* $T_a C$*; % Module temperature in Kelvin*

V_c *=* V_a */ Ns; % Cell voltage*

% Calculate short-circuit current for $T_a K$

I_{sc} *=* $I_{sc\_}T_{ref}$ ** (1 + (A * (*$T_a K$ *-* T_{ref}*)));*

% Calculate photon generated current @ given irradiance

I_{ph} *= (G/Go) **I_{sc}*;*

```
% Define thermal potential (V_t) at temp T_ref
V_t_T_ref = A * k * Tref / q;
% Define b = E_g * q/(A*k);
b = E_g * q /(A * k);
% Calculate reverse saturation current for given temperature
Io_T_ref = I_sc_Tref / (exp(Voc_Tref / Vt_Tref) -1);
Io = Io_T_ref * (T_aK / T_ref)^(3/A) * exp(-b * (1 / T_aK -1 / Tref));
% calculate series resistance per cell
dVdI_Voc = -1.07/Ns; % Take dV/dI @ Voc from I-V curve of datasheet
Xv = Io_T_ref / Vt_T_ref * exp(Voc_T_ref / Vt_T_ref);
R_S = - dVdI_Voc - 1/Xv;
% Define thermal potential (V_t) at temp Ta
V_t_Ta = A * k * T_aK/ q;
%  I_a = Iph - Ir * (exp((Vc +  I_a * R_S) / Vt_Ta) -1)
% f(I_a) = Iph -  I_a - Ir * ( exp((Vc + Ia * Rs) / Vt_Ta) -1) = 0
% Solve for  I_a by Newton's method: Ia2 = I_a1 - f(Ia1)/f'(Ia1)
I_a=3; % initial value of  I_a
for j=1:5;
I_a =  I_a - (I_ph -  I_a - Io .* ( exp((Vc +  I_a .* Rs) ./ Vt_Ta) -1))./ (-1 - Io * (Rs ./ Vt_Ta) .* exp((Vc +  I_a .* Rs) ./ Vt_Ta));
end
```

A.1.2 MATLAB Functions script for P&O Algorithm

```
function D_k = fun (D_k2,D_k1,V_k,V_k1,I_k,I_k1,ds)
P_k1=I_k1*V_k1;
P_k=I_k*V_k;
dP=P_k1-P_k;
dD=D_k2-D_k1;
if dP>0
if dD>0
D_k=D_k2+ds;
else
D_k=D_k2-ds;
end
else
if dD>0
D_k=D_k2-ds;
else
D_k=D_k2+ds;
end
end
%P_k=P_k1
%D_k2=D_k1
```

Appendix B

B.1 PV water pumping system MPPT controls simulation

B.1.1 FIS of FLC based MPPT of PV water pumping system MATLAB/SIMULINK

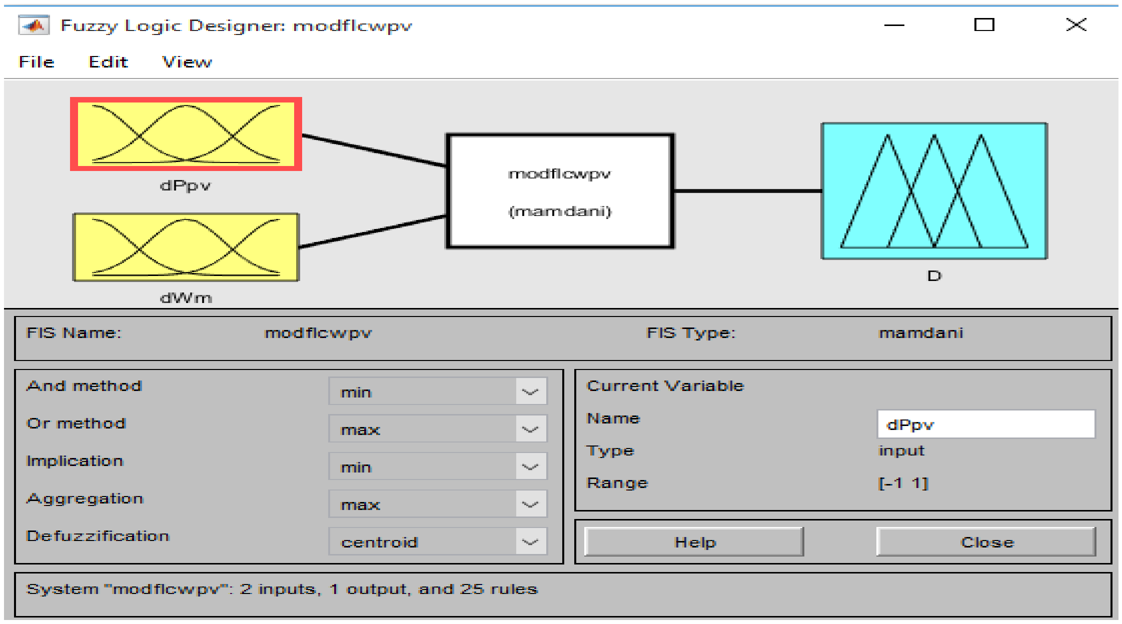

Fig. B.1 FIS editor.

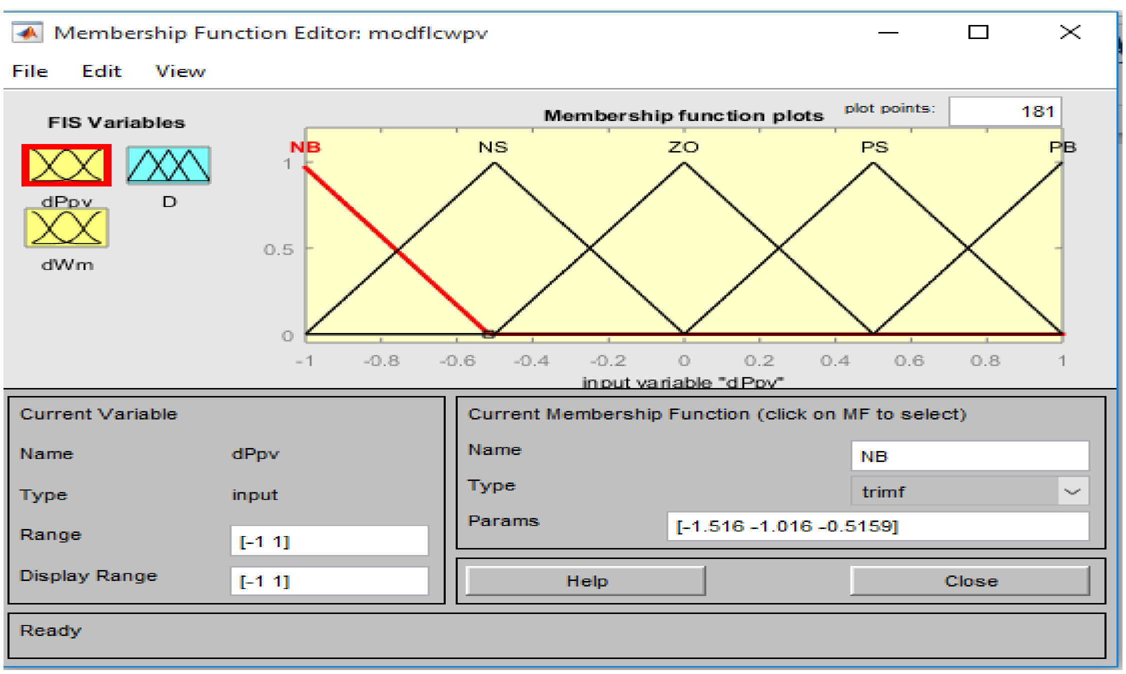

Fig. B.2 Membership function editor of the input variable (D_{ppv}).

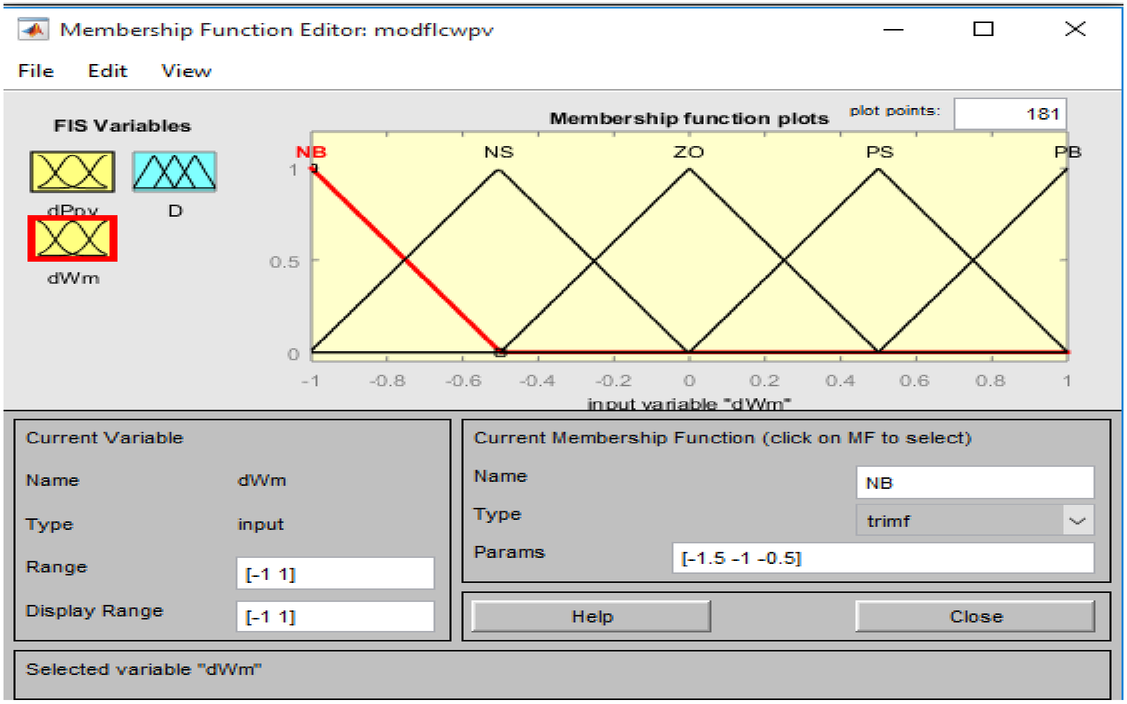

Fig. B.3 Membership function editor of the input variable ($d\omega_m$).

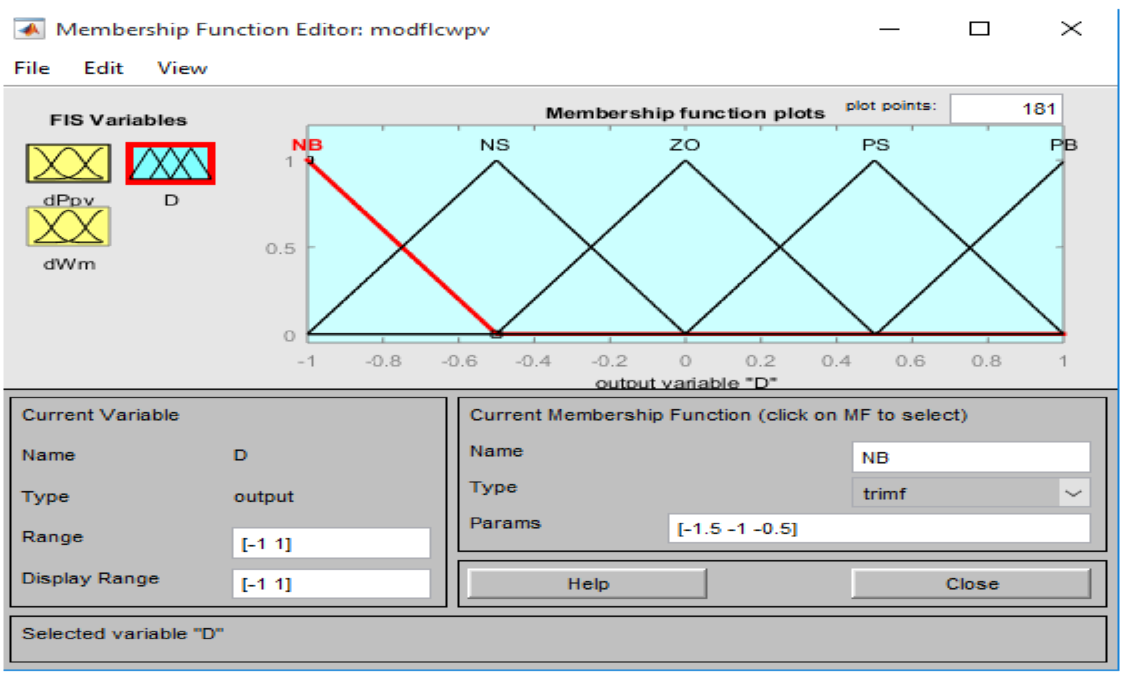

Fig. B.4 Membership function editor of the output variable (D).

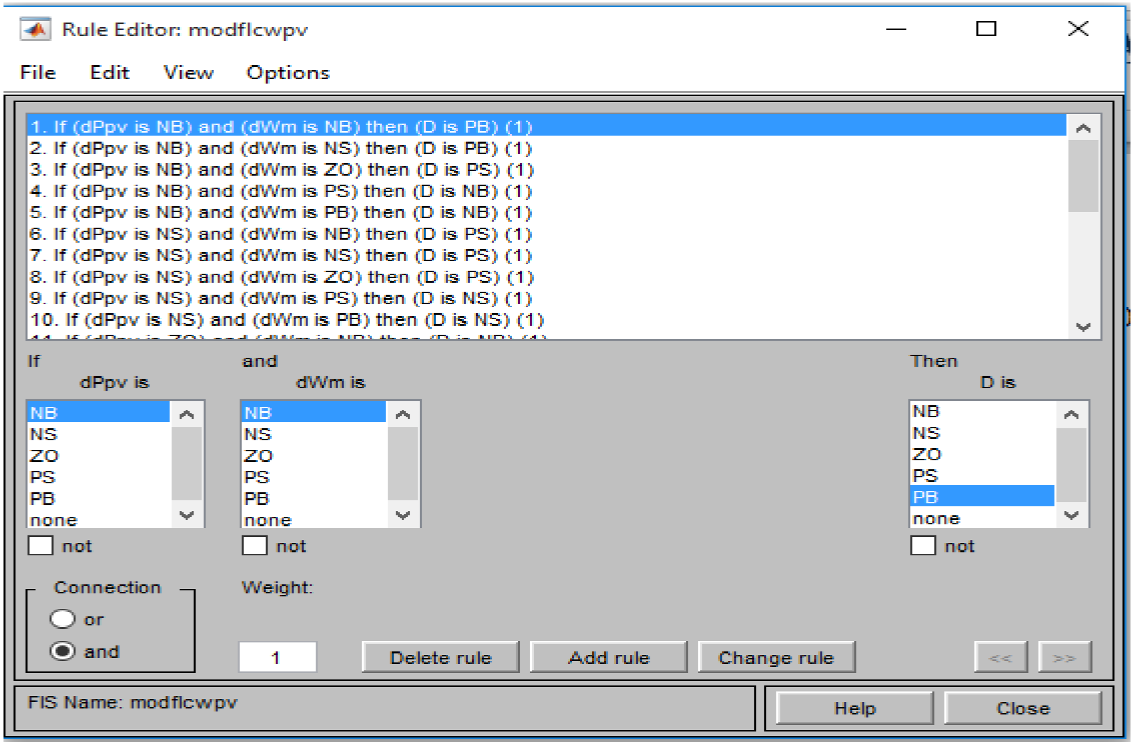

Fig. B.5 Rule-base editor.

Appendix C

C.1 Specification of PV module provided to market from Ethiopian Power Engineering Industry

METEC/EPEI solar technology

Specification

Cell type	multi crystalline silicon solar cells
Cell size	156 mm * 156 mm
No. of cells & connections	72(6*12)
Dimension of module (mm)	1965*992*40 mm
weight	20 kg $\pm$ 0.5 kg

Electrical characteristics

Model	EM300P
Maximum power rating at STC (p_m)	300W
Open circuit voltage (Voc)	45.20V
Short circuit current (Isc)	8.73A
Voltage at Pmax (Vmp)	36.41V
Current at Pmax (Imp)	8.24A
Power tolerance	-0~+3%
Standard test conditions	Irradiance 1000 W/m^2, cell temprature25°c, air mass 1.5

Limits

Fuse rating	15A
Maximum system voltage	1000VDC
Operating temperature	-40 ~ +85 $^\circ$c

Temperature and coefficients

NOCT (nominal operating cell temperature)	48 $^\circ$c $\pm$ 2 $^\circ$c
Temp coefficients of Voc	-(115 $\pm$ 5)mv/$^\circ$c
Temp coefficients of Isc	(0.08 $\pm$ 0.015)%/$^\circ$c
Temp coefficients of power	-(0.4 $\pm$ 0.05))%/$^\circ$c

Out put

Type of output terminal	Junction box
Cable size	4mm^2
Cable length	1500mm
Connector	Plug type